

**Development and Characterisation of Novel Squalene  
Based Adjuvant Formulations for Yeast Vaccines  
Against IBDV**

Dissertation

zur Erlangung des  
Doktorgrades der Naturwissenschaften (Dr. rer. nat.)

der

Naturwissenschaftlichen Fakultät I  
Biowissenschaften  
der Martin-Luther-Universität Halle-Wittenberg

vorgelegt von

Herrn Dipl.-Pharm. Johannes Jörg Stelzner  
geboren am 16.01.1989 in Dresden

Gutachter:

1. Prof. Dr. Karsten Mäder
2. Prof. Dr. Sven-Erik Behrens
3. Prof. Dr. Judith Kuntsche

Halle (Saale), 02.02.2018

## **Table of Contents**

List of Abbreviations .....	iv
<b>1 Introduction .....</b>	<b>1</b>
1.1 Vaccines and the Need for Adjuvants .....	1
1.2 Adjuvant Mechanisms.....	3
1.2.1 Classification of Adjuvants .....	3
1.2.2 Squalene Adjuvants.....	5
1.2.3 Nanoparticle Adjuvants.....	7
1.3 Infectious Bursal Disease Virus .....	9
1.4 Research Objectives .....	10
<b>2 Materials .....</b>	<b>13</b>
2.1 Genetic Background of the Yeast Vaccines.....	13
2.2 Adjuvants and Materials for Adjuvants Preparation.....	14
2.3 Miscellaneous.....	15
<b>3 Experimental .....</b>	<b>16</b>
3.1 Preparation of the Nanoparticles .....	16
3.2 Methods for Physicochemical and Size Characterisation .....	17
3.2.1 Static Light Scattering.....	17
3.2.2 Photon Correlation Spectroscopy.....	17
3.2.3 Nano Tracking Analysis.....	17
3.2.4 Asymmetrical Flow Field-Flow Fractionation.....	18
3.2.5 Electron Microscopy .....	20
3.2.6 Differential Scanning Calorimetry (DSC) .....	21
3.2.7 X-Ray Diffraction .....	21
3.2.8 <sup>1</sup> H-Nuclear Magnetic Resonance ( <sup>1</sup> H-NMR).....	21
3.2.9 Zeta Potential .....	21
3.3 Laboratory Equipment .....	22
3.3.1 Miscellaneous Laboratory Equipment .....	22
3.3.2 Lyophilisation .....	23
3.3.3 Gamma Sterilisation.....	23
3.4 Biological and Biochemical Methods .....	23
3.4.1 Sample Preparation for SDS-PAGE.....	23
3.4.2 SDS-Polyacrylamide Gel Electrophoresis (PAGE) .....	24
3.4.3 Western Blot Analysis.....	24
3.4.4 Preparation of Blood Serum.....	24
3.4.5 Enzyme-Linked Immunosorbent Assay (ELISA).....	25
3.4.6 Antibodies .....	25
3.4.7 Beta-Galactosidase Assay .....	25
3.4.8 <i>In Vitro</i> Cytotoxicity Test .....	26
3.4.9 Cultivation of Yeast .....	27
3.5 Animal Trials .....	28

---

3.5.1	Trials in Mice .....	28
3.5.2	Immunisation Trials in Mice .....	28
3.5.3	Immunisation Trials in Chickens .....	29
3.5.4	Multispectral Fluorescence Imaging .....	30
<b>4</b>	<b>Results and Discussion.....</b>	<b>32</b>
4.1	Optimisation Downstream Processing .....	32
4.1.1	Cell Disruption .....	32
4.1.2	Yeast Cell Disaggregation.....	35
4.1.2.1	Process Optimisation and Size Determination .....	35
4.1.2.2	Cell Wall Integrity - Beta-Galactosidase Assay and VP2-Detection .....	38
4.1.2.3	Immunisation Trials in Mice .....	40
4.1.3	Alternative Inactivation Methods.....	40
4.1.3.1	Inactivation and Antigen Verification .....	40
4.1.3.2	Immunisation Trials in Mice .....	42
4.2	Test of Commercial Adjuvants .....	43
4.3	Development and Characterisation of Nanoscaled Adjuvant Systems .....	46
4.3.1	Formulation Development and Evaluation of Critical Processing Parameters ...	46
4.3.2	Lyophilisation and Sterilisation .....	52
4.3.3	Long Term Stability .....	56
4.3.4	Size Determination and Physicochemical Characterisation.....	60
4.3.4.1	Static Light Scattering and Photon Correlation Spectroscopy (PCS) .....	60
4.3.4.2	Nanoparticle Tracking Analysis (NTA) .....	63
4.3.4.3	Asymmetrical Flow Field-Flow Fractionation (AF4) .....	65
4.3.4.4	Electron Microscopy .....	67
4.3.4.5	Zeta Potential .....	69
4.3.4.6	Differential Scanning Calorimetry (DSC).....	73
4.3.4.7	X-Ray Diffraction.....	76
4.3.4.8	<sup>1</sup> H-Nuclear Magnetic Resonance .....	77
4.3.5	Cytotoxicity Assay .....	80
4.3.6	<i>In Vivo</i> Experiments Adjuvants Development.....	83
4.3.6.1	Immunisation Trials in Mice .....	83
4.3.6.2	Tracking of the Squalene Based SLN Formulation.....	88
4.3.6.3	Immunisation Trials in the Target Organism Chicken.....	95
<b>5</b>	<b>Conclusion and Outlook.....</b>	<b>101</b>
<b>6</b>	<b>Appendix.....</b>	<b>I</b>
6.1	References .....	I
6.2	Supplementary Material .....	XIX
6.3	Acknowledgement.....	XXIII
6.4	Curriculum Vitae.....	XXIV
6.5	Selbstständigkeitserklärung.....	XXV
6.6	Publications .....	XXVI

---

## List of Abbreviations

AF4	Asymmetrical Flow Field-Flow Fractionation
<sup>1</sup> H-NMR	<sup>1</sup> H-Nuclear Magnetic Resonance
AT XX	Animal Trial XX
BSA	Bovine Serum Albumin
CFA	Complete Freund's Adjuvant
CFU	Colony Forming Units
DSC	Differential Scanning Calorimetry
EB	ELISA Buffer
EDTA	Ethylenediaminetetraacetate
EID	Egg Infectious Dose
ELISA	Enzyme-Linked Immunosorbent Assay
EPR	Electron Paramagnetic Resonance
HLB	Hydrophilic-Lipophilic Balance
HTV XX	Animal trial XX in chicken
IBDV	Infectious Bursal Disease Virus
IFA	Incomplete Freund's Adjuvant
ISCOM	Immune Stimulating Complexes
JS-1	Adjuvant formulation 1
JS-2	Adjuvant formulation 2
JS-3	Adjuvant formulation 3
JS-3o	Optimised adjuvant formulation 3
JS-4	Adjuvant formulation 4
mab63	Monoclonal Antibody 63 against IBDV
MALLS	Multi Angle Laser Light Scattering
MEM	Minimal Essential Medium
MMO	Mannide Monooleate
NIR	Near Infrared
NTA	Nano Tracking Analysis
OPNG	o-nitrophenyl- $\beta$ -D-galactopyranosid
PBS	Phosphate Buffered Saline
PCS	Photon Correlation Spectroscopy
PDI	Polydispersity Index
PEG	Polyethylene Glycol
PES	Polyethersulfone
PS154	Placebo squalene-free formulation of JS-3o
PVA	Polyvinyl Alcohol
PVDF	Polyvinylidene Difluoride

---

PVP	Polyvinylpyrrolidone
RC	Regenerated Cellulose
RES	Reticuloendothelial System
RMS	Root Mean Square radius
SDS	Sodium Dodecyl Sulfate
SLN	Solid Lipid Nanoparticle
SPF	Specific-Pathogen-Free
SRB	Sulforhodamin B
TBS	Tris Buffered Saline
TBS-T	Tris Buffered Saline with Tween 20
TEM	Transmission Electron Microscopy
TRIS	Tris(hydroxymethyl)aminomethane
VAKXXX	Yeast Vaccine XXX
VLP	Virus Like Particle
VP2	Virus Protein 2 of IBDV
WAX	Wide Angle X-ray scattering
WB	Western Blot
WT367	Antigen free yeast
YP	Yeast Peptone media
YPD	Yeast Peptone Dextrose media

# **1 Introduction**

## **1.1 Vaccines and the Need for Adjuvants**

The active immunisation of humans and animals provides the unique possibility of a reliable protection from infectious diseases [1]. Inoculation or variolation are regarded as the earliest forms of vaccinations. Infectious material from mild smallpox pustules was administered to healthy people to protect them from severe forms of smallpox already in the 10<sup>th</sup> century in China [2]. Although this method caused often serious infections, 2-3 % died by the inoculation, it can be regarded as the first live attenuated vaccine [1].

In 1796, Edward Jenner used cow pox to immunise an eight years old boy against smallpox. In the following, the inoculation with smallpox did not cause signs of the disease and a protectivity of the cow pox vaccination against smallpox was concluded [3]. Although Jenner was not the first who described the vaccination with cow pox against smallpox, he is regarded as the founder of modern immunology and vaccination [4,5]. Before the invention of the vaccine, 800 thousand people died annually of smallpox [6]. The introduction of a mandatory smallpox vaccination in 1874 in the German Empire led to a massive decrease in the death rate of smallpox in comparison to Austria without compulsory vaccinations [7,8]. The eradication of the smallpox by worldwide vaccination programs is considered as one of the largest achievements of medical care. While smallpox were the world's most devastating disease for thousands of years [6], the world was declared as smallpox free in 1980, after the last case in Somalia in 1977 [9,10].

Vaccines are divided into live attenuated, inactivated, subunit and toxoid vaccines [11]. Live attenuated vaccines base on viable pathogens with a decreased virulence. Although attenuated vaccines provide a good protection after only one immunisation, its use is restricted in immune suppressed patients like under chemotherapy or with HIV infection [12]. Attenuated vaccines are well recognised by the immune system as dangerous pathogens via multiple mechanisms, like size, cell wall composition, surface charge, hydrophobicity, pathogenic DNA and specific characteristics [13–16]. Thus, they provide excellent protectivity by mimicking the infection. Nevertheless, viable

pathogens carry the risk of remutation into the virulent form [17]. Inactivated vaccines of killed pathogens provide a better security profile, as the pathogen cannot reproduce [11]. Inactivated vaccines present the second main group. As they consist of whole or disrupted killed pathogens, their biocompatibility is increased, but is accompanied with a lower immunogenicity. Thus, larger doses or multiple administrations are necessary to ensure a sufficient protectivity [12].

Further purification led to subunit vaccines containing the specific epitopes which are the target of the antibodies, like neuraminidase or hemagglutinin of influenza [18]. Vaccines against diphtheria and tetanus are examples of toxoid vaccines. Detoxified bacterial exotoxins were administered as antigen [19]. Without an appropriate adjuvant, subunit vaccines often do not raise a sufficient immune response [20,21]. Polysaccharide vaccines are a special form of subunit vaccines and consist of polysaccharides of the bacterial surface capsules e.g. from meningococcus or pneumococcus [22]. Polysaccharides induces a T-cell independent immunity, thus they do not provide a reliable protectivity in young children [23,24]. The low immunogenicity of the polysaccharides has been overcome by the conjugation of the polysaccharides to proteins. This changed the immune response to a T-cell dependent response with good protectivity in small children [19]. Promising experimental vaccines base on DNA and RNA, which encode the antigen. After their uptake in the cells of the target organism, they are translated into the antigen [25].

The processing and purification of vaccines from live attenuated to single antigen vaccines or DNA vaccines changed the recognition of the vaccine by the immune system. Complete pathogens are well recognised by numerous specific markers (size, charge, cell wall and nucleic acid composition) as dangerous pathogen. In contrast, the recognition of single antigens is restricted [13–16]. Therefore, the inherent immune stimulating effect of pathogens is missing. Thus, a lower antibody titre is affected which does not provide a sufficient protectivity. While an increase of the antigen dose and the number of boosts can provide a sufficient immunity in some vaccines, others require the use of adjuvants to increase the immunogenicity [12]. The use of adjuvants ensures a reliable protectivity and can reduce the required antigen dose. In the case of a pandemic, many vaccine doses can be provided and the high costs of the antigen can be decreased by a reasonable adjuvant [26]. The adjuvant alone does not induce immunogenicity. Just

in combination with an antigen, it stimulates the immune reaction against the antigen [27].

Le Moignic and Pinoy have already shown the immune stimulating effect of water in oil emulsions by the incorporation of *Salmonella typhimurium* into mineral oil in 1916 [28]. Glenny *et al.* observed in 1926 the immune stimulating effect of precipitated aluminium on a diphtheria toxoid vaccination [29]. Jules Freund developed the complete and incomplete Freund's Adjuvant in 1937. He is known as the father of the adjuvant principles [27,30]. Freund's Adjuvant is regarded till today as the gold standard in immune stimulation, but it is accompanied with massive side effects [31]. Although adjuvants were developed for many years and many experimental adjuvants have been examined in animal trials, the number of adjuvants for human use is limited [32]. The most commonly used adjuvants in humans are aluminium salts and squalene nanoemulsions.

## 1.2 Adjuvant Mechanisms

### 1.2.1 Classification of Adjuvants

Although adjuvants can be classified according to their origin, chemical properties or type of the strengthened immune response, a classification according to the main adjuvant principles was preferred [33]. Understanding the basic adjuvant principles provides the chance to develop and optimise adjuvant formulations. Cox and Coulter suggested the following detailed classification [34]:

1. Depot generation
2. Induction of cytotoxic T-lymphocytes
3. Targeting
4. Antigen presentation
5. Immunomodulation

The formation of an antigen depot is a basic principle of water in oil emulsions like Freund's Adjuvant, TiterMax<sup>®</sup> Gold or Montanide ISA720 VG. Aim is to increase the contact time between the antigen and the immune system by an antigen release over several days and the protection of the antigen from degradation [33,34]. The same effect is attributed by multiple booster injections. In addition to the depot effect, inactivated

*Mycobacteria tuberculosis* and non-biodegradable paraffin oil were made responsible for the strong adjuvant effect of Freund's Adjuvant and its poor biocompatibility [35]. Paraffin oil induces a local inflammation with ulcers and granulomas [36].

Implants and microparticles are modern systems for a controlled and extended antigen release. The antigen release is controlled by degradation of the matrix or diffusion of the antigen. Even *et al.* described the release of ovalbumin from a lipid implant of cholesterol, lecithin and glycerol trimyristate over 14 days, making a booster injection redundant [37]. The most promising and intensively investigated release systems are Polylactide-co-glycolide (PLGA) microspheres [38–40]. Although no commercial vaccine uses PLGA microspheres, the market product Enantone<sup>®</sup> releases a peptide of 9 amino acids over a period of 4 weeks [41]. The release over 4 weeks covers the time of an initial immunisation and 2 booster injections.

The adjuvant effect of saponins, mainly from the bark of *Quillaja saponaria*, is attributed to the activation of cytotoxic T-cells. As crude saponins are toxic and cause haemolysis after intravenous administration, its purified fractions Quil-A, QS-21 or immune stimulation complexes (ISCOM) of cholesterol, phospholipids and saponins are preferred [42]. The covalent binding between a reactive aldehyde group in the saponin and an amine of the cytotoxic T-cell activates the cytotoxic T-cell [43].

Targeting describes the specific delivery of the antigen to immune competent cells like dendritic cells and macrophages. Size and charge of the antigen are important factors to mimic the pathogen and optimise the recognition by the immune system [14,44]. Virus like particles and virosomes are prominent examples for an immune stimulation by aggregates [45,46]. Virus like particles are composed of noninfective virus capsid or envelope proteins and the antigen [45]. In the virosomal hepatitis A vaccine HAVpur<sup>®</sup>, the antigen is absorbed on a unilamellar liposome of 150 nm. For better recognition by the immune system, a hemagglutinin of influenza was incorporated in the phospholipid bilayer. Both adjuvant systems are recognised as a virus because of their size (22 nm – 150 nm) and structure [46]. Therefore, they are taken up rapidly by macrophages and dendritic cells and provide a much stronger immune response than the soluble antigen [46]. A positive surface charge promotes the uptake of nano- and microparticles by macrophages and dendritic cells [14,15]. In the following, cationic emulsifiers like quaternary ammonium compounds were used as adjuvants [47].

Enhanced antigen presentation describes the stabilisation of the antigen in its native conformation and its presentation to immune effector cells. The adsorption of antigens on oil in water emulsions, ISCOMs or particles stabilises the conformation of the antigen and thus present the antigen to immune competent cells [34]. This mechanism is accompanied with the targeting of immune competent cells. Many adjuvants provide several modes of action and cannot be classified strictly into one group. Freund's Adjuvant combines the depot effect with the immunomodulatory effect of the paraffin oil and the *Mycobacteria tuberculosis*. The use of multiple mechanisms is preferred in the development of new adjuvant systems. Several adjuvants are combined to achieve a superior immune stimulation. The malaria vaccine Mosquirix combines the adjuvant effects of monophosphoryl lipid A (MPL), saponin (QS-21) and liposomes [48].

Immunomodulation comprises small molecules and proteins which modify the cytokine network. Especially the immune stimulation via Toll-like (TLR), Nod-like (NLR) and RIG-I-like (RLR) receptors, recognising pathogen associated molecular patterns (PAMP) like bacterial DNA, viral RNA, muramyl dipeptide, lipopolysaccharides, mannose oligosaccharides as well as synthetic analogs like CpG dinucleotide rich sequences or monophosphoryl lipid A, induces the innate immune response [49]. The most frequently used adjuvant aluminium activates the innate immune system via the NALP3-Inflammasome [50]. In the following, the proinflammatory cytokines IL-1b, IL-18 and IL-33 are released. Additionally, the adsorption of the antigen at the precipitated aluminium hydroxide lead to an improved presentation of the antigen to the immune system [51]. The monophosphoryl lipid A adjuvanted hepatitis B vaccine Fendrix was the first approved vaccine adjuvanted with an TLR ligand [52].

### 1.2.2 Squalene Adjuvants

Squalene emulsions have been widely used as vaccine adjuvants and drug delivery systems [53]. Because of its chemical structure as linear triterpene (Figure 1) and precursor in the endogenous cholesterol biosynthesis, it is biodegradable and provides good biocompatibility [54].

Water in squalene emulsions, like Montanide ISA720 VG and TiterMax<sup>®</sup>, were developed to overcome the toxicity of mineral oil based adjuvants like Freund's Adjuvant [53]. In Montanide ISA720 VG, the 30 % aqueous phase is stabilised with

mannide monooleate in the lipid squalene phase. It has been widely used as adjuvant in experimental malaria and HIV vaccines [55]. The adjuvant mechanisms were mainly attributed to the W/O emulsions, by the formation of an antigen depot at the injection site [55,56].

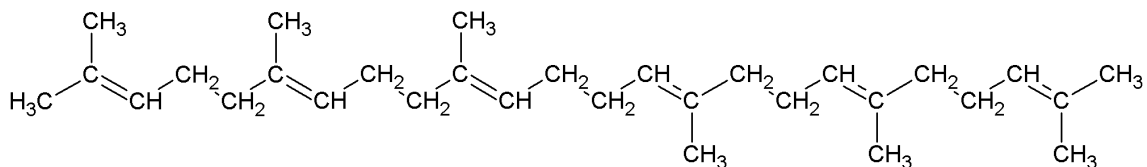


**Figure 1.** Chemical structure of squalene.

Additional, squalene in water emulsions were developed as adjuvants. The initially developed squalene nanoemulsion, Syntex adjuvant formulation, based on a squalene nanoemulsion and the immune stimulant muramyl dipeptide, but had severe side effects [57,58]. Later, the adjuvant effect of squalene nanoemulsions, without a further immune stimulant, was discovered [59]. AddaVax<sup>TM</sup>, AS-03 in the pandemic flu vaccine Pandemrix<sup>®</sup> and MF59<sup>®</sup> in the seasonal flu vaccine Fludax<sup>®</sup> are comparable squalene nanoemulsions. The most established squalene adjuvant is the squalene nanoemulsion MF59<sup>®</sup>. Since its approval in 1997, more than 150 million doses have been applied and it is known for its excellent biocompatibility [60]. Nevertheless, squalene adjuvants were made responsible for the gulf war syndrome, a multisymptom disorder of gulf war veterans, caused by vaccination with a squalene adjuvanted anthrax vaccine. Initial data suggested that anti-squalene antibodies were detectable in the blood serum of affected veterans [61]. Further studies could not prove a correlation between anti-squalene antibodies and the gulf war syndrome [62]. Moreover, squalene nanoemulsions have shown no induction of anti-squalene antibodies in immunisation trials [63]. Today, squalene nanoemulsions are regarded as safe and potent adjuvant formulations [60].

In MF59<sup>®</sup>, the lipophilic squalene phase of 4.3 % is stabilised with 0.5 % Tween 80 and 0.5 % Span 85 in the nanometre range around 160 nm [64]. The particle size plays an important role for the immune stimulating effect. Application of the single ingredients did not stimulate the immune system and the immune response remained at the level of the PBS negative control [65]. Also a squalene in water emulsion with a particle size of 1 µm has shown no comparable immune stimulating effects [66]. As the antigen was not incorporated in the lipophilic phase, a depot effect could not be assumed. A study with <sup>3</sup>H labelled squalene has shown a rapid elimination from the injection side. Within

4 h resp. 2 days, the squalene amount decreased to 36 % resp. 24 % [67]. For squalene nanoemulsions, the formation of a local inflamed and immunocompetent area at the injection side is assumed. Even the application of MF59<sup>®</sup> at the injection side 24 h before the immunisation led to a comparable stimulation. In contrast, the injection at a different side and the application 24 h after the antigen application at the same injection side did not cause an adjuvant effect [68]. The cytokine release after the injection attracts subsequently monocytes and granulocytes in the immune competent area [69]. This promotes the transport of the antigen into the lymph nodes and thus stimulated the activation of T-cells and B-cells [70].

### 1.2.3 Nanoparticle Adjuvants

Nanoparticles have been used frequently as delivery systems for vaccines [71]. Nanoscaled vaccine delivery systems act by the protection and prolonged release of the antigen [72]. Furthermore, nanoparticles stimulate the antigen resorption via the ocular, nasal and oral route [73–75]. Incorporation or adsorption of the antigen at the surface allowed to mimic the typical pathogen size, promoting the recognition by the immune system, the uptake by immune competent cells and the delivery to the lymphatic system [46,76].

Reddy *et al.* have shown the transport of nanoparticles into lymphatic capillaries and draining lymph nodes after intradermal injection. They observed a strong size dependency for the accumulation in lymph nodes and dendritic cells. Hereafter, the investigated 25 nm particles, containing ovalbumin as model antigen, raised a stronger immunity than the 100 nm particles [76].

Liposomes were used as versatile drug delivery system for antigens. The structure of liposomes allows to incorporate antigens and to modify the particle size and surface structure easily [46,48,77]. Both were applied to mimic the surface of pathogens. Oligomannose and yeast mannan coated liposomes have shown a dramatic increase in cell mediated immunity by mimicking the polysaccharide moieties of pathogens [78,79]. A vaccine of coated liposomes, containing soluble leishmania antigen, resulted in a nearly full protectivity against *Leishmania major* in comparison to the oligomannose free liposomal vaccine [78]. Similar nanoparticle structures, composed of virus capsid proteins and antigens, are virosomes and virus like particles. They can be

classified as reconstituted viruses. Their use and high potential is discussed in section 1.2.1.

Poly(lactide-co-glycolide) acid has been intensively studied as biodegradable polymer for vaccine drug delivery systems. Poly(lactide-co-glycolide) nanoparticles have been used successfully via the nasal, oral and parenteral route [80–82]. Ovalbumin loaded poly(lactide-co-glycolide) nanoparticles have shown a strong size dependency of the adjuvant effect. While microparticles with a mean diameter of 17  $\mu\text{m}$  did not raise antibody titres, the immune stimulation increased with smaller particles of 1  $\mu\text{m}$  and 300 nm [40].

Chitosan nanoparticles have been widely used for the mucosal application of vaccines via the nasal and oral route [74,83,84]. The cationic structure of chitosan particles is made responsible for the mucoadhesive properties. A chitosan based vaccine against hepatitis B induced high antibody titres in female BALB/c mice after intramuscular administration. The antibody titre of the chitosan nanoparticles vaccine with a particle size of 200 nm was up to 8 fold higher than the alum adjuvanted vaccine [85].

Different from the delivery systems, nanodispersions itself can also stimulate the immune system. Squalene nanoemulsions are the most prominent immune stimulating nanodispersions [60]. They are described in detail in section 1.2.2. In addition to the discussed squalene nanoemulsion, solid lipid nanoparticles (SLN) have been described as stable biocompatible adjuvant (SBA) by Müller *et al.* [86]. It was shown that the expression of proinflammatory cytokines were dependent on the hydrophobicity of nanoparticles [87]. An activation of the innate immune system by the lipid nanoparticles was assumed, as the lipids are recognised as damage associated molecular patterns (DAMP), like hydrophobic cell compartments which are released after cell lysis [16]. In contrast to this, the *in vivo* evaluated stable and biocompatible adjuvants always contained an immune stimulant. The successfully tested formulations based on paraffin or esterquat (N,N-di-[beta-stearylethyl]-N,N-dimethylammonium chloride) [88]. The adjuvant effect of paraffin and its bad biocompatibility with the formation of granulomas was already described by Freund in 1937 [36]. Additionally, cationic charged particles are well known to stimulate the immune response [14,89].

The formulation of saponins with phosphatidylcholine and cholesterol resulted in nanoparticles of 40 nm. The formed cage like structures acted immune stimulating by

the delivery of saponins and controlled the toxicity of saponins [90]. ISCOMS are approved for veterinary use in the equine influenza vaccine Equilis [91]. Additional, several antigens, like influenza A virus envelope glycoproteins, measles viral membrane antigens and bovine serum albumin, were incorporated into ISCOMs and used as antigen delivery systems [92–94].

### **1.3 Infectious Bursal Disease Virus**

The infectious bursal disease or Gumboro disease is a highly contagious disease mainly in chickens. It is caused by the double-stranded RNA infectious bursal disease virus from the family of birnaviridae and reaches morbidity rates up to 100 % [95,96]. Mainly young chickens of 3-6 weeks are affected and show unspecific clinical signs like decreased feed intake, ruffled feathers and prostration. Clinical signs of severe forms are a watery diarrhea and dehydration [97].

The animals are infected via the faecal-oral route. After the infection, the virus replicates initially in macrophages of the gut-associated tissues and spreads via the blood stream. The main target of the virus are proliferating B-lymphocytes in the bursa of Fabricius [98]. As the bursa develops during the 3-6 week of life, the chickens are most susceptible during this time. Earlier infections often occur without clinical symptoms, but with the same long lasting immunosuppression. The immunosuppression is caused by a depletion of the lymphoid follicles in the bursa. During the bursa infection, the replication of the virus lyses the bursa lymphocytes, which leads to depletion and necrosis of the bursa follicles [99]. The destruction of the lymphoid follicles in the bursa of Fabricius induces a growth deficit and makes the chickens susceptible for secondary infections [100]. Furthermore, the immunosuppression reduces the efficacy of future vaccinations [101]. Later on, the virus also infects and damages the spleen, bone marrow and thymus lymphocytes [102].

Gumboro disease was described as the most important disease in the global chicken production and occurs worldwide [103]. High economic losses in poultry farms are caused by its mortality, exceeding 50 % for very virulent strains, and long lasting immunosuppression [99]. Until the end of the 1980s, mainly mild forms of IBDV caused losses by a reduced yield in poultry farms and secondary infections [104].

There is no causal therapy for IBDV. Because of the high viability and resistance against heat, pH value and chemicals, the virus can remain infectious for 122 days. Therefore, a strict hygiene management is necessary, as the virus can be transmitted easily via water, nutrition and dust [105,106]. Although there are vaccines against IBDV, the occurrence of very virulent strains in 1987 led to vaccination failures and following increased morbidity and mortality [107].

Müller *et al.* gave an excellent overview about the current status of vaccines against infectious bursal disease [106]. The majority of commercially available IBDV vaccines bases on live attenuated classical virulent strains. Unfortunately, they do not provide sufficient protection against very virulent IBDV strains [106]. More stimulating strains in intermediate, intermediate plus and hot vaccines raise higher antibody titres and protectivity, but they can cause bursa lesions itself. The bursa lesions and immunosuppression may be comparable with the effects of infections [102]. The safety profile and vaccine breakthroughs are typical phenomena for live vaccines, especially for only mild attenuated vaccines. Nevertheless, even the intermediate plus vaccines were not able to achieve full protectivity against very virulent IBDV strains [108]. The presence of maternal antibodies is a further limiting factor in field vaccinations and requests for more potent vaccines [109]. The vector vaccine VAXXITEK<sup>®</sup> was developed to overcome the interference with maternal antibodies and potential immunosuppression of live vaccines. It bases on the herpes virus of turkey as vector for VP2. Thus, it ensures the necessary immune stimulation by the virus and the delivery of a potent and safe antigen [110,111].

## 1.4 Research Objectives

The aim of this work was to develop a vaccine formulation for a novel yeast based vaccine against the infectious bursal disease virus in chicken. The long-term goal was to achieve a competitive ready-to-use formulation of the yeast vaccine, a potent adjuvant system and excipients to ensure excellent biocompatibility. To be competitive with available market products, it should be focused on established adjuvant principles and preparation methods for large scale production. Genetic optimisation of the yeast vaccines and improvements during the fermentation were applied in parallel by project partners to increase the antigen amount and to achieve a stable and defined product.

This work focused on the following aspects of downstream processing and adjuvants development:

**1. Optimisation of the downstream processing:**

The yeast material should be processed to examine the influence of the particle size on the immune stimulation. Additionally, a uniform small particle size is requested to standardise the yeast vaccine and for the incorporation into a controlled release formulation. As yeast is well known to act as an adjuvant [56], the disrupted yeast material should be investigated for an increased adjuvant effect and to enhance the accessibility of immune competent cells to the antigen. Sterilisation trials with  $\gamma$ -irradiation should be carried out to inactivate the yeast material and to apply a validated sterilisation method in accordance with the pharmacopoeia.

**2. Test of commercial adjuvants:**

The adjuvant effect is highly dependent on the antigen, animal species and route of administration [49,112]. Commercial adjuvants should be investigated to ensure excellent immune stimulating properties and to select candidates for further adjuvants development.

**3. Development of adjuvant systems**

After the test of commercial adjuvants, the adjuvant system AddaVax<sup>TM</sup>, similar to MF59<sup>®</sup>, should be improved for easier preparation in large scales and to induce a stronger immune response by introducing a second adjuvant principle. Most adjuvants need to be prepared directly before the administration or they are available as aqueous emulsion. Therefore, it was the aim to develop a squalene containing adjuvants which could be stored as dry powder together with the freeze-dried and inactivated yeast material.

**4. Detailed physicochemical characterisation of the adjuvant systems**

The size of nanosized adjuvants is the most critical parameter for the adjuvant properties [66]. Therefore, detailed size measurements has to be performed, using static light scattering, photon correlation spectroscopy, nano tracking analysis and asymmetrical flow field-flow fractionation in combination with

multi angle laser light scattering. Differential scanning calorimetry,  $^1\text{H-NMR}$  and X-ray diffraction are applied additionally to characterise the combination of the solid and liquid lipids in the final adjuvant formulations.

#### **5. *In vitro* and *in vivo* testing of the developed adjuvant systems**

*In vitro* cytotoxicity tests should be performed on CCD-Co18 cells to determine the biocompatibility. The adjuvant effects of the developed formulations are evaluated initially in mice experiments. To provide results about the biodistribution and bioelimination of the final adjuvant system, fluorescently labelled formulations are tracked non-invasively. Furthermore, the distribution study can clarify the adjuvant mechanism of squalene nanoparticles.

#### **6. Immunisation trials in the target organism**

Final immunisation trials with the leading adjuvant formulation should be carried out in the target organism chicken. Continuous determination of the antibody titres and a final challenge experiment with a very virulent IBDV strain provide detailed data about the protectivity in chicken. Histopathological investigations of the bursa of Fabricius give a detailed overview about the protectivity of the vaccine formulation.

## 2 Materials

### 2.1 Genetic Background of the Yeast Vaccines

The yeast vaccines were developed and grown in the laboratory of the project partner Prof. Dr. Karin Breunig, Institute of Biology, Department of Genetics, at the Martin-Luther-University Halle-Wittenberg. For detailed information about the construction of the yeast strains and their genetic background, it is referred to the original works of Arnold *et al.* and Krijger *et al.* [104,113,114].

All yeast strains based on the antigen free *Kluyveromyces lactis* strain WT367, which was used as negative control in the immunisation studies. The growth of *Kluyveromyces lactis* on lactose is mainly dependent on the enzymes  $\beta$ -galactosidase, encoded by *LAC4*, and the lactose permease, encoded by *LAC12* [115]. The expression of both genes is induced in the presence of lactose or galactose. In the non-induced state, the inhibitor KIGal80 represses the transcription activator KIGal4 [116]. Thus, no expression of the *LAC4* and *LAC12* gene occurs. The recombinant antigen was stably inserted into the genome, downstream of the strong *LAC4* promoter [117] to ensure a reproducible, lactose dependent protein expression.

As reported by Saugar *et al.*, a capsid forming region of 456 amino acids from IBDV VP2 was selected as antigen to be expressed in *K. lactis* [118]. The amino acid sequence derived from IBDV strain D78 (GenBank: EU162087.1). To increase the amount of VP2 synthesised intracellularly, the protein was stabilised by replacing the threonine at position 2 of VP2 D78 by serine, in accordance with the N-end rule [119]. Furthermore, in VAK890 the VP2 expression was promoted by stable integration of additional *KIGAL4* transcription activator gene copies. For obtaining VAK911, the same principles were applied, but additionally the VP2 sequence was codon optimised by Mr. Gene GmbH (Regensburg, Germany) using the *S. cerevisiae* algorithm [14]. Strain VAKJS27 and VAKJS71 relied on the same principles and were optimised further, to grant high genetic stability and good growth properties, to facilitate the fermentation processes.

The antigen amount (VP2) was determined as 1.1  $\mu\text{g}$  per mg dry yeast for VAK890, 2.1-3.6  $\mu\text{g}$  per mg dry yeast for VAK911, 2.2-4.1  $\mu\text{g}$  per mg dry yeast for VAKJS27 and 3.5  $\mu\text{g}$  per mg dry yeast for VAKJS71.

## 2.2 Adjuvants and Materials for Adjuvants Preparation

**Table 1.** *Adjuvants and materials for adjuvants preparation.*

<b>Material</b>	<b>Lot</b>	<b>Producer</b>
<b>Adjuvants</b>		
AddaVax™	Various	Invivogen (Toulouse, France)
Montanide ISA720 VG	GWT24040-2316103	Seppic (Köln, Germany)
Complete Freund's Adjuvant	SLBC5082	Sigma Aldrich (Darmstadt, Germany)
Incomplete Freund's Adjuvant	SLBD7682	Sigma Aldrich (Darmstadt, Germany)
<b>Lipids</b>		
Squalene	MKBH3446V MKBQ5948V	Sigma Aldrich (Darmstadt, Germany)
Softisan 154	111225	Cremer Oleo (Witten, Germany)
<b>Emulsifiers</b>		
Span 85 LQ	870965	Croda (Nettetal, Germany)
Tween 80 HP	SD43361	Croda (Nettetal, Germany)
Cithrol MMO	607808	Croda (Nettetal, Germany)
Lecithin S100	790571-4/903	Lipoid (Ludwigshafen, Germany)
Kolliphor P188 micro	WPEI553T	BASF (Ludwigshafen, Germany)
Saponin (from quillaja bark)	010M7015V	Sigma Aldrich (Darmstadt, Germany)
<b>Fluorescence dyes</b>		
DiR (DiIC18(7) or 1,1'-dioctadecyltetramethyl indotricarbocyanine Iodide)	1654313	Life Technologies (Ober-Olm, Germany)
<b>Excipients for freeze-drying</b>		
Gohsenol EG-05PW	23N01	Nippon Gohsei (Düsseldorf, Germany)
PEG 1500S	DEG4127470	Clariant (Muttenz, Switzerland)
Trehalose	1250745	Fluka (Buchs, Switzerland)
Sucrose	133902	Fluka (Buchs, Switzerland)
Glucose	2228	Grüssing (Filsum, Germany)
Mannitol	M620019020	Merck (Darmstadt, Germany)
Dextran 500	241/03	Serumwerk Bernburg (Bernburg, Germany)
PVP 25	33420	Serva (Heidelberg, Germany)
<b>Others</b>		
Na Citrate*2 H <sub>2</sub> O	12E04-N05	Fagron (Barsbüttel, Germany)

---

## **2.3 Miscellaneous**

The exact composition of feeding solutions and buffers for biological and biochemical methods are given in the appendix. All other substances were of analytical grade, if not stated otherwise.

## 3 Experimental

### 3.1 Preparation of the Nanoparticles

The nanoparticles and nanoemulsions were produced with a high pressure homogeniser (Avestin C5, Ottawa, Canada) by using a pre-emulsion, prepared with a high speed mixer (Ultra-Turrax<sup>®</sup> T18, IKA, Staufen, Germany). For the formulation JS-2, the saponin was dissolved in bidistilled water and the lecithin was dissolved in squalene at 65°C. All other emulsifiers were dispersed in 10 mM sodium citrate solution pH 6.5 at 45°C. For the preparation of the pre-emulsion, squalene was added under continuous stirring at 20000 rpm at room temperature. The pre-emulsion of the solid lipid nanoparticle formulation JS-3 and JS-3o was formed by emulsifying the previously molten and mixed lipid phase of squalene and Softisan 154 under the same conditions at 65°C. Subsequently, the pre-emulsions were further processed with a high pressure homogeniser (EmulsiFlex C5, Avestin, Ottawa, Canada) at room temperature and at 65°C for JS-3 and JS-3o, resp. The homogenisation pressure and cycle number were dependent on the formulation and were evaluated for each formulation to achieve a comparable size distribution like AddaVax<sup>™</sup> (120-170 nm).

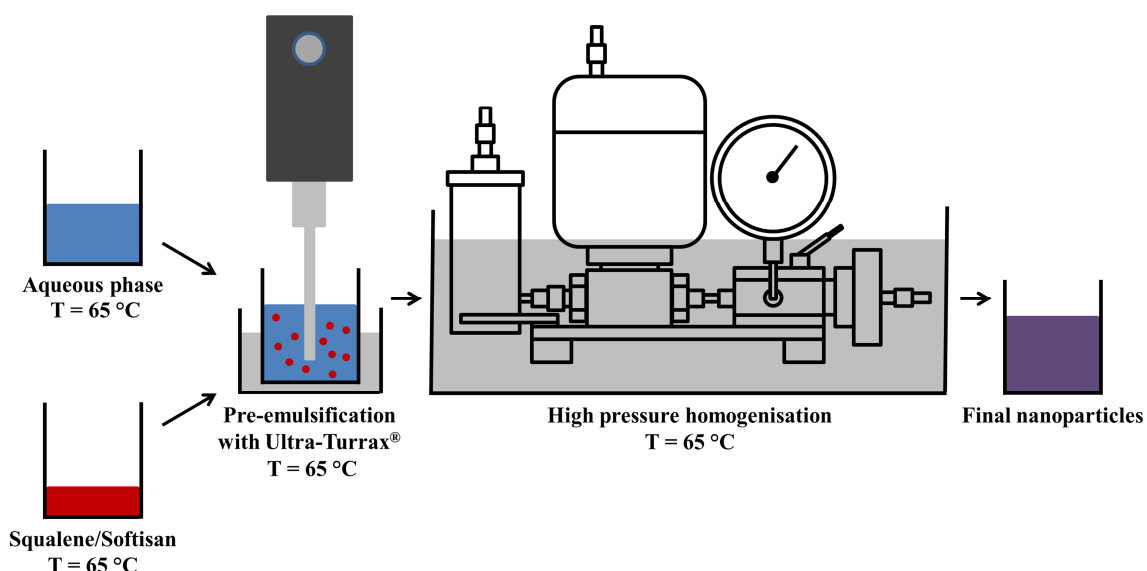


**Figure 2.** Preparation method for the solid lipid nanoparticles.

For animal experiments and cytotoxicity tests, the formulations were filtered after high pressure homogenisation through a 0.2  $\mu\text{m}$  filter of regenerated cellulose or polyethersulfone to ensure sterility. The solid lipid nanoparticles were filtered using preheated filters and syringes of 80°C to use the flexibility of the emulsified droplets

and for not changing the size distribution. Afterwards, the Softisan containing samples were cooled down on ice. For long time storage, the formulations were preserved with 0.02 % sodium azide and stored in the fridge at 4°C. The exact composition of the formulations is given in section 4.3.1.

## **3.2 Methods for Physicochemical and Size Characterisation**

### **3.2.1 Static Light Scattering**

Routine measurements of the size distribution were carried out by laser diffractometry on a Mastersizer 2000 (Malvern Instruments, Malvern, United Kingdom) combined with a Hydro 2000 S wet dispersion unit. The samples were measured at a laser obscuration of 5 %, corresponding to 11-15 % obscuration of the blue laser, in purified water. A series of 5 runs was evaluated by the Mastersizer 2000 software version 5.60, using the Mie theory, assuming spherical particles with a refractive index of 1.494, absorption of 0.001 and a refractive index of 1.33 for the dispersant as optical properties.

### **3.2.2 Photon Correlation Spectroscopy**

PCS measurements were carried out on a Zetasizer Nano ZS (Malvern Instruments, Malvern, United Kingdom) and the Zetasizer software 6.30. All samples were diluted with 0.22 µm filtered bidistilled water to a lipid concentration of 0.025 % and measured in quintuplicate in the automatic mode, suggesting 12-14 sub runs each. The samples were given 180 s to equilibrate at 25 °C. Measurements were performed in the backscattering mode at 173° to prevent multiple scattering events.

### **3.2.3 Nano Tracking Analysis**

Nano tracking analysis is a novel technique visualising nanoparticles. As the Abbe limit of half of the wavelength limits the resolution of bright field microscopes, it is not possible to examine nanoparticles there. However, the scattered light of nanoparticles can be tracked as point scatters in a microscope. The nano tracking analysis uses this principle to measure the size by tracking each single particle in the measurement chamber, preventing from multiple scattering events. Like in the PCS, the particle

movement is caused by the Brownian motion. In the following, the hydrodynamic particle radius can be calculated with the Stokes-Einstein equation. In contrast to the dynamic light scattering, the particle size is calculated for every single particle. Especially for broad and multimodal distributions, this offers a more detailed view on the particle size distribution [120].

The particle concentration was adjusted with 0.2  $\mu\text{m}$  filtered citrate buffer to 60 particles in the measurement area and was measured at five positions for 30 s to overcome the drawback of a limited sample size. The experiments were carried out on a NanoSight NS300 (Malvern Instruments, Malvern, United Kingdom) at a controlled temperature of 25°C. The samples were illuminated by a red laser beam at 642 nm and the particle movement was captured by a sCMOS camera. In the following, the data were analysed with the corresponding software NTA 3.1.

### 3.2.4 Asymmetrical Flow Field-Flow Fractionation

Asymmetrical Flow Field-Flow Fractionation (AF4) in combination with Multi Angle Laser Light Scattering (MALLS) has been used intensively as powerful tool to characterise the molecular weight distribution of polymers and macromolecules, size distribution and shape of nanoparticles [121–123]. The measurement bases on the previous separation of the particles in a flow channel. An applied cross flow decelerates especially larger particles on an accumulation wall, while smaller particles diffuse back to the faster elution profile in the middle of the flow channel and are eluted first. Thus, heterogeneous and broad particle size distributions can be examined accurately by static light scattering. For the detailed measurement principles of AF4/MALLS it is referred to the publications of Giddings and Wittgren *et al.* [124,125].

The separation of nanoemulsions and lipid nanoparticles was carried out with an Eclipse F asymmetrical flow field-flow fractionation (Wyatt Technology Europe, Dernbach, Germany) and analysed by a DAWN EOS multi angle laser light scattering detector (Wyatt Technology Europe, Dernbach, Germany), measuring the angle dependent light scattering intensity. A membrane of regenerated cellulose with a molecular weight cut off of 10 kDa (Microdyn-Nadir GmbH, Wiesbaden, Germany) was set up in a trapezoidal flow channel of 265 mm length and 350  $\mu\text{m}$  height as accumulation membrane. The eluent, 10 mM sodium citrate buffer pH 6.5 preserved

with 0.02 % sodium azide and filtered through 0.1  $\mu\text{m}$ , was provided by a HPLC pump and a micro vacuum degasser (Agilent 1100 Series, Agilent Technologies, Ratingen, Germany). Before the measurements, the formulations were adjusted with citrate buffer to 0.1 % lipid, meaning that 100  $\mu\text{g}$  lipid in 100  $\mu\text{l}$  buffer were investigated per run. The separation method is described in detail in Table 2. Initially, elution and focus steps with cross flows of 2 ml/min were applied to provide a homogeneous flow at the beginning of the injection. In the following, the samples were injected with a flow of 0.2 ml/min for 2 min, meaning that the injection loop of 100  $\mu\text{l}$  was flushed four times. The elution and separation of the nanosized formulations were performed with two isocratic cross flow gradients from 2 ml/min to 0.5 ml/min and in the following to 0 ml/min at a detector flow of 1 ml/min. The final elution step without crossflow was applied to remove contaminants from the channel, as well as the permanent elution mode with injection was applied to remove samples residuals in the injection loop.

**Table 2.** Method for AF4/MALLS separation analysis.

Step	Time (min)	Mode	Focus flow (ml/min)	Cross flow (ml/min)	
				Start	End
1	2	Elution	-	2	2
2	1	Focus	2	-	-
3	2	Focus + Injection	2	-	-
4	1	Focus	2	-	-
5	4	Focus + Injection	2	-	-
6	5	Elution + Injection	-	2	0.5
8	50	Elution + Injection	-	0.5	0
9	10	Elution + Injection	-	0	0
<b>Eluent:</b>	10 mM Na-citrate pH 6.5		<b>Inject flow:</b>	0.20 ml/min	
<b>Spacer:</b>	350 $\mu\text{m}$		<b>Detector flow:</b>	1.00 ml/min	

Data analysis of the raw data was performed with the Astra software 4.90 (Wyatt Technology Europe, Dernbach, Germany). The shape of the nanoemulsions and solid lipid nanoparticles was known from electron microscopic investigations as spheres. Hence, the data were fitted using the sphere model with a 3<sup>rd</sup> order polynomial fit. All samples were measured in triplicate and results are given as mean. The primary size information of the MALLS is the root mean square radius (RMS) which was

transformed to the geometric radius of spherical particles to ensure comparability by the following equation [126]:

$$d_{\text{geo}} = 2 r_{\text{geo}} = 2 \sqrt{\frac{5}{3}} RMS \quad (\text{Equation 1})$$

The characteristic  $D_{(0.1)}$ ,  $D_{(0.5)}$  and  $D_{(0.9)}$  values were calculated from the volume weighted cumulative particle size distribution over the whole peak.

### 3.2.5 Electron Microscopy

#### Cryo TEM

Vitrified samples of 2 mg/ml lipid were prepared using an EM GP grid plunger (LEICA, Wetzlar, Germany) under controlled temperature and humidity. Initially, the formulation was filter through a 0.22  $\mu\text{m}$  sterile filter to get rid of minimal parts of interfering larger particles. A thin film of the formulation was applied to a holey carbon film coated EM grid (C-flat<sup>TM</sup>, Protochips Inc., Raleigh, USA) by placing a drop on the grid and removing the excess with a filter paper. In the following, the samples were vitrified by plunging them into liquid ethane and kept in liquid nitrogen until they were transferred via a Gatan 626 cryotransfer system to the electron microscope. Electron microscopic pictures were taken on a Libra 120 Plus (Carl Zeiss Microscopy GmbH, Oberkochen, Germany) transmission electron microscope, running at 120 kV with a dual-speed on axis SSCCD camera (BM-2k-120, TRS, Moorenweis, Germany).

#### Negative Stain TEM

The negative stains were prepared by placing 3  $\mu\text{l}$  of the formulation, diluted to 10 mg/ml, onto a copper grid coated with a formvar film. Excessive liquid was removed with filter paper after 1 minute. After three following washing steps with water, the samples were stained with one drop of 1 % aqueous uranyl acetate. After 1 minute the liquid was drained of with filter paper and air dried. The prepared samples were investigated on a Zeiss Em900 (Carl Zeiss SMT, Oberkochen, Germany) electron microscope, operating at 80 kV and equipped with a slow scan camera (Variospeed SSCCD camera SM-1 k-120, TRS, Moorenweis, Germany).

### 3.2.6 Differential Scanning Calorimetry (DSC)

Thermal analysis was performed on a Differential Scanning Calorimeter 200 (Netzsch, Selb, Germany). If not stated otherwise, closed aluminum pans were used. Sample masses from 4 mg to 30 mg were weighted out accurately, depending on the lipid concentration in the sample. An empty closed aluminum pan was used as reference. The measurement cycle consisted of a heating segment from 5°C to 85°C, followed by a cooling step to 5°C and a second heating cycle to 85°C. Between the steps, a dwell time of 3 min was applied at the last temperature. DSC scans were performed with heating and cooling rates of 5 K per minute and under continuous nitrogen flow of 10 litres per minute. The maxima and minima of the DSC curves were assumed as melting resp. solidification points.

### 3.2.7 X-Ray Diffraction

Wide angle X-ray scattering was performed on a STOE STADI MP (STOE & Cie GmbH, Darmstadt, Germany) powder diffractometer, equipped with a cobalt anode (40 kV and 30 mA) and a Ge (111) monochromator to select the Co  $K_{\alpha}$  radiation at 0.1788965 nm. Data of the rotating samples were collected in the transmission mode from  $2\theta = 4-45^{\circ}$  in  $0.5^{\circ}$  steps for 60 s each. Prior X-ray analysis, the solid lipid nanoparticle formulations were concentrated by ultracentrifugation at 100000 g for 30 min on an Optima MAX XP (Beckmann Coulter, Brea, USA).

### 3.2.8 $^1\text{H}$ -Nuclear Magnetic Resonance ( $^1\text{H}$ -NMR)

$^1\text{H}$ -NMR experiments were carried out on a 500 MHz spectrometer (Unity Inova 500, Varian, Palo Alto, USA). The formulations were measured at 25°C and contained 20 %  $\text{D}_2\text{O}$  with 0.75 % trimethylsilylpropionate as internal standard. 32 spectra were accumulated to improve the signal to noise ratio.

### 3.2.9 Zeta Potential

Zeta potential measurements were performed on a Zetasizer Nano-ZS (Malvern Instruments, Malvern, United Kingdom) using laser Doppler electrophoresis. The zeta potential was calculated from the measured electrophoretic mobility by using the Helmholtz-Smoluchowski equation [127].



### **3.3.2 Lyophilisation**

For freeze-drying, the samples were frozen rapidly with liquid nitrogen at  $-196^{\circ}\text{C}$  and lyophilised on a Christ Alpha 2-4 freeze dryer (Martin Christ Gefriertrocknungsanlagen GmbH, Osterode am Harz, Germany) in combination with a Vacuubrand RC 6 vacuum pump (Vacuubrand GmbH, Wertheim, Germany) for 24 h. The chamber was evacuated to 0.05 mbar, corresponding to  $-48^{\circ}\text{C}$  on the sublimation curve of ice.

### **3.3.3 Gamma Sterilisation**

Gamma sterilisation was carried out as service by the Synergy Health Radeberg GmbH, using cobalt 60 as radiation source. In accordance with the European Pharmacopoeia, single or double doses of 25 kGy with target doses of 25-33 kGy resp. 50-60 kGy were applied to ensure sterility. The exact applied doses were evaluated dosimetrically. Shipping and irradiation were performed on dry ice at  $-78^{\circ}\text{C}$ . Prior sterilisation, the samples were aliquoted into radiation resistant polyethylene terephthalate tubes.

## **3.4 Biological and Biochemical Methods**

### **3.4.1 Sample Preparation for SDS-PAGE**

1 ml with 30 OD units of the yeast material was collected by centrifugation at 5000 rpm on an Eppendorf Centrifuge 5417R (Eppendorf AG, Hamburg, Germany) at  $4^{\circ}\text{C}$  for 5 min. After adding 600 mg glass beads and 500  $\mu\text{l}$  B60 buffer to the cells, they were disrupted by 4 times vortexing on a Multi-Pulse Vortexer (Glas-Col, Terre Haute, USA) for 3 min at  $4^{\circ}\text{C}$  and 5 min storage on ice. In the following, the supernatant was purified by centrifugation at 14000 rpm for 5 min at  $4^{\circ}\text{C}$ . The protein concentration was measured as described by Bradford in 1976 [128], using a Bio-Rad protein assay (Bio-Rad Laboratories, Hercules, USA) and bovine serum albumin as standard. The proteins in the supernatant were denaturated by heating with 10x Laemmli buffer at  $95^{\circ}\text{C}$  for 20 min and stored at  $-20^{\circ}\text{C}$ . All samples were adjusted to a constant protein amount to avoid differences caused by incomplete protein extraction.

### **3.4.2 SDS-Polyacrylamide Gel Electrophoresis (PAGE)**

The proteins were separated by electrophoresis in SDS-Polyacrylamide gels, based on their molecular weights, as described by Laemmli in 1970 [129]. Samples were run in a separation gel of 12 % and a stacking gel of 4.8 % polyacrylamide at constant amperage of 25 mA for 45 min in SDS-PAGE running buffer. PageRuler™ Prestained Protein Ladder (Thermo Fisher Scientific, Waltham, USA) was used as molecular weight standard in a range of 10-170 kDa.

### **3.4.3 Western Blot Analysis**

The weight dependent separated proteins were transferred onto a 0.45 µm PVDF membrane (Merck Millipore, Billerica, USA) to be detected by specific antibodies [130]. They were transferred at 100 V under continuous cooling with ice in transfer buffer for 1 hour. The membrane was blocked with 5 % milk powder and 3 % BSA in TBS-T for 1 hour. In the following, the membrane was incubated with the primary anti-IBDV (rabbit) antibody, diluted 1:10000 in blocking solution, overnight. Unbound antibody was removed by thoroughly washing with TBS-T. After the incubation with a horseradish peroxidase conjugated secondary antibody (1:5000) and thoroughly washing with TBS-T, the VP2 was visualised on X-ray films, using ECL reagent (GE Healthcare, Little Chalfont, UK). Additionally to the immunological protein detection, the membranes were stained with Ponceau S to verify their protein load semi-quantitatively.

### **3.4.4 Preparation of Blood Serum**

#### **Preparation of mouse serum**

After blood sampling, it was clotted for 1 hour at room temperature and for the following 16 h at 4°C. Serum was obtained by centrifugation with 10000 g at 4°C for 90 s. The supernatant was purified by a second identical centrifugation step and inactivated for 30 min at 56°C. Serum samples were preserved with 0.02 % sodium azide and stored at 4°C to ensure stability.

#### **Preparation of chicken serum**

Serum was gained by centrifugation at 3000 rpm for 30 min after clotting the blood at room temperature for half an hour. Finally, it was kept at -20°C.

### 3.4.5 Enzyme-Linked Immunosorbent Assay (ELISA)

An IDEXX (IDEXX Laboratories, Westbrook (Maine) USA) IBD enzyme linked immune assay for chicken was modified for the use in mice to determine the antibody titre against IBDV in mice. The tests were carried out as described in the manual with the following modifications. Mice sera were diluted 1:50. An anti-mouse-HRP antibody was used instead of the supplied anti-chicken:HRP (goat) as secondary antibody. The 2<sup>nd</sup> antibody was diluted 1:5000 in 50 mM tris-HCl pH 8.0, 140 mM sodium chloride and 1 % fetal calf serum. Mab63, a monoclonal antibody against IBDV diluted 1:100, was used as positive control. The sample buffer and the secondary antibody were measured as negative controls to verify the performance of the test itself. The changes prevented from the calculation of antibody titres. Instead, the absorption at 650 nm was used for quantification.

In chicken, the antibody titre was determined with an anitProFLOK<sup>®</sup> PLUS IBD ELISA (Zoetis, Florham Park, USA), following the producer`s instructions.

### 3.4.6 Antibodies

**Table 4.** *Overview about the used antibodies in Western Blot (WB) and ELISA of mice sera.*

Name	Host	Epitopes	Use	Supplier/Reference
anti-mouse-HRP	goat	IgG	ELISA	Sigma-Aldrich
anti-VP2 (mab63)	mouse	VP2	ELISA	Snyder 1988 [131]
anti-IBDV	rabbit	IBDV-VP2;- VP3;-VP4	WB/ELISA	Granzow 1997 [132]
anti-rabbit-HRP	goat	IgG	WB	Jackson Immuno Research

### 3.4.7 Beta-Galactosidase Assay

The activity of beta-galactosidase was used as a parameter to determine the integrity of the yeast cell wall. The yeasts were washed twice by centrifugation for 10 min at 4°C and a speed of 6000 rpm on an Eppendorf Centrifuge 5810R (Eppendorf AG, Hamburg, Germany) and resuspended in beta-Gal buffer. Subsequently, the cells were lysated with glass beads. The enzyme activity was measured spectrometrically at 420 nm and 30°C by following the degradation of 0.4 % ortho-nitrophenyl- $\beta$ -galactoside solution for 3 minutes every 30 seconds.

The activity of beta galactosidase was calculated by:

$$\text{beta – galactosidase activity} = \frac{\Delta OD \times d}{\epsilon \times c \times V} \quad (\text{Equation 3})$$

$\epsilon$  extinction coefficient of OPNG       $d$  layer thickness

$c$  protein concentration       $V$  used sample volume

### 3.4.8 *In Vitro* Cytotoxicity Test

Cytotoxicity was estimated with a sulforhodamin B (SRB) assay on human colon fibroblasts (CCD-Co18) cells in cooperation with the Erasmus master student Hanne Debergh. The test based on a modified protocol of the test introduced by Skehan et al. [133]. Cells were cultured in minimum essential medium (MEM), supplemented with 1 % penicillin-streptomycin, 1 % sodium pyruvate, 1 % non-essential amino acids and 15 % fetal bovine serum at 37°C under 5 % pCO<sub>2</sub> atmosphere. Medium without cells was used as blank and non-treated cells were used as negative control. Prior analysis, samples were diluted to a lipid concentration of 2.15 %. Emulsifier samples were diluted by the same factor as the nanoparticles. Osmolarity and pH-value were adjusted with 10x PBS to ensure biocompatibility. In the following, each formulation was tested at four different concentrations containing 1.075 % (Dilution 1), 0.215 % (Dilution 1:5), 0.043 % (Dilution 1:25) and 0.0086 % (Dilution 1:125) lipid after mixing 100 µl sample with 100 µl medium containing 2000 cells. The concentrations of the components in dilution 1 are given in Table 5. The cells interacted with the samples on 96 well plates and were incubated for 48 h at 37°C under 5 % pCO<sub>2</sub>. After 48 h, the medium was removed and the cells were fixed by adding TCA at 4°C for 1 h. After four washing steps with water, it was incubated for 30 min with 0.057 % sulforhodamin B solution. Subsequently, the 96 well plates were washed with 1 % acetic acid. After resuspending in 10 mM Tris (pH 10.5), measurements of the protein content were carried out calorimetrically at 570 nm. Cell viability was calculated by the following formula:

$$\text{cell viability} = \frac{A_{\text{sample}} - A_{\text{blank}}}{A_{\text{control}} - A_{\text{blank}}} \quad (\text{Equation 4})$$

$A_{\text{control}}$  absorption of untreated cells

$A_{\text{blank}}$  absorption of MEM

$A_{\text{sample}}$  absorption of with SLN incubated cells

**Table 5.** *Composition of the formulations for the cytotoxicity test in the highest applied concentration in dilution 1.*

<b>Formulation</b>	<b>Emulsifier A</b>	<b>Emulsifier B</b>	<b>Lipid</b>
<b>JS-1</b>	0.125 % Tween 80	0.125 % Span 85	1.075 % Squalene
<b>JS-2</b>	0.03125 % Saponin	0.0625 % Lecithin S100	1.075 % Squalene
<b>JS-3</b>	0.195 % Tween 80	0.195 % Span 85	0.5375 % Softisan 154 0.5375 % Squalene
<b>JS-3o</b>	0.5375 % Poloxamer 188		0.5375 % Softisan 154 0.5375 % Squalene
<b>JS-4</b>	0.125 % Tween 80	0.125 % MMO	1.075 % Squalene

### 3.4.9 Cultivation of Yeast

Yeast vaccines were produced by the project partners from the Institute of Biology, Department of Genetics Prof. Dr. Karin Breunig. For mice immunisation studies, yeast was cultured at 30 °C in shaking flasks (140 rpm). The precultures were prepared by inoculating 20 ml YPD medium with a single yeast colony from YPD plates. After growing overnight, the preculture was transferred to a second preculture in YPD media with an OD of 0.7 and grown for 10 h. The main culture of 500 ml was started at an OD of 0.3 in YP medium with 2 % lactose to induce expression of the VP2 antigen. VAK890, VAK911, VAKJS27 and WT367 were induced for 15 h. VAKJS71 was induced for 12 h in the main culture.

Large scale fermentation of VAKJS71 for chicken trials was carried out in a DasGip parallel bioreactor system (DasGip AG, Jülich, Germany). The system worked in parallel with two 1 litre media batches and was fully equipped to adjust the following conditions pO<sub>2</sub> 30 %, pH 5.0 and 30°C. The fermentation was conducted as fed batch process over 46 hours. Precultures of 100 ml and secondary precultures of 500 ml were cultivated for 8 h resp. 12 h in YPD to inoculate the fermenter. The exact composition of the media and feed solutions is given in the appendix. After fermentation, the cells were harvested by centrifugation using an Avanti J-25 centrifuge (Beckmann Coulter, Brea, USA) at 6000 rpm for 10 min. The yeast material was frozen at -20°C for 24 h and lyophilised on a Christ Alpha 2-4 freeze dryer (Martin Christ Gefriertrocknungsanlagen GmbH, Osterode am Harz, Germany) for another 24 h. In the following, it was crushed using mortar and pestle and heat inactivated at 90°C for 2 h. In the end, the content of the IBDV antigen was determined by SDS-PAGE and western blot.

## 3.5 Animal Trials

All animal trials were approved by the local authorities of Saxony-Anhalt and performed in accordance with the animal welfare act.

### 3.5.1 Trials in Mice

Mice were housed under controlled conditions (22°C and 12 h dark/light cycle) in groups of 5 animals and provided with water and nutrition *ad libitum*. Biodistribution and elimination experiments were performed in female hairless, immunocompetent SKH1-Elite (CRL:SKH1-*Hr<sup>hr</sup>*) mice (Charles River Laboratories, Wilmington, USA) at an age of 9 weeks. Female BALB/c mice (Charles River Laboratories, Wilmington, USA; Harlan Laboratories, Indianapolis, USA or Janvier Labs, Saint-Berthevin, France) at an age of 6 weeks were used for immunisation studies. For the application and blood sampling, the mice were anaesthetised with isoflurane/oxygen mixture with 4 % isoflurane initially for 1 min and 2 % isoflurane as maintenance dose. The mice were placed on a heat plate (35°C) to prevent from cooling of the body. Finally, the mice were sacrificed by cervical dislocation.

### 3.5.2 Immunisation Trials in Mice

Immunisation trials in mice were performed in groups of 5 animals. All samples were prepared freshly of yeast, the adjuvant, water for injection and 10x PBS to ensure isotonicity and euhydrie. In general, each mouse received three doses of each 0.1 mg yeast vaccine at day 0; 14 and 28 subcutaneously. During the experiments, they were monitored daily by visual inspection and weighted weekly. Five weeks after the first immunisation, their blood was collected terminally from the *Vena cava caudalis* to estimate the antibody titre. An overview about the standard immunisation protocol 2-2-1 is shown in Table 6.

The samples of the developed adjuvants and AddaVax<sup>TM</sup> were adjusted to 2.15 mg squalene in 100 µl for injection at one side or in 200 µl for injection of 100 µl at both sides of the abdomen. The CFA and IFA containing vaccines were prepared by emulsifying the resuspended yeast in 50 µl PBS buffer into 50 µl of the lipophilic adjuvant. The formulation was vortexed until it was stable. The stability was confirmed by the water drop test, meaning that a drop of the prepared formulation stayed in its

shape on the water surface. Samples with Montanide ISA720 VG were prepared like the other W/O emulsions, but 30 µl of the hydrophilic and 70 µl of the lipophilic phase were used. Multiples of the described ratios of hydrophilic and lipophilic phases were prepared for easier handling. Antigen free yeast WT367 and PBS were used as negative controls.

**Table 6.** *Immunisation and experimental protocol for the chicken and mouse trials.*

Day	Events in chicken trials		Events in mouse trials
0	Immunisation	1 <sup>st</sup> blood donation	Immunisation
10		2 <sup>nd</sup> blood donation	
14	1 <sup>st</sup> boost		1 <sup>st</sup> boost
20		3 <sup>rd</sup> blood donation	
27		4 <sup>th</sup> blood donation	
28	Challenge		2 <sup>nd</sup> boost
35	Section	5 <sup>th</sup> blood donation	Blood donation + Section

### 3.5.3 Immunisation Trials in Chickens

Immunisation studies in chickens were performed in cooperation with Prof. Dr. Silke Rautenschlein at the Clinic for Poultry at the University of Veterinary Medicine Hannover, Foundation. The chickens were bred and hatched from SPF-eggs from VALO<sup>®</sup> (Lohmann Tierzucht, Cuxhaven, Germany). After a primary breeding period of 18 days at 37°C and 65 % humidity, the fertilised eggs were placed in the hatch incubator at 35°C and 80 % humidity till hatch at day 21. At the age of 2 weeks, groups of 18 – 20 chickens were immunised subcutaneously with 0.5 ml PBS, 10 mg yeast vaccine VAKJS71 or placebo yeast WT367. The chickens received a booster immunisation 14 days after their first immunisation. The adjuvants preparation was proceeded as described for the mice experiments. Blood samples were taken from the wing vein four times and the exact immunisation protocol is given in Table 6.

Before challenging the chickens, the groups were subdivided into 2 groups of 9-10 chickens each. One group was challenged with each 10<sup>4</sup> EID of a very virulent IBDV strain (vvIBDV strain 89163/7.3, Etteradossi *et al.* [134]) via the ocular route and the other group was kept as negative control group by receiving 50 µl PBS per eye. The subgroups of 9-10 animals were kept in isolator units. At any time the chickens received feed and water *ad libitum*. After their challenge, the chickens were observed daily for

severe clinical symptoms. Ruffled feathers, closed eyes, depression together with lying down led to immediate euthanasia of the birds. At day 35, the surviving birds and the control group were sacrificed. Post mortem, all chickens were autopsied and all organs were investigated for pathological lesions. Additionally, histopathological samples were prepared of the bursa, spleen and caecal tonsils. The bursa and the animals were weighted to determine the bursa to bodyweight ratio.

### 3.5.4 Multispectral Fluorescence Imaging

Biodistribution and elimination studies of the novel solid squalene based adjuvant were performed on a Maestro<sup>TM</sup> fluorescence imaging system from CRi (Cambridge Research and Instrumentation, Hopkinton, USA). The system based on the principles of fluorescence. Therefore, DiR was used as fluorescence tracer and incorporated into the solid lipid nanoparticles. Data analysis was carried out with the corresponding software Maestro<sup>TM</sup> (Version 2.10.0). The excitation light was emitted from a xenon lamp and filtered by a bandpass filter (710-760 nm). The emission light was preselected by an 800 nm longpass filter. In the following, a tunable liquid crystal filter selected the emission light in the range from 780-950 nm. A CCD camera acquired the fluorescence spectrum in 5 nm steps. A binning of 2x2 was used for the image acquisition, meaning that 4 pixels of the detector were combined to improve the signal quality. The exposure time was chosen as calculated by the software to prevent from over or under exposure.

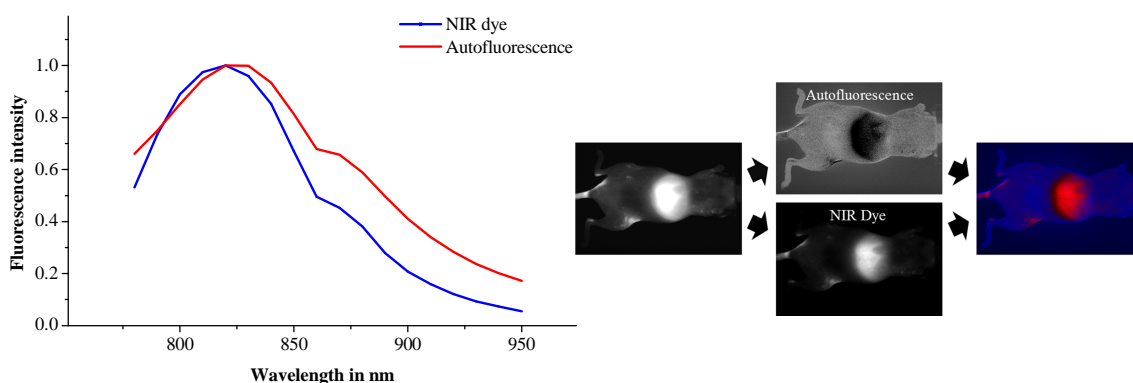


**Figure 3.** Principles for the unmixing of fluorescence images by the use of previously recorded reference spectra at the example of auto and background fluorescence from the added NIR tracer molecule.

Grey scale pictures were obtained as primary data, representing an addition of all measured intensities over the wavelength range from 780-950 nm. In the background, this data consisted of the exact spectral information for each pixel. By the use of

previously recorded reference spectra, it was possible to subtract auto and background fluorescences from the tracer signal or to distinguish between different tracers with different spectral properties. Figure 3 is pointing out the principles of the unmixing between different fluorescence spectra at the example of auto fluorescence from the added NIR tracer molecule.

As the fluorescence intensity is dependent on the exposure time, excitation intensity and the size of the measurement region, it was normalised on them. For *in vitro* experiments, like quantification of the dye load or SLN content, the fluorescence was measured in 96 well microtitre plates. As region of interest (ROI) a round area of 28.11 mm<sup>2</sup> in the center of the well was used to ensure homogeneous light distribution. For the *in vivo* elimination and biodistribution studies, the blank of an untreated mouse was subtracted from the measured intensities.

## **4 Results and Discussion**

### **4.1 Optimisation Downstream Processing**

#### **4.1.1 Cell Disruption**

The yeast cells were either disrupted as described in the method section for SDS-PAGE sample preparation or they were disrupted on an EmulsiFlex-C5 high pressure homogeniser (Avestin, Ottawa, Canada). Instead of lysis buffer, PBS pH 7.2 was used as biocompatible aqueous phase. To ensure protein stability, cell lysis was performed under controlled conditions on ice directly before the application. In accordance with the literature and microscopic in process controls, 15 cycles at 1750 bar were performed on the high pressure homogeniser [135].

In animal trial 12 (AT12) and 14 (AT14) the effect of disrupted yeast cells on the strength of the immune response was evaluated. The rigid cell wall ensures a high stability of the foreign protein, but it makes the immunogen hardly accessible to immunocompetent cells. It is necessary for the immunogen to be released out of the yeast to trigger an immune reaction. The yeast itself is recognised as pathogen and thus, the immune response against the yeast is stimulated. As the immune stimulation is not limited to the yeast and comprises the antigen as well, this makes the yeast an adjuvant [137]. The yeast cell wall mainly consists of an outer mannan and an inner glucan layer. Both polysaccharides can bind to C-type lectin receptors which are expressed on macrophages and immature dendritic cells. C-type lectins are a subgroup of pattern recognition receptors and led to an immune stimulation by the innate immune response [138,139]. Additionally,  $\beta$ -glucans can activate toll like receptors and can stimulate the production of the proinflammatory cytokine TNF- $\alpha$  [140]. Cell disruption can make the inner  $\beta$ -1,3-glucan layers more accessible to immune cells [141]. Yeast cell particles with a reduced mannan amount in their outer cell wall layer have been patented as vaccine system. This resulted in an increase of the  $\beta$ -1,3-glucan content at the outer cell surface [142]. Oligomannose and yeast mannan coated liposomes have shown a dramatic increase in cell mediated immunity. A vaccine of coated liposomes, containing soluble leishmania antigen, resulted in a nearly full protectivity against *Leishmania major* in comparison to the oligomannose free liposomal vaccine [78,79].

Intact yeast cells were tested against lysated VAK890 and were compared to the more optimised strain VAK911 (Figure 4). Each mouse was immunised with 0.1 mg yeast, adjuvanted with CFA for the first application and IFA for the boosts, 2 and 4 weeks after the first immunisation. Placebo yeast WT367 was used as negative control group and induced antibodies at the same level like the ELISA negative control. This confirmed that there was no immune response to naive yeast except a potential adjuvant effect which would just work together with an antigen.

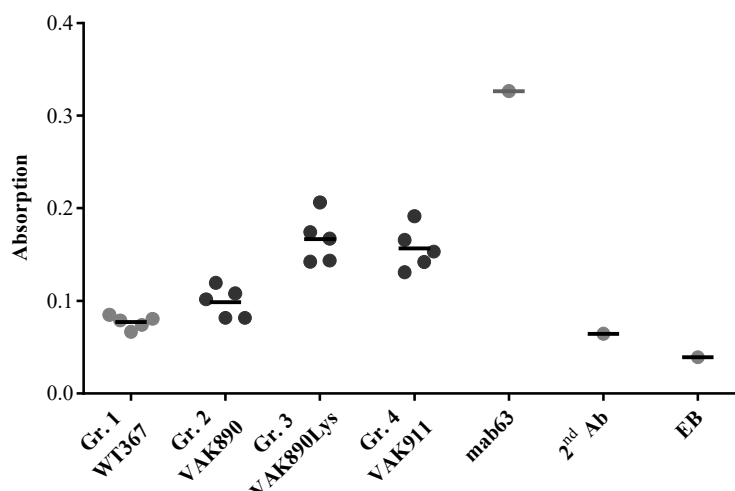


**Figure 4.** ELISA results of AT 12: The absorption was determined as parameter for the immune response in mice against intact VAK890, lysated yeast material VAK890, optimised VAK911 and antigen free yeast WT367. ELISA buffer (EB), mab63 and 2<sup>nd</sup> antibody were examined as controls for the ELISA. The exact group arrangement is explained in Table 7.

**Table 7.** Group arrangement and immunisation conditions of AT12, investigating lysated yeast vaccines and an optimised yeast strain.

Group	Yeast	Adjuvant	Amount	Schedule	Processing
1	WT367	CFA/IFA/IFA	3x 0.1 mg	2-2-1	Standard
2	VAK890	CFA/IFA/IFA	3x 0.1 mg	2-2-1	Standard
3	VAK890 Lysate	CFA/IFA/IFA	3x 0.1 mg	2-2-1	Glass bead disruption
4	VAK911	CFA/IFA/IFA	3x 0.1 mg	2-2-1	Standard

All mice treated with VAK911 or lysated VAK890 reacted on the applied vaccine formulation with good antibody titres, there were no nonresponders. In contrast, the intact VAK890 group showed only a slight immune response, compared to the wild type yeast WT367 without a VP2 antigen. Two mice did not react on VAK890. The higher antigen amount in VAK911 caused an increased antibody production against VP2. The VP2 concentration in VAK911 was twofold higher than in VAK890. A high

antigen amount is a key parameter for a strong immune response [47,143]. Nevertheless, the aim was to reach a sufficient immune response with the lowest possible amount of antigen, as this provides fast and economic antigen production. Lysated VAK890 showed a massive increase in the antibody titres compared to the intact yeast cells. The antibody response was at the same level as the optimised strain VAK911. This result indicated that there is an effect of the cell disruption, although the mechanism was not investigated in this experiment. It could lead to a reduction of the applied amount of VAK911. The stability of the lysated samples have been ensured by the fresh preparation of the samples and confirmed retrospectively by SDS-PAGE and western blot. Nevertheless, stability experiments with lysated cells indicated a lower stability of disrupted yeast vaccines in aqueous suspensions and freeze-dried powders, making lysated cells as market product questionable.

The animal trial AT14 was performed to evaluate the effect of disrupted cells and to understand the mechanism of the improved immune stimulation. The massive increase in the antibody titres by disruption could be an effect of better accessibility to the yeast encapsulated antigen or due to higher immunogenicity resp. an adjuvant effect of the disrupted yeast cells. Adding lysated antigen free WT367 to VAK911 was chosen to investigate the influence of an adjuvant effect of disrupted cells. Trials with intact and treated VAK911 were performed to check the effect of a promoted antigen release.

The comparison of intact and disrupted VAK911 had no influence on the antibody response in this experiment, as shown in Figure 5. On the other hand, additionally added lysated VAK367 decreased the immune response. All groups resulted in responding mice. However, large deviations between the individual mice within the groups have to be taken in account. A final statement about the effect and mechanism was not possible from AT14.

Concluding the results of AT12 and AT14, together with results performed with BVDV E2, two main factors for an increased immune response by lysated cells emerged. Yeast with a relative low antigen amount which was not able to induce a sufficient immune response in intact cells and yeasts with rigid cell walls benefited from the lysis. An upper limit in the dependency between antigen amount and antibody titre was reached in the immunisation trials with IBDV VP2 in VAK911. An additional adjuvant effect of lysated yeast cells to the adjuvant effect of the intact cells could not be confirmed. The

investigations of sonicated yeasts in group 5 belongs to the yeast cell disaggregation experiments and are discussed in Chapter 4.1.2.

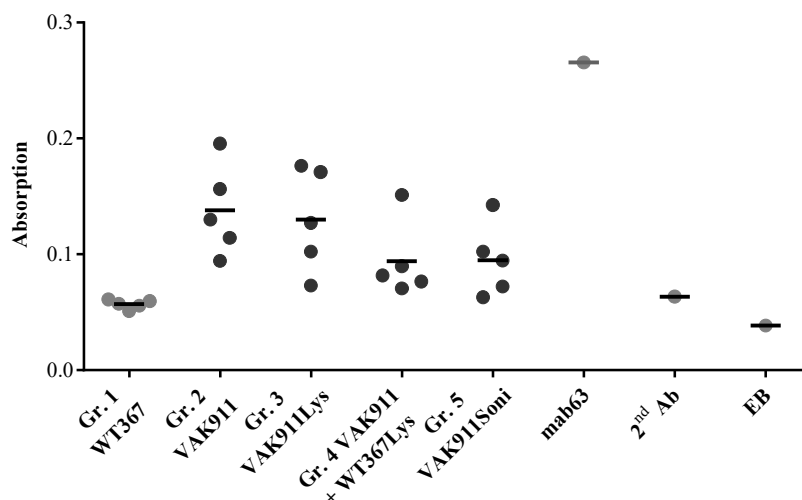


**Figure 5.** ELISA results of AT14: The absorption was determined as parameter for the immune response in mice against VAK911, lysated yeast material VAK911, intact yeast material VAK911 containing lysated WT367, VAK911 treated by ultrasonication and antigen free yeast VAK367. ELISA buffer (EB), mab63 and 2<sup>nd</sup> antibody were examined as controls for the ELISA. The exact group arrangement is explained in Table 8.

**Table 8.** Group arrangement and immunisation conditions of AT14, investigating lysated yeast vaccines and particle size effects.

Group	Yeast	Adjuvant	Amount	Schedule	Processing
1	WT367	CFA/IFA/IFA	3x 0.1 mg	2-2-1	Standard
2	VAK911	CFA/IFA/IFA	3x 0.1 mg	2-2-1	Standard
3	VAK911	CFA/IFA/IFA	3x 0.1 mg	2-2-1	Glass bead disruption
4	VAK911 WT367	CFA/IFA/IFA	3x 0.1 mg 3x 0.1 mg	2-2-1	Standard Glass bead disruption
5	VAK911	CFA/IFA/IFA	3x 0.1 mg	2-2-1	Sonication 2 min 15 W

## 4.1.2 Yeast Cell Disaggregation

### 4.1.2.1 Process Optimisation and Size Determination

The processed and resuspended yeast vaccines showed aggregates of several yeast cells instead of single cells. As the recognition of immunogens is dependent on the particle size, it was the aim to achieve a specific size distribution of the yeast material by disaggregation [40]. Furthermore, smaller particles were necessary to incorporate them into microparticles for adjuvants formulations with a sustained antigen release to replace the initial and booster injections by just one immunisation. *Kluyveromyces lactis* is growing as budding yeast, meaning that during the asexual replication the daughter

cell buds from the mother cell [144]. In the following, the cells do not exist as single cells, but are sticking closely together. Furthermore, the clumping could be caused by the processing of the fermented yeast. Especially during centrifugation and heat inactivation at 90°C for 2 h, they could stick together. The single yeast cells should remain intact, as they provide a stable compartment, due to their rigid cell wall. Although many mechanical and chemical methods are known from daily routine, only ultrasonication is used standardly to disaggregate cells [145]. Neither EDTA, citric acid, sodium chloride nor acidic and basic pH conditions had a positive effect to singularize the cells. Applying mechanical forces with the high-revving stirrer Ultra-Turrax T18 and SilentCrusher did not disaggregate the yeast cells. High pressure homogenisation on an Avestin EmulsiFlex-C5 had no influence on the particle size, but cracked yeast cells at higher homogenisation pressures. The only successful disaggregation method was ultrasonication on a cell disrupter (Branson Sonifier 250, Emerson, St. Louis, USA).

The disaggregation experiments were performed with 2 mg/ml to 30 mg/ml yeast at sonifier output powers of 10-20 W. Different yeast concentrations had no influence on the size distribution and on the process time.

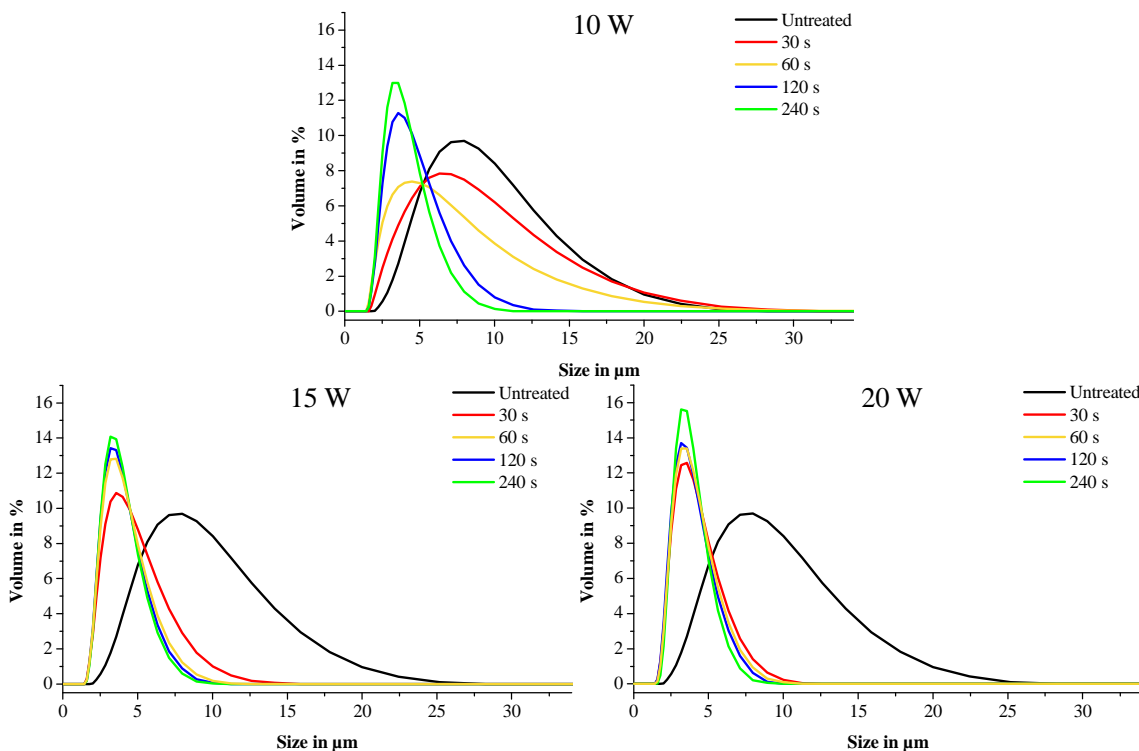


**Figure 6.** Impact of the ultrasonication power and time on the particle size distribution of yeast. Sonication powers of 10 W, 15 W and 20 W were applied for 30 s, 60 s, 120 s and 240 s.

The time and power dependent effect of the disaggregation is shown in Figure 6. Especially the lowest output power of 10 W showed a strong time dependent effect. While the median of the particle size changed from 7.2  $\mu\text{m}$  to 6.1  $\mu\text{m}$  after 30 s of sonication, the  $D_{(0.9)}$  value remained around 12.5  $\mu\text{m}$ . Longer application times up to 4 min led to a size distribution of 3.3  $\mu\text{m}$  in median and 5.3  $\mu\text{m}$  in  $D_{(0.9)}$ , which were comparable with the shortest treatment of 30 s at the highest output power. Nevertheless, with the lowest power it was not possible to reach a narrow size distribution as with the high output power. After 30 s treatment at 20 W, the size distribution was comparable with the treatment of 10 W after 240 s. Longer application times at 20 W had nearly no influence on the particle size distribution. In the following, they were mainly performed as stress conditions to investigate the stability during ultrasonication. At 15 W there was a size dependency between 30 s and 60 s, decreasing the  $D_{(0.9)}$  from 6.4  $\mu\text{m}$  to 5.4  $\mu\text{m}$ . Conditions with an output power of 15 W for 1 min resulted in the desired and uniform size distribution of the yeast cells.

Microscopic investigations of the untreated yeast proved the occurrence and dominance of larger particle aggregates from 20  $\mu\text{m}$  to 80  $\mu\text{m}$ . After sonication, mainly single cells, dimers and trimers were present in the microscopic view (Figure 7 right). Dimers and trimers originated from replicating cells.

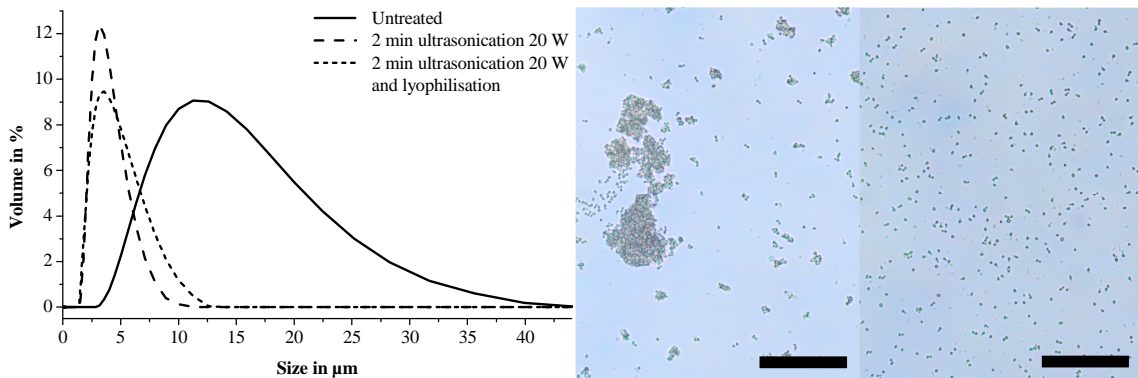


**Figure 7.** *Left: Size distribution of yeast after ultrasonication with 20 W for 2 min, untreated yeast material and resuspended yeast after ultrasonication and lyophilisation. Right: Microscopic view of untreated yeast in water and after sonication for 2 min with 20 W. Scale bars represent 100  $\mu\text{m}$ .*

From the microscopic view, the cells remained intact and their vitality was confirmed by a methylene blue stain. To enable long time storage of the disaggregated cell material, it was lyophilised after sonication. The resuspended sonified and lyophilised material did not show reaggregation tendencies. Nevertheless, the  $D_{(0.9)}$  value increased

slightly from 5.8  $\mu\text{m}$  to 6.6  $\mu\text{m}$ . The  $D_{(0.1)}$  and  $D_{(0.5)}$  values remained constant at 2.1  $\mu\text{m}$  and 3.3  $\mu\text{m}$ , confirming that the lower limit was the single yeast cell.

#### 4.1.2.2 Cell Wall Integrity - Beta-Galactosidase Assay and VP2-Detection

Ultrasonication is a frequently used procedure to crack cells, especially for bacteria like *E. coli* [146]. Due to their more rigid cell wall structure, yeast cells are known to be more stable against ultrasonication [136]. The activity of beta-galactosidase was used as a surrogate parameter to evaluate the integrity of the cell wall. Beta-Galactosidase is expressed in the cells of *K. lactis*, if it is grown on lactose, to make it available as nutrient [147,148]. Already small cracks in the cell wall and membrane make the enzyme accessible for the substrate OPNG. Therefore, the released enzyme activity can be linked directly to the amount of damaged cells. Especially for long term storage, an intact cell wall was required as natural barrier for stability reasons.

VAK911 was grown on YP medium containing 2 % lactose overnight up to an optical density of 7.76. After harvesting and washing, it was resuspended in beta-Gal buffer. The yeast was treated with a Branson Sonifier 250 for 0.5; 1; 2 or 4 minutes with an output power of 15 W or 20 W. The enzyme activity was measured in the buffer after centrifugation for 10 min at 1000 rpm and 4°C. The activity was measured in untreated yeast as control group and in lysated yeast after sonication at 20 W to determine the remaining activity.

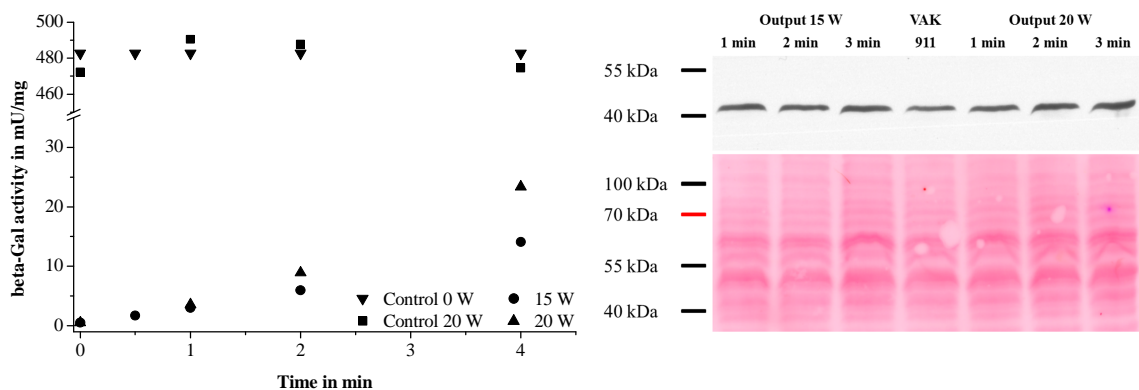


**Figure 8.** Left: Beta-Galactosidase activity vs. sonication time and power. The beta-galactosidase activity was determined in the supernatant of sonicated yeast cells (20 W upright triangles and 15 W circles) and after cell lysis of sonicated yeast (20 W squares) and lysated control yeast (reversed triangles). Right: Western blot for VP2 detection after ultrasonication and Ponceau S stain for the semi-quantitative protein load verification.

Ultrasonication led only to minor damage of the cell wall and release of beta-galactosidase. Both, increased power and longer application time, resulted in higher

enzyme activities outside the cells, as shown in Figure 8. The standard procedure with 2 min sonication at an output power of 15 W released 1.25 % of the enzyme. Also the most stressing conditions with 4 min at 20 W caused only damage on 5 % of the cells. After treatment with 20 W, the remaining enzyme activity in lysated samples resulted in no decrease of the enzyme activity. This indicated that the sonication itself just cracked a very small amount of yeast cells.

To evaluate the stability of VP2 after sonication, 1 ml with 30 OD units of the treated yeast were harvested by centrifugation for 5 min at 5000 rpm and 5°C. The samples were prepared for SDS-PAGE and western blot as described in the method section. The primary antibody  $\alpha$ -IBDV was used in 1:6000 dilution. Sonication had no influence on the protein stability. All sonicated samples, up to most stressing conditions of 20 W and 4 min application time, contained the same level of VP2 as the control group of untreated VAK911. A Ponceau S stain proofed the load of the same amount of overall protein. Additional, a part of the sonicated samples was plated to check the viability of the sonicated samples. The plated volume was calculated to contain around 100 CFU before ultrasonication and was incubated for 48 h at 30°C. No single sample showed a decrease in their viability. Instead the amount of CFU increased by ongoing sonication up to 200 CFU. Untreated yeast existed as association of some single cells, but they were just counted as one CFU on the agar plate. After disaggregation, smaller aggregates or even single cells could be counted. The number of cells in all samples was constant, just their recognition differed. All samples were treated and plated at the same time to prevent from potential differences by reproduction of the yeast.

The results of the stability tests concluded that there was no negative effect of the sonication on the cell viability, the integrity of the cell membrane and the VP2 antigen. From literature, a much higher energy intake is known to crack yeast cells [149,150]. Operating between 120 W and 600 W resulted in a time and power dependent size decrease and protein release of *Saccharomyces cerevisiae*. The lowest energy intake of 120 W for 3 min released less than 10 % protein, correlating with the cracked cell amount [149].

### **4.1.2.3 Immunisation Trials in Mice**

The results of the immunisation trial with disaggregated yeast cells were carried out together with the investigation of lysated yeast cells in AT14. The results and exact conditions are given in Figure 5 and Table 8, respectively. The sonicated yeast samples were prepared directly before the applications under controlled conditions on ice with 15 W sonication for 2 min at a Branson Sonifier 250 (Emerson, St. Louis, USA).

Although ultrasonication did not affect the stability of VP2 and did not crack the cells, the antibody titres of sonicated VAK911 were lower. The immune response of the sonicated samples differed drastically between the single mice. While one animal reacted with good antibody titres to the sonicated yeast, two other mice showed only an intermediate antibody response. Two mice showed only minimal immune reaction to the disaggregated yeast material. However, the large deviations of the antibody titres in all investigated groups did not permit conclusions about a lower immune reaction. Altogether, it was concluded that the sonic treatment was not able to increase the immune response. For the development of lipid based controlled release formulations of the yeast vaccines, small and specified size distribution of the yeast material was a main requirement.

## **4.1.3 Alternative Inactivation Methods**

### **4.1.3.1 Inactivation and Antigen Verification**

The standard inactivation method of the lyophilised yeast material with dry heat at 90°C for 2 hours was introduced by Marina Arnold [104]. The heat treatment did not degrade VP2 and the yeast material could induce antibodies in immunisation studies [104]. Subviral particles of VP2 were described as stable in 20 % ethanol and 20 % dimethyl sulfoxide as well within a pH range from pH 2.5 to pH 9 [151]. Although the heat stability of VP2 is contradictive in aqueous suspension, VP2 subviral particles remained stable up to 60°C VP2 [151,152]. Due to the partial stability against heat, steam sterilisation at 121°C and dry heat at 160°C, 170°C and 180°C were tested as described in the pharmacopoeia. Additional, gamma irradiation on dry ice was tested as gentle alternative inactivation and sterilisation method. As the fermented yeast material fully consisted of microorganisms, it was distinguished between inactivation and sterilisation in accordance with the pharmacopoeia. D10 values up to 2.7 kGy were reported for the gamma sterilisation of yeast, meaning that each dose of 2.7 kGy kills 90 % of the

remaining living yeast cells [153,154]. A dose of 25 kGy would affect a survival rate of  $10^{-9}$  which was not sufficient to reach a security assurance level of  $10^{-6}$  for assumed  $10^8$  yeast cells per vaccine dose. As it was not possible to follow the applied dose of gamma irradiation in real-time, dose ranges of 25-33 kGy and 50-60 kGy were chosen. The exact applied dose was confirmed dosimetrically with 28.0 kGy for the 25 kGy group and 53.6 kGy for the 50 kGy group. The gamma irradiation was performed on lyophilised yeast material on dry ice, as these were the gentlest conditions for proteins [155].

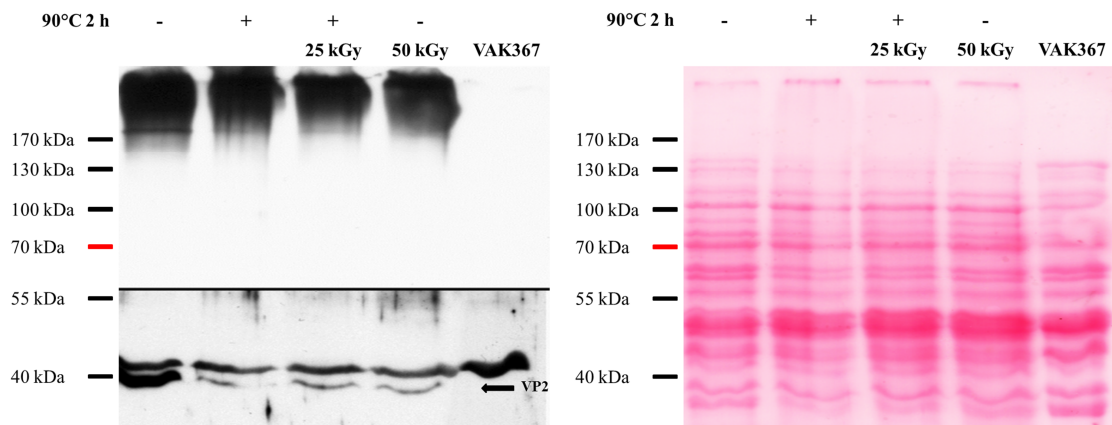


**Figure 9.** Left: Western blot of the VP2 detection of untreated, heat inactivated ( $90^{\circ}\text{C}$  2 h), heat inactivated and gamma radiated ( $90^{\circ}\text{C}$  2 h and 25 kGy) and gamma radiated (50 kGy) VAKJS27. Antigen free WT367 is given as negative control. Right: Ponceau S stain for the semi-quantitative protein load verification.

All sterilisation experiments with dry heat between  $160^{\circ}\text{C}$  and  $180^{\circ}\text{C}$  led to a complete degradation of all proteins. Steam sterilisation caused notable degradation on VLPs, VP2 and all other cellular proteins. Gamma sterilisation was more suitable. The results of the inactivation experiments with the standard procedure and gamma irradiation are shown in Figure 9. Although there was a decrease of the VP2 band around 40 kDa by the heat inactivation at  $90^{\circ}\text{C}$ , the VLPs above 170 kDa remained unchanged. The formation of VLPs with a diameter of 23 nm of IBDV-VP2 was described in the literature [156]. Because of the size and structure of VLPs, they are able to mimic the virus and represented the main immunogenic fraction. Thus, they provide an excellent adjuvant itself, as they are recognised by the immune system as virus [45].

Applying additional 25 kGy gamma irradiation to the heat inactivated yeast vaccine VAKJS27 or just applying 50 kGy to lyophilised yeast did not decrease the VP2 content. Although the final adjuvant formulation could be sterilised by steam

sterilisation, the gamma irradiation provided the possibility to sterilise the freeze-dried adjuvant formulation and yeast vaccine by gamma irradiation in the final containers.

#### 4.1.3.2 Immunisation Trials in Mice

The influence of gamma irradiation as inactivation and sterilisation method was examined on the immunogenicity. After the lyophilisation, the yeast material was inactivated at 90°C for 2 hours as standard procedure. To assure sterility, with a security assurance level of  $10^{-6}$  as requested by the European Pharmacopoeia, 25 kGy gamma irradiation was applied to inactivated material (group 4). Applying 50 kGy was used to inactivate and sterilise the yeast material in one step.

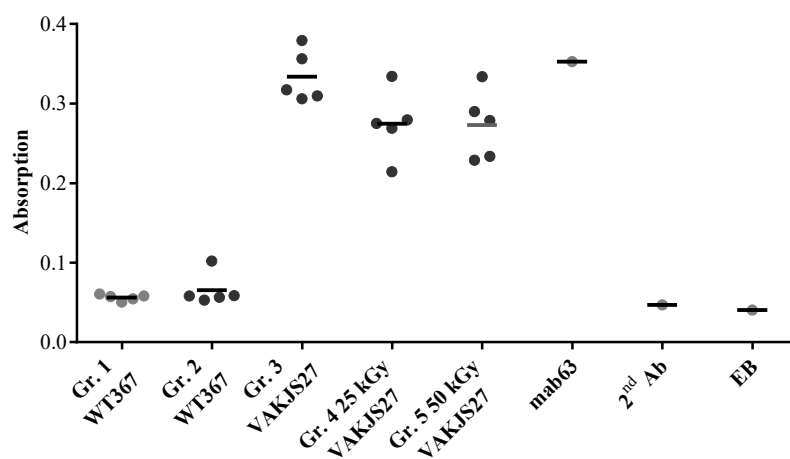


**Figure 10.** ELISA results of AT18: The absorption was determined as parameter for the immune response in mice against heat inactivated (90°C 2 h), heat inactivated and gamma radiated (90°C 2 h and 25 kGy), gamma radiated (50 kGy) VAKJS27 and antigen free yeast WT367. ELISA buffer (EB), mab63 and 2<sup>nd</sup> antibody were examined as controls for the ELISA. The exact group arrangement is explained in Table 9.

**Table 9.** Group arrangement and immunisation conditions of AT18, examining the effect of gamma irradiation. \* Serum samples of group 2 were added from AT17, as WT367 was examined in AT18 without adjuvant (group 1).

Group	Yeast	Adjuvant	Amount	Schedule	Processing
1	WT367	no	3x 1 mg	2-2-1	Standard
2*	WT367	AddaVax™	3x 1 mg	2-2-1	Standard
3	VAKJS27	AddaVax™	3x 1 mg	2-2-1	Standard
4	VAKJS27	AddaVax™	3x 1 mg	2-2-1	Additional sterilisation with 25 kGy
5	VAKJS27	AddaVax™	3x 1 mg	2-2-1	Inactivation with 25 kGy Sterilisation with 25 kGy

The radiated samples were investigated in an immunisation trial with the 10-fold dose of yeast and adjuvanted with AddaVax™. Sera of an AddaVax™ adjuvanted negative control group with WT367 was added as control group from AT17, as the WT367 group was applied without adjuvant in AT18. Independent of the inactivation method, all vaccinated animals have shown a strong immune response. As determined by SDS-PAGE and western blot, gamma irradiation caused a decrease in the antigen amount. Although the immunogenic VLP fraction remained nearly unchanged, the decreased antigen amount led to lower antibody titres, compared with the standard heat inactivation. The results are given in Figure 10 and indicated that the antibody production against IBDV was not dependent on the irradiation dose. According to the small group size and the large deviations in the groups, the results should be interpreted carefully.

The adjuvant effect of the yeast itself is discussed in detail in Chapter 4.1.1. A major fact is the exposure of  $\beta$ -1,3-glucans on the yeast surface. Heat treatment at 65°C for 1 hour is known to promote exposure of  $\beta$ -1,3-glucans on *Kluyveromyces lactis* and *Saccharomyces cerevisiae*. Additional, it has been demonstrated an enhanced production of reactive oxygen species in blood phagocytes after treatment with heat treated yeast, as important pathway in the antifungal response. In an immunisation trial with *Saccharomyces cerevisiae* and *Pichia pastoris*, carrying pp65 of the human cytomegalovirus, Bazan *et al.* found a massive activation of pp65-specific CD4<sup>+</sup> and CD8<sup>+</sup> T-lymphocytes by  $\beta$ -1,3-glucan exposed yeast [157]. Comparing heat inactivated and with 25 kGy radiated yeast in group 4 with the 50 kGy radiated yeast in group 5 made a heat stimulating effect improbable in the experimental setting. The effect could also be caused by a similar effect of gamma irradiation or an overcompensation of the stimulating effect of glucans by the used adjuvants.

## 4.2 Test of Commercial Adjuvants

The immune stimulating effect of adjuvants is dependent on the animal species and the antigen [34,49,112]. Although the Freund's Adjuvant is known as the gold standard [31], its use is limited, because of its bad biocompatibility [36]. To evaluate the adjuvant effect for further adjuvants development, CFA, IFA, Montanide ISA720 VG and AddaVax™ were tested in mice using VAK911 as vaccine formulation. Additional, the effect of the antigen amount was investigated with the 10-fold dose of VAK911.

All adjuvants have stimulated the antibody formation against IBDV (Figure 11). In contrast, the control yeast WT367 did not induce antibody formation, as it was antigen free. AddaVax<sup>TM</sup>, Montanide ISA720 and CFA (boosts with IFA) showed a good and comparable antibody response against IBDV. Increasing the antigen amount by a factor of 10 strengthened the immune reaction dramatically. Although it is a possible principle to reach sufficient high antibody titres, this strategy was unfavoured because of the production cost and production time of the antigen. Each single animal in these groups has shown an immune reaction. In contrast, the immunisation with incomplete Freund's Adjuvant caused a lower immune response, whereby two animals had an antibody response at the level of the antigen free yeast WT367.

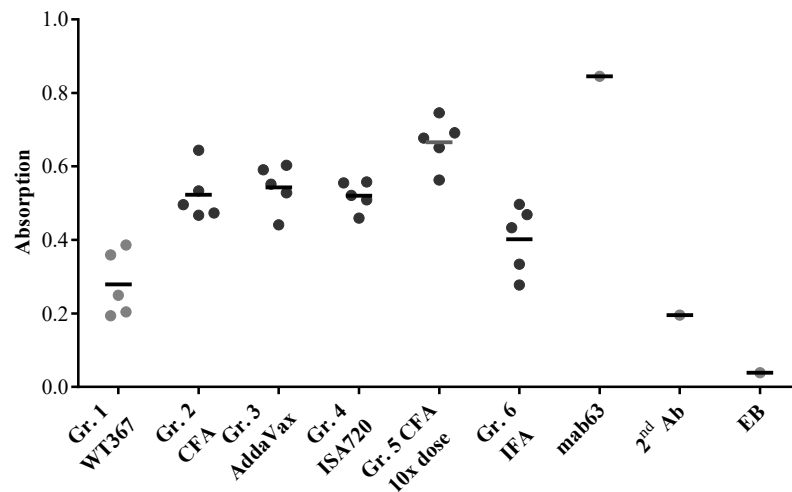


**Figure 11.** ELISA results of AT16: The absorption was determined as parameter for the immune response in mice against VAK911, adjuvanted with CFA, AddaVax<sup>TM</sup>, Montanide ISA720 VG and IFA, and a 10x dose VAK911 in comparison to the response against WT367. ELISA buffer (EB), mab63 and 2<sup>nd</sup> antibody were examined as controls for the ELISA. The exact group arrangement is explained in Table 10.

**Table 10.** Group arrangement and immunisations conditions of AT16, comparing the immune stimulating effect of commercially available adjuvants and the antigen dose effect.

Group	Yeast	Adjuvant	Amount	Schedule	Processing
1	WT367	CFA/IFA/IFA	3x 0.1 mg	2-2-1	Standard
2	VAK911	CFA/IFA/IFA	3x 0.1 mg	2-2-1	Standard
3	VAK911	AddaVax <sup>TM</sup>	3x 0.1 mg	2-2-1	Standard
4	VAK911	Montanide ISA720 VG	3x 0.1 mg	2-2-1	Standard
5	VAK911	CFA/IFA/IFA	3x 1.0 mg	2-2-1	Standard
6	VAK911	IFA/IFA/IFA	3x 0.1 mg	2-2-1	Standard

The initial immunisation with complete Freund's Adjuvant was important to induce a strong antibody response. Nevertheless, the good adjuvant activity of CFA was associated with bad biocompatibility. The Freund's Adjuvant, especially the CFA, caused severe irritation, inflammation and hair loss at the injection side after some days. The side effects progressed during the experiment, until the animals were sacrificed at the end of the experiment. In contrast to the best compatible adjuvant AddaVax™, CFA was a water in oil emulsion instead of an oil in water nanoemulsion and its lipid amount was 20-fold higher than the squalene amount. Furthermore, paraffin is neither biodegradable nor biocompatible and it is known to cause granulomas and ulcers at the injection side [36]. Killed *Mycobacteria tuberculosis* in the complete Freund's Adjuvant can further promote the irritations. Montanide ISA720 remained at the injection side like Freund's Adjuvant because of its lipophilic composition. Despite the remaining squalene volume, it showed no signs of irritation, as squalene is biocompatible and occurs in the body as precursor of cholesterol and in the skin [54,158]. The squalene nanoemulsion AddaVax™, its composition is also known as MF59®, was the best biocompatible adjuvant. Within two days, the injected vaccine was fully absorbed without showing any signs of irritation. Despite the low injected squalene amount (2.15 mg) it could be distributed by the lymphatics because of its size in the nanometre range [159]. MF59® has been approved in 1992 and has shown its excellent biocompatibility with several millions of applied doses in humans [60]. Because of the excellent compatibility and strong adjuvant effect of squalene, especially of the nanosized squalene emulsion AddaVax™, it was focused on squalene containing nanoparticles for the further adjuvants development. Furthermore, AddaVax™ was selected as standard adjuvant for further immunisation studies.

## 4.3 Development and Characterisation of Nanoscaled Adjuvant Systems

### 4.3.1 Formulation Development and Evaluation of Critical Processing Parameters

As described previously, MF59<sup>®</sup> is a well characterised and established adjuvant system. Several million doses of MF59<sup>®</sup> and other nanosized squalene formulations have been used successfully since 1992 [60]. Following, the goal for all developed formulations was to formulate squalene in the nanometre range. The formulation JS-1 was composed of the same ingredients as MF59<sup>®</sup>. It was used as control to compare the immune stimulating effects and to reveal possible contaminations during the preparation process, for example with pyrogens, due to the impossibility of an aseptic preparation in the high pressure homogeniser. Derived from JS-1, the lipophilic emulsifier Span 85 was substituted by mannide monooleate to obtain JS-4. Mannide monooleate is known for its immunostimulatory effect itself. It is part of several adjuvant systems, including the gold standard for adjuvants Freund's Adjuvant and Montanide ISA720 VG [31,160,161]. Span 85 and mannide monooleate are both non-ionic water in oil emulsifiers with HLB values of 1.8 for Span 85 and 4.3 for MMO, differing in the degree of esterification with oleic acid and in the stereo chemistry of their hydrophilic part. Both emulsifiers derived from sugar alcohols.

The aim of the development in the formulation JS-2 was the parallel use of the adjuvant effects of squalene and saponins. Crude saponin derived from the bark of *Quillaja saponaria*. Its purified forms Quil A and QS-21 were used as adjuvants [162]. The application of crude saponins and Quil A was limited, because of their bad biocompatibility. Together with phosphatidylcholine and cholesterol they form cage like structures around 40 nm. These ISCOMs (immune stimulating complexes) were approved for equine influenza and showed reduced toxic effects in comparison with the unformulated saponin fractions [90]. Further purification of the crude saponins to QS-21, with a comparable adjuvant effect, and formulation with liposomes and monophosphoryl lipid A led to the adjuvant system AS01, which was approved in the malaria vaccine Mosquirix [48].

Aim for the formulation JS-3 and its improved form JS-3o was to develop solid lipid nanoparticles containing squalene. Solid particle suspensions have the possibility to be transformed into powder by drying. The transformation into a dry powder is expected to increase the storage stability and reduces the shipping cost and storage volume. For the yeast vaccine, dried and inactivated yeast powder is the preferred and most stable storage form. Thus, a ready to use formulation, by just adding water for injection, composed of antigen, adjuvant, buffer and isotonicating agents should be developed. Nanostructured lipid carriers of a lipid mixture of squalene and cetylpalmitate, stabilised with soybean phosphatidylcholine and Poloxamer 188, have already been developed by Lin *et al.* The lipid particles with a size of 200-260 nm were developed for the dermal delivery of diphencyprone [163]. Similar lipid particles have been developed for the topical psoralen therapy and as drug carrier system for breast cancer [164,165].

**Table 11.** *Composition of the final squalene containing nanosized formulations JS-1 – JS-4.*

<b>Formulation</b>	<b>Emulsifier A</b>	<b>Emulsifier B</b>	<b>Lipid</b>
<b>JS-1</b>	0.5 % Tween 80	0.5 % Span 85	4.3 % Squalene
<b>JS-2</b>	0.125 % Saponin	0.25 % Lecithin S100	4.3 % Squalene
<b>JS-3</b>	0.5 % Tween 80	0.5 % Span 85	1.375 % Softisan 154 1.375 % Squalene
<b>JS-3o</b>	5 % Poloxamer 188		5 % Softisan 154 5 % Squalene
<b>JS-4</b>	0.5 % Tween 80	0.5 % MMO	4.3 % Squalene

The first step of the emulsions preparation was the preparation of the preemulsions with an Ultra-Turrax<sup>®</sup>. High speed rotor stator mixers are known for the production of nanoparticles and nanoemulsions [166,167]. Nevertheless, the preemulsions had size maxima in the lower  $\mu\text{m}$  range. Except the preemulsions for JS-1 and JS-4, they were not stable for a longer time. Additional homogenisation steps of the preemulsion on an EmulsiflexC5 high pressure homogeniser achieved the size of the market product AddaVax<sup>™</sup>. The homogenisation experiments have shown that there is no change in the size distribution of all formulations after five homogenisation cycles at constant homogenisation pressures. In the following, all homogenisation experiments were carried out with five cycles at each selected pressure.

### Development of JS-1 and JS-4

As JS-1 was a replica of AddaVax<sup>TM</sup>, its composition was given. Tween 80 was replaced by MMO to get JS-4. Because of the similarity of both emulsifiers, there was no need to change the emulsifier concentration. The development of these formulations was limited to the optimisation of the production process. Both squalene emulsions behaved similar during the homogenisation process. Already stirring with an Ultra-Turrax<sup>®</sup> at 20000 rpm for 5 min resulted in a stable emulsion between 1  $\mu\text{m}$  and 20  $\mu\text{m}$  (Figure 12). The application of low homogenisation pressures of 600 bar was sufficient to obtain a nanoemulsion, although there was still a considerable fraction larger than 400 nm. Further increase of the homogenisation pressure resulted in a smaller particle size and narrower size distribution. Although a pressure of more than 1200 bar had just minor effects, larger particles were fully removed at 1800 bar and resulted in the best size distribution.

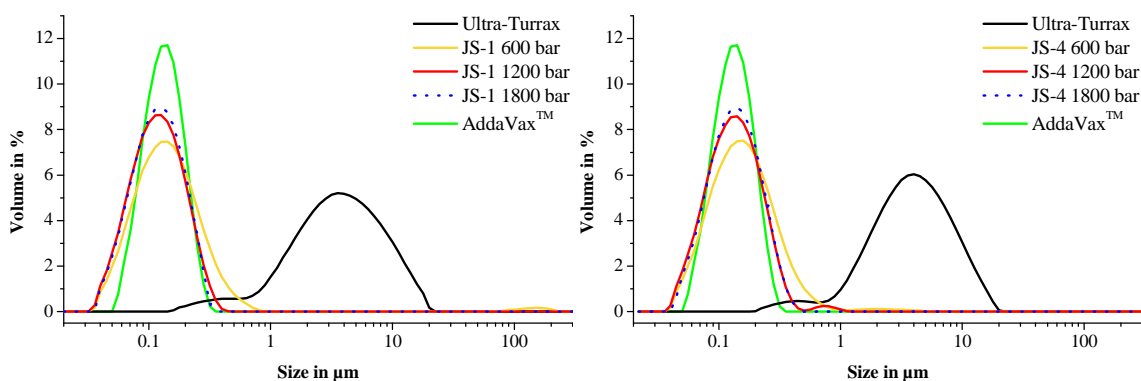


**Figure 12.** Influence of the homogenisation pressure on the particle size distribution of JS-1 (left) and JS-4 (right).

### Development of JS-2

The aim of developing a stable squalene nanoemulsion, using saponin as stabiliser, interfered with the high toxicity of *Quillaja* saponins. There were several publications about the LD<sub>50</sub> values of saponin and its purified subfractions Quil A and QS-21. A LD<sub>50</sub> dose of 50 mg/kg bodyweight has been reported for Quil A, corresponding 1 mg for a mouse of 20 g [168]. Even *et al.* incorporated 100  $\mu\text{g}$  of Quil A into lipid implants for controlled antigen release in mice and observed no side effects [37]. The use of purified fractions like Quil A or QS-21 is preferred, because of the higher toxicity of crude saponins. Injecting 200  $\mu\text{g}$  crude *Quillaja* saponin extract (Spikoside) in mice killed 6 of 10 mice [90]. As saponins can stimulate the immune response in mice at

concentrations below 1  $\mu\text{g}$ , aim of the development was a stable formulation with the lowest possible amount of saponin [169].

The saponin containing emulsions were not producible in the standardly used 10 mM sodium citrate buffer. Even adding citrate to the prepared emulsion caused an immediate increase in the particle size. Citrate is known to act as a peptisator, meaning it can overcompensate the Nernst potential. The assumed effect is discussed in detail in the zeta potential section. In initial experiments, the hydrophilic emulsifier Tween 80 of AddaVax<sup>TM</sup> was substituted by the same amount of saponin. Although this formulation accomplished the requirements stability and uniform size distribution (120-170 nm z-average), the saponin content had to be decreased, due to its high toxicity. Decreasing the saponin amount and substitution of Span 85 by lecithin were applied to reduce the toxicity. There were just minor influences on the size distribution of lecithin above a concentration of 0.25 %. Different from the preparation method of the other formulations, the lecithin was not dispersed in the aqueous phase. It was dissolved in the squalene at 65°C using an Ultra-Turrax<sup>®</sup> T10. The size and stability of the emulsion was mainly dependent on the saponin content. Decreasing the saponin content up to 0.05 % had dramatic influence on the particle size distribution and stability. At 0.05 % the z-average of 187 nm was above the required 120-170 nm of AddaVax<sup>TM</sup>. Increasing the concentration resulted in the desired size range of 155 nm at 0.125 % and 133 nm at 0.5 % saponin (Figure 13).

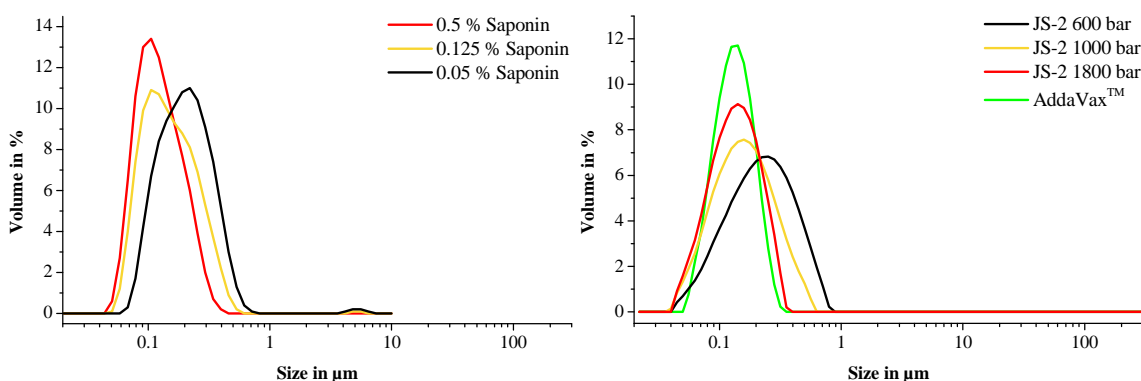


**Figure 13.** Influence of the emulsifier concentration at 1800 bar (left, PCS results) and the homogenisation regime (right, static light scattering) on the particle size distribution of JS-2.

It was possible to compensate the lower emulsifier amount by applying higher homogenisation pressures, whereas the lower stability could not be improved. A saponin amount of 0.125 % matched acceptable stability, toxicity and size distribution for initial animal experiments. In contrast to JS-1 and JS-4, a higher energy intake was

needed to get a nanoemulsion. Each increase in the homogenisation pressure up to 1800 bar resulted in a smaller and narrower size distribution. Increasing the homogenisation pressure from 1000 bar to 1800 bar changed the  $D_{(0.9)}$  value from 310 nm to 220 nm. For the most formulations 600 bar were often sufficient to acquire an acceptable size. In this case, a very broad distributed emulsion below 1  $\mu\text{m}$  was accomplished for JS-2, but it differed dramatically from the intended size range of AddaVax<sup>TM</sup>.

The low amounts of emulsifiers were made responsible for the necessity of high homogenisation pressures, as well for the instability and floating of the lipophilic phase of the initially prepared preemulsion of JS-2. Results of haemolysis tests showed that the addition of lecithin to saponin did not prevent from the haemolytic activity of saponins, like it is known for ISCOMs [90]. Nevertheless, as vaccine formulations are mainly applied subcutaneously or intramuscularly, the formulation was examined in animal experiments.

### **Development of JS-3 and JS-3o**

The preferred preparation method for the solid lipid nanoparticles was hot melt homogenisation. This standard method offered the possibility of a high scale production and did not need any organic solvent. As squalene was the immune stimulant in the formulation, the lipid phase should contain at least 50 % squalene to apply a sufficient squalene amount per injection. The solid lipids were selected because of their biocompatibility and their incorporation capacity of the liquid lipid. The melting point should be above the body temperature of 37°C but below 65°C to be processed in the EmulsiflexC5 homogeniser. Although Dynasan 114 (glycerol trimyristate) provided these requirements, it was withdrawn as solid liquid, because squalene was released under mechanical stress. In contrast to Dynasan 114, Softisan 154 provided a much better incorporation of the squalene. It was assumed that the high purity of glycerol myristate forced the squalene release during the crystallisation. As Softisan 154 consists of chains from C10 to C18, the crystal structure is less regular and can incorporate a liquid lipid. Softisan 154 fulfilled all requirements. It is biocompatible and chemical inert, due to its structure of saturated triglycerides. The mixture with squalene was homogeneous and solid up to a squalene concentration of 75 %.

For the solid formulation JS-3 it was necessary to decrease the lipid content to get a size distribution comparable to AddaVax<sup>TM</sup>. An acceptable size was reached with 2.75 % of the lipid mixture. Increasing the emulsifier concentration had just minimal effects on the size distribution. The emulsifying properties of Tween 80 are highly temperature dependent, due to the temperature dependent interaction of water with the polyethylene oxide part of Tween 80 via hydrogen bridge bonds. At the cloud point at 73°C, Tween 80 loses its emulsifying properties and precipitates [170]. Although it was not possible to mimic the size distribution of AddaVax<sup>TM</sup> with the formulation JS-3, 90 % of the particle volume was below 300 nm. Figure 14 shows the size dependency of the production conditions. The optimal homogenisation pressure was at 1000 bar. Above this pressure, there was no further size decrease. Contrary at high homogenisation pressures, the particle size distribution broadened and a residual in the lower  $\mu\text{m}$  range occurred. This behaviour was in contrast to the liquid squalene emulsions, where an increase in the homogenisation pressure always led to a narrower size distribution. This effect has already been described by Innocente *et al.* and was attributed to the coalescence of small particles in the homogenisation chamber directly after their disaggregation [171]. Lower pressures e.g. at 600 bar caused a second larger particle population around 150  $\mu\text{m}$ . Because of the size dependent solubility of nanoparticles, this could lead to massive instabilities by Ostwald ripening [172].

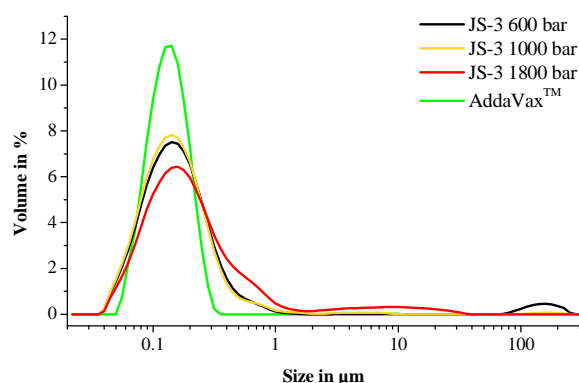


**Figure 14.** Influence of the homogenisation pressure on the particle size distribution of JS-3.

The change of the emulsifier to Poloxamer 188 resulted in a narrower size distribution and the possibility of higher lipid contents. The final formulation consisting of equal parts of each 5 % of Poloxamer 188, Softisan 154 and squalene had a similar size distribution like AddaVax<sup>TM</sup>. A ratio of 1 part emulsifier on 2 parts lipid has shown the best properties. Hot melt homogenisation with 10 % lipid and 5 % Poloxamer 188 resp. 4.3 % lipid and 2.5 % Poloxamer 188 at 1400 bar resulted in a size distribution like

AddaVax<sup>TM</sup> (Figure 15). The high emulsifier content of 5 % prevented from the formation of a second particle species around 1  $\mu\text{m}$ . This particle species occurred on higher homogenisation pressures and could be overcome by applying a final homogenisation step at low pressures. Although the size distribution of 2.5 % emulsifier and 10 % lipid was still acceptable, the  $D_{(0.9)}$  increased from 200 nm to 260 nm. Lower emulsifier contents, like 1.25 % Poloxamer, resulted in a very broad size distribution.

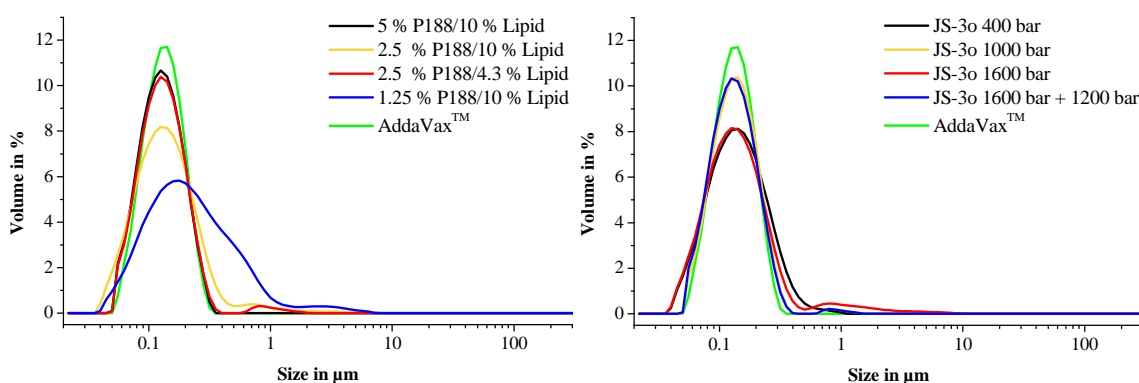


**Figure 15.** Influence of the lipid and emulsifier composition (left) and the homogenisation regime (right) on the particle size distribution of JS-3o.

The homogenisation regime had just minor influence on the formulation. As shown in Figure 15 right, already a low homogenisation pressure of 400 bar resulted in nanoparticles with a median of 130 nm. Applying higher pressures, with an optimum between 1000 bar and 1400 bar, narrowed the particle size distribution. A further increase broadened the size distribution at low particle size as well at larger particle sizes around 1  $\mu\text{m}$ . The addition of a final homogenisation step at lower homogenisation pressures removed the larger particles and generated the narrowest size distribution.

### 4.3.2 Lyophilisation and Sterilisation

Aim of the work was to develop ready to use formulations, consisting of the yeast vaccine, an adjuvant, buffers and further excipient e.g. for tonicity. Storage as dry powder was the most stable form of the yeast vaccine. Even at room temperature it was stable for several months. Therefore, the squalene containing solid lipid nanoparticle formulations JS-3 and JS-3o were the most promising ones to be dried. Lyophilisation is the method of choice for sensitive and heat instable material. After rapid freezing under the eutectic temperature, the ice will sublime without heating the sample by applying vacuum. Cryoprotectants were needed to protect the formulation from collapsing and to ensure good redispersibility. Especially polyalcohols and saccharides have been widely

used as cryoprotectants [173,174]. The investigations of the lyophilisation experiments were divided into the freezing and the lyophilisation process. Freeze thaw experiments were carried out to investigate the first necessary step of rapid freezing in liquid nitrogen. In the following, the formulation was thawed at room temperature and investigated macroscopically and by static light scattering.

Mannitol and trehalose are known as effective cryoprotectants for lipid nanoparticles [174]. Nonetheless, the exact behaviour is unpredictable. Mannitol, trehalose, sucrose and glucose have been tested in concentrations from 5 % to 15 %. The most promising results are given in Figure 16. Mannitol formed a non redispersible cake with both formulations in all investigated concentrations. Although the Tween 80 and Span 85 containing formulation JS-3 was fully redispersible without any cryoprotectant after freezing, the volume weighted median ( $D_{(0.5)}$ ) changed dramatically from 0.127  $\mu\text{m}$  to 6.54  $\mu\text{m}$ . Trehalose could improve the stability slightly, but even 15 % were not able to protect the formulation sufficiently. Glucose and sucrose had the same dose depending effect. More than 10 % of the saccharides had just minimal influence on the particle size than lower concentrations. The optimal concentration of 10 % broadened the size distribution ( $D_{(0.1)} - D_{(0.9)}$ ), but remained the mean particle size ( $D_{(0.5)}$ ).

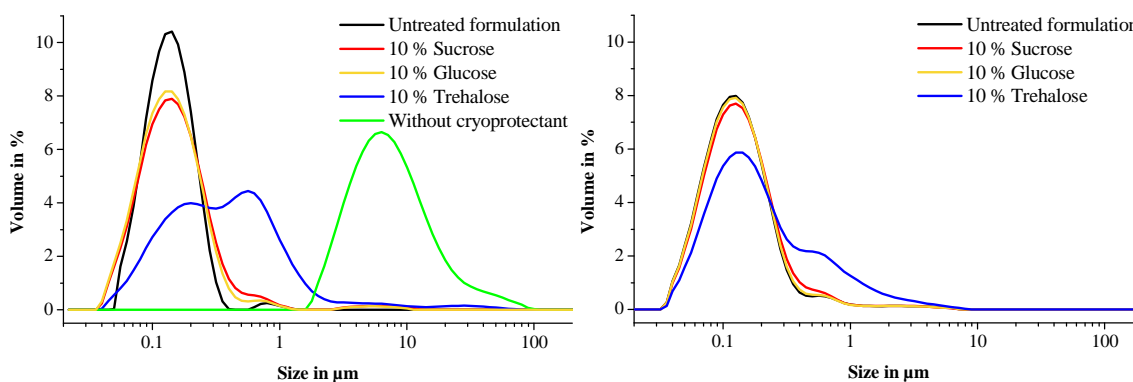


**Figure 16.** Freeze thaw experiments of JS-3 (left) and JS-3o (right). Influence of sucrose, glucose and trehalose as cryoprotectants on the particle size distribution.

The formulation JS-3o was not redispersible without a cryoprotectant. The addition of 10 % of glucose or sucrose led to no change in the particles size distribution after the freeze thaw cycle. There was no difference in the size distribution between the raw formulation and the freeze-thawed formulation with these cryoprotectants. In contrast, the gold standard trehalose was not able to fully protect the formulation from caking. The formulation aggregated at low concentrations of 5 % trehalose and higher concentration increased the droplet size ( $D_{(0.5)}$ ) remarkably from 131 nm to 179 nm.

Higher amounts of cryoprotectants could not improve the stability and were withdrawn, because of the higher tonicity of the redispersed samples. Further freeze drying experiments were performed for both formulations with glucose and sucrose as cryoprotectants.

Lyophilisation of JS-3 was not successful with the selected cryoprotectants. A bimodal size distribution around 0.1  $\mu\text{m}$  and 10  $\mu\text{m}$  occurred after lyophilisation (Figure 17). Although increasing amounts of sucrose stabilised the nanorange, it was not possible to get an acceptable result. About 45 % of the with 10 % sucrose stabilised particles were larger than 400 nm. In contrast to the freeze-thaw experiments, sucrose was superior to glucose and provided a smaller particle size after lyophilisation. It could be concluded that the liquid emulsifiers were not able to stabilise the redispersed solid nanoparticles. During the drying process the liquid emulsifiers, especially the hydrophilic Tween 80, adsorbed on the saccharides. When water was added, the emulsifiers were still interacting with the saccharides and could not stabilise the lipid nanoparticles. Furthermore, the relative low emulsifier concentration could not be sufficient to protect the particles.

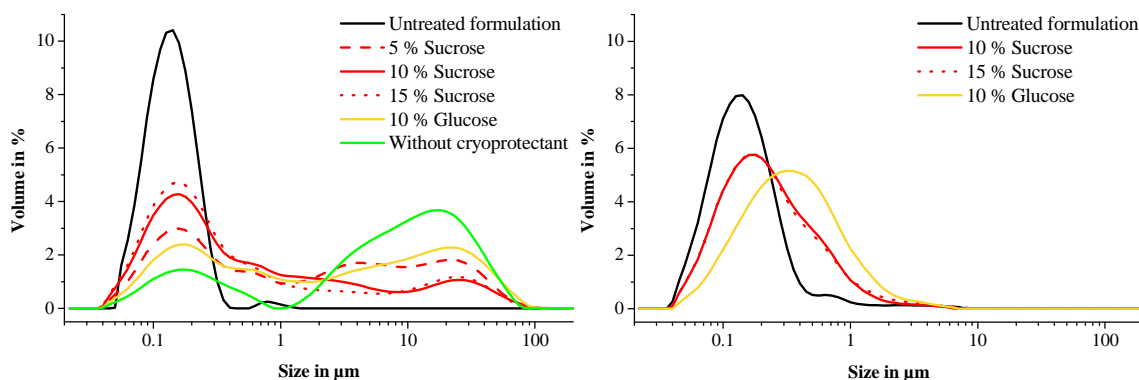


**Figure 17.** Influence of sucrose and glucose as cryoprotectants on the particle size distribution after lyophilisation of JS-3 (left) and JS-3o diluted to 2.5 % lipid (right).

It was not possible to redisperse the Poloxamer 188 containing formulation with 10 % lipid with any cryoprotectant after lyophilisation. The high lipid concentration minimised the distance between the single particles and thus, they aggregated during the freeze drying. Decreasing the lipid concentration to 2.5 % by diluting with 10 mM sodium citrate solution resulted in acceptable results. Sucrose was superior to glucose and an increase from 10 % to 15 % did not improve the redispersibility. The median increased after lyophilisation from 0.131  $\mu\text{m}$  to 0.193  $\mu\text{m}$  for 10 % sucrose and 0.314  $\mu\text{m}$  for 10 % glucose. An amount of 10 % sucrose ensured the best protecting

effects and isotonicity. However, untypically for freeze-dried products it was challenging to resuspend the formulations. Therefore, dextran, polyvinyl alcohol (PVA), polyethyleneglycol (PEG) and polyvinyl pyrrolidone (PVP) have been examined to enhance the redispersibility after freeze drying.

While Dextran 500 was not able to improve the stability, just adding 2 % of PEG 1500, PVP 25 or PVA made it rapidly redispersable and stable. The addition of 2 % PVA resulted in a comparable size distribution to the untreated formulation. Especially for low PVA concentrations and PEG, aggregates above 1  $\mu\text{m}$  occurred, but they were less than 5 % of the particle volume (Figure 18). PVA or PEG alone were not able to stabilise the formulation. Nevertheless, the z-average increased from 127 nm to 165 nm with a constant PDI of 0.1, indicating a larger hydrodynamic diameter. It has been assumed that the single particles were in contact during the lyophilisation. Hence, they could not be fully protected from sticking together. Under stirring and dilution, like in the static light scattering, the particles could disaggregate. The influence of the lyophilisation on the particle size has also been investigated by electron microscopy in section 4.3.4.4.

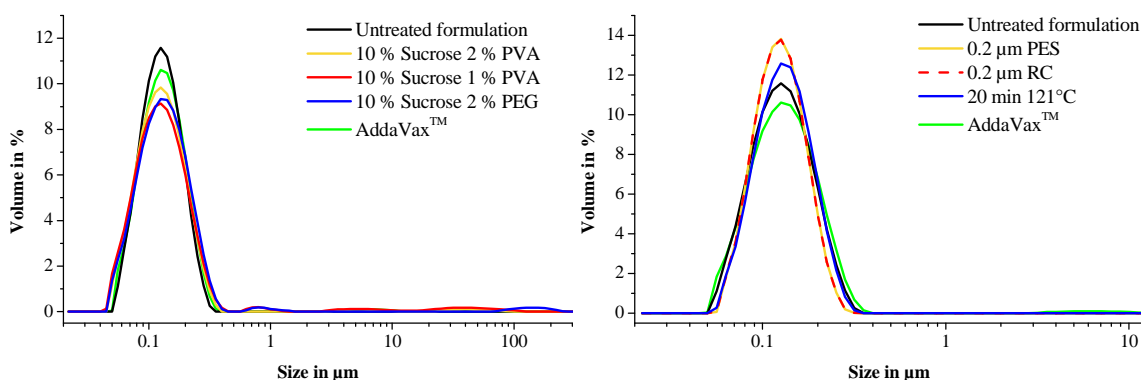


**Figure 18.** *Left: Influence of polyvinyl alcohol and polyethylene glycol on the particle size distribution in the lyophilisation of JS-3o (2.5 % lipid content) with 10 % sucrose. Right: Influence of steam sterilisation (121°C 20 min) and aseptic filtration by PES and RC filters on the particle size distribution of JS-3o.*

In accordance with the European Pharmacopoeia, parenteral formulations have to be sterile. All liquid squalene formulations were filtered through a 0.2  $\mu\text{m}$  filter of regenerated cellulose or polyethersulfone. For the solid formulations, it was necessary to filter the hot emulsions to take advantage of the deformability of the liquid lipid droplets. A terminal sterilisation processes like heat and steam sterilisation is always favored. Parenteral fat emulsion for parenteral nutrition are routinely autoclaved [175]. Due to the strong temperature dependency of the HLB value and a cloud point of

Tween 80 at 73°C, it was not possible to autoclave all developed adjuvants except JS-3o [170].

The filtration of the hot nanoemulsion through a 0.2 µm filter led to a small size decrease and narrower size distribution by retaining larger particles. Figure 18 shows the influence of the sterilisation procedure of JS-3o on the size distribution. While the  $D_{(0.5)}$  values were constant the  $D_{(0.9)}$  values decreased from 190 nm to 180 nm. In contrast, the z-average and PDI remained constant at 127 nm and 0.09. No different effects between filters, made of regenerated cellulose and polyethersulfone, have occurred for JS-3o. Steam sterilisation caused no effects on the particle size. For the Softisan 154 free nanoemulsion, it was not necessary to filter them at higher temperatures. Squalene was already liquid at room temperature and thus, the emulsion droplets were flexible enough to be filtered through a 200 nm filter. Larger particles were retained, too, but in general there was no influence on the size distribution. Filtration was performed with filters made of polyethersulfone or regenerated cellulose. While there were no differences between the filter materials for the most formulations, it was not possible to use polyethersulfone filters for the saponin and lecithin stabilised emulsion JS-2. Probably due to adsorption of the emulsifiers on the filter material, the nanoemulsion was not stabilised anymore and showed a massive size increase.

### 4.3.3 Long Term Stability

As size is the most important factor to guarantee the adjuvant effect of squalene, the stability of the successfully tested squalene nanoformulations was investigated over 12 months at 4°C. Additional, the stability at 25°C was tested for the freeze-dried formulation of JS-3o. Figure 19 shows the stability of JS-1, JS-2, JS-3 and JS-4 up to 12 months, measured by static light scattering. Additional measurements using dynamic light scattering were performed at the same time points. Although the high stability of JS-1, JS-4 and JS-3o was confirmed by PCS, static light scattering provided more detailed information about the size increase, especially in the µm range.

The most stable formulations JS-1 and JS-4 differed just in their composition of the lipophilic emulsifier. Although they were nearly similar in their hydrophilic part and differed just in their stereochemistry, they differed in the HLB value of 1.8 for Tween 80, by esterification with three oleic acids, and 4.3 for mannide monooleate, by

just adding one oleic acid. Nevertheless, the stability of both formulations was excellent over 12 months at 4°C. The static light scattering showed identical size distributions after 12 months storage. These results were confirmed by z-averages and PDI of 139 nm 0.09 and 140 nm 0.09 after 12 months for JS-1. For JS-4 the parameters remained at 141 nm 0.06. Minimal deviations occurred, due to the inherent measuring errors of the instruments. The stability of MF59<sup>®</sup> has been investigated by Ott *et al.* throughout the shelf-life of 3 years at 2-8°C. Neither the mean particle size nor the amount of large particles above 1.2 µm have changed during storage [176].

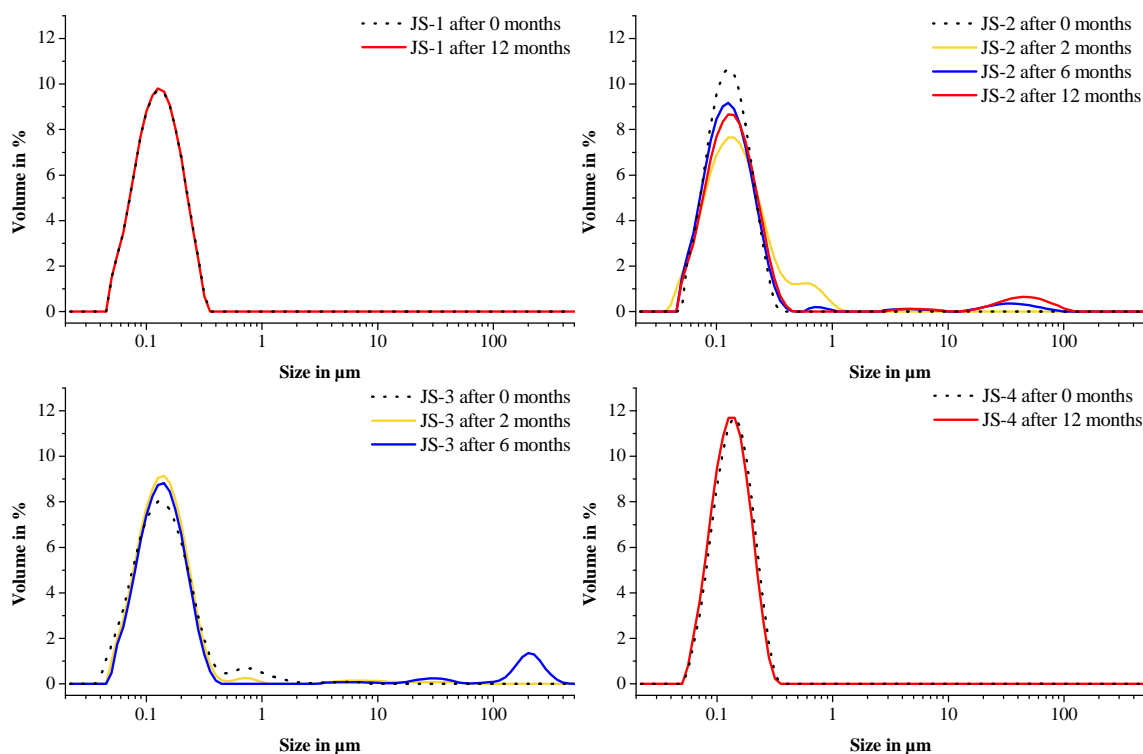


**Figure 19.** Influence of the storage time on the particle size distribution of JS-1, JS-2, JS-3 and JS-4 up to 12 months storage at 4°C.

In contrast to the stable formulations, JS-2 and JS-3 were not fully stable over one year. JS-2 based on a very low amount of 0.125 % of the hydrophilic emulsifier saponin, because of the high toxicity of *Quillaja* saponins [90]. Nevertheless, its stability was surprisingly high. Although a second particle species between 400 nm and 1 µm appeared after 2 months, more than 90 % of the particles remained below 400 nm, even after 12 months. While the  $D_{(0.1)}$  value remained at 0.07 µm and the median remained constant at 0.13 µm, the  $D_{(0.9)}$  value increased with the storage time. After 4 months, the size increase was visible macroscopically. Coalesced droplets between 20 µm and 100 µm floated and formed a white foam on the top of the emulsion. The foam was fully redispersible. During the storage time, the species around 60 µm increased, while

the species between 400 nm and 1  $\mu\text{m}$  disappeared. After one year, the volume distribution of the squalene emulsion consisted of two size maxima below 400 nm and around 60  $\mu\text{m}$ .

The SLN formulation JS-3 was just stable for 2 months. During this time, the size distribution was nearly identical, except a decrease of particles larger than 400 nm which could be followed by a decrease of the  $D_{(0.9)}$  value from 292 nm to 249 nm and a slight decrease of the  $z$ -average after two months. This behaviour was explained by aggregation and floating of the particles during storage. In this early stage, the large particle aggregates were not visible on the wall of the tubes. Although the samples were slightly shaken before the measurements, the large particles were not redispersed and thus excluded from the measurements. After three months, a ring of aggregated and floated lipids appeared on the wall of the tubes. The concentrated lipid ring was hardly redispersible and was responsible for the second particle species around 200  $\mu\text{m}$  after 6 months storage. One year of storage resulted in a nearly translucent aqueous solution with concentrated lipids on the top. Although light scattering data indicated that there was a main part of the formulation in the preferred size range below 400 nm after 6 months, the exact lipid amount remained unclear, as the aggregated lipid particles were not fully redispersible. This effect was clearly classified as instability, especially as the apparent initial size decrease was caused by the same effect. Lipid aggregates tended to stick on the wall of the tubes and could float during the measurement because their density was lower than water. After the formation of a second larger particle species, they grew at cost of smaller particles, which is known as Ostwald ripening. Smaller particles dissolved and accumulated on larger particles due to the size dependent solubility. According to Ostwald-Freundlich, the solubility of smaller particles was increased because of the higher curvature of the surface on smaller particles [172].

The results of the stability tests of the optimised SLN formulation JS-3o are given in Figure 20. Changing the emulsifiers to Poloxamer 188 and increasing the lipid content to 10 % resulted in an outstanding stability. Even after one year, there was no change in the particle size distribution. In contrast, a squalene-free placebo formulation of JS-3o, consisting of 10 % Softisan 154 and 5 % Poloxamer 188, was not stable for more than four weeks. The size distribution changed from monomodal around 150 nm to a bimodal distribution around 150 nm and 30  $\mu\text{m}$ . At the same time, the viscosity increased. Because of the lipophilic structure of squalene, it had no emulsifying

properties itself. Although Softisan 154 was characterised by a hydroxyl value of 7.1, implying very low amounts of mono- and diglycerides, it was expected that the residual mono- and diglycerides can bind water. Swelling of the particles led to the increase in size and viscosity. In addition, the gelation of low viscous SLN formulations into viscous gels is a well-known phenomenon. This process is promoted by high shear forces, like shaking or injecting through a syringe needle, and high lipid concentrations [177]. As described by Siekmann and Westesen, the gelation process can be induced by crystallisation or change of the lipid modification. The transformation of the instable  $\alpha$ -modification into the favored  $\beta$ -modification caused the formation of lipid platelets with an increased particle surface. In the following, the stabiliser was unable to cover the new surface areas [178]. Section 4.3.4.6 discusses the crystallisation process of the solid lipid nanoparticles. During the first 10 days after production, the instable  $\alpha$ -modification was transferred completely into the stable  $\beta$ -modification. The increase in size of the squalene-free formulation became present after 4 weeks, delayed to the change of the lipid modification. The high amount of 5 % Poloxamer 188 should also ensure the coverage of all lipid surfaces with the stabiliser.

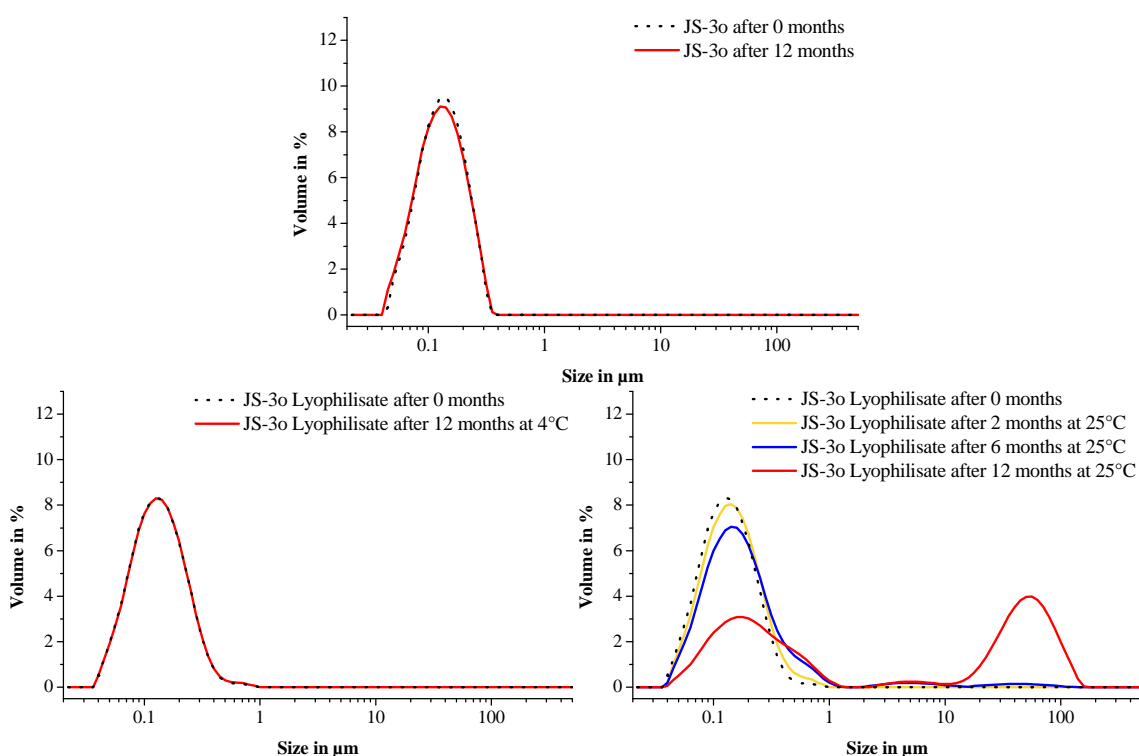


**Figure 20.** Influence of the storage time on the particle size distribution of JS-3o at 4°C (top) and its lyophilisates at 4°C (left) and 25°C (right) up to 12 months.

Also the lyophilisate of JS-3o presented perfect stability properties at 4°C over one year, albeit the lyophilisation broadened the size distribution. In contrast, storage of the

lyophilisate at 25°C influenced the particle size. There was a continuous size increase in the first 6 months, without changing the size characteristics dramatically. After one year, the size characteristics have completely changed to a bimodal particle size distribution with a main fraction of 50 % between 10 µm and 200 µm. The desired fraction below 400 nm was reduced to 42 %. The size increase is expected to decrease the immune stimulating effects after 12 months.

The MF59<sup>®</sup> derived standard formulation JS-1, JS-4 and the leading formulation JS-3o provided excellent stability properties at 4°C. The lyophilisate of JS-3o could be stored for 6 months at room temperature without change of its characteristics. A vaccine formulation, composed of the dried yeast vaccine and the developed and dried adjuvant JS-3o, can be stored as dry powder. Although this formulation should be stored at 4°C, it is possible to be stored at room temperature for a limited time. It should be stored at 4°C until the dispensing of the vaccine formulation to the user resp. veterinarian, then the application of the formulation has to be assured for the next 6 months.

### **4.3.4 Size Determination and Physicochemical Characterisation**

#### **4.3.4.1 Static Light Scattering and Photon Correlation Spectroscopy (PCS)**

As the size is the main factor for the adjuvant effect of squalene in water emulsions [66], the size distribution of the final formulations was investigated intensively using several techniques. A z-average of 120 – 170 nm was required for AddaVax<sup>™</sup> in accordance with the supplier information. In the following, it was set as reference for all developed formulations. Static light scattering and photon correlation spectroscopy were used as basic methods for the formulation development and as in-process controls for the adjuvants preparation.

The targeted z-average between 120 nm and 170 nm was reached by all developed formulations, except the freeze-dried form of JS-3o with 185 nm. Table 12 presents the results of the PCS and static light scattering measurements. The AddaVax<sup>™</sup> replica JS-1 and the nanoemulsion JS-4, stabilised with Tween 80 and mannose monooleate, provided with 140 nm and 141 nm a nearly identical z-average like AddaVax<sup>™</sup> of 146 nm. A polydispersity index around 0.065 indicated a monomodal, narrow and comparable particle size distribution. The z-average is the intensity weighted mean hydrodynamic diameter, thus it is not fully comparable with the static light scattering

data. Especially emulsifiers with long polyoxyethylene chains like Poloxamer 188 can result in larger hydrodynamic diameters [179]. However, the structure of the emulsifiers in AddaVax<sup>TM</sup> and JS-1 were identical resp. comparable for JS-4. Both measurement methods conformed in their assumption of spherical particles for their calculations, as they can be assumed for nanoemulsions [180]. In contrast, the primary result of the static light scattering is the root mean square radius or radius of gyration, which can be calculated under the assumption of compact spheres into the geometric radius [126]. The three nanoemulsions agreed in their mean diameter around 130 nm, 10 nm lower than the z-average. As the z-average is intensity weighted and the light scattering intensity of nanoparticles increases with the size to the power of six, large particles were overestimated in the z-average. Different from the PCS data the distribution width increased in the order AddaVax<sup>TM</sup> < JS-1 < JS-4. While the  $D_{(0.1)} - D_{(0.9)}$  width of Addavax<sup>TM</sup> was estimated with 120 nm, it increased to 133 nm for JS-1 and 141 nm for JS-4. The graphic visualisation of these size distributions in Figure 21 illustrates the narrower distribution of AddaVax<sup>TM</sup> and higher particle amounts around a size of 100 nm.

**Table 12.** Size distribution of the developed formulations and AddaVax<sup>TM</sup> determined by PCS and static light scattering.

Formulation	PCS		Static light scattering			
	Z-Average	PDI	$D_{(0.1)}$	$D_{(0.5)}$	Mean	$D_{(0.9)}$
AddaVax <sup>TM</sup>	146 nm	0.069	77 nm	124 nm	132 nm	197 nm
JS-1	140 nm	0.067	71 nm	121 nm	130 nm	204 nm
JS-2	164 nm	0.118	65 nm	129 nm	153 nm	268 nm
JS-3	166 nm	0.085	67 nm	127 nm	137 nm	224 nm
JS-3o	141 nm	0.097	63 nm	118 nm	128 nm	212 nm
JS-3o Lyo	185 nm	0.116	65 nm	125 nm	146 nm	242 nm
JS-4	141 nm	0.063	67 nm	119 nm	129 nm	208 nm

Because of the low emulsifier amount of saponin and lecithin, JS-2 had a much larger particle size and broader size distribution. The PCS measurements of the nanoemulsion with 164 nm z-average and a PDI of 0.118 confirmed with the static light scattering results with the largest mean of 153 nm and largest  $D_{(0.1)} - D_{(0.9)}$  width of 203 nm. Figure 21 (left) visualises the monomodal and broad distribution of JS-2, comprising particles from 35 – 850 nm.

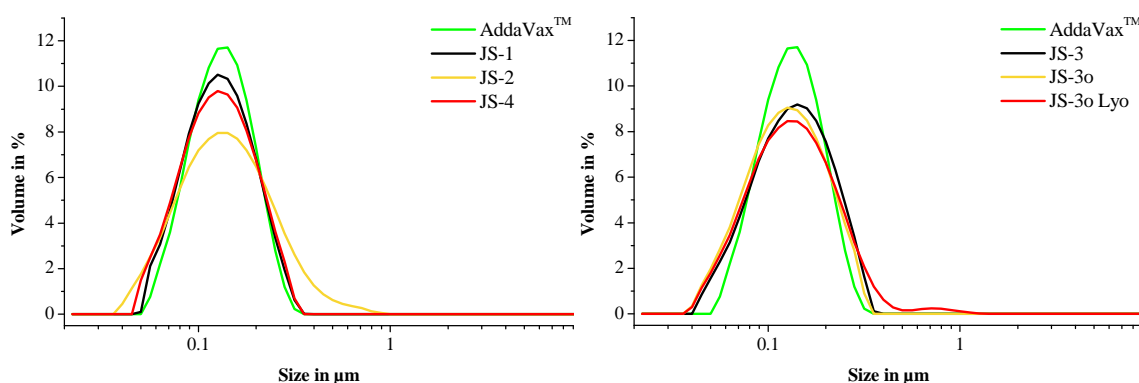


**Figure 21.** Size distribution (determined by static light scattering) of the developed formulations JS-1, JS-2 and JS-4 in comparison to AddaVax™ (left) and of the solid lipid nanoparticle formulations JS-3, JS-3o and the lyophilisate of JS-3o in comparison to AddaVax™ (right).

The z-average of the Poloxamer 188 stabilised solid lipid formulation JS-3o of 141 nm and a PDI of 0.097 was in the targeted size range. Although an increase of the hydrodynamic diameter had been described for steric stabilised nanoparticles [179], static light scattering proofed a mean geometric diameter of 128 nm, nearly identical to AddaVax™. Lyophilisation led to a size increase of JS-3o to 185 nm z-average and 0.116 in PDI. In comparison with JS-2, JS-3o Lyo had a lower mean and  $D_{(0.9)}$  value, but the z-average of JS-3o Lyo was increased dramatically. This was caused by the overestimation of large particles in the z-average. PCS was not able to resolve the second particle species in JS-3o Lyo around 1  $\mu\text{m}$ , but the second particle species contributed to the z-average. Although the second species comprised only 1.5 % of the particle volume, it had large influence on the z-average. Static light scattering data clarified this findings, while the  $D_{(0.1)}$  and  $D_{(0.5)}$  values remained in the range of the unprocessed formulation around 65 nm and 120 nm, the  $D_{(0.9)}$  increased by 30 nm to 242 nm. As the majority of the particle mass confirmed with the standard AddaVax™, it was further characterised and investigated in animal trials, although it was not in the target range of 120 – 170 nm (z-average).

The previously developed solid lipid nanoparticle formulation JS-3 resulted in contrary results between the static and dynamic light scattering. Although the mean particle size and the  $D_{(0.9)}$  value just differed 10 nm from JS-3o, the z-average was increased by 25 nm to 166 nm. Both formulations agreed in the occurrence of their largest particles around 350 nm, thus the increase in z-average could not be attributed to the overestimation of larger particles. Additionally, the PDI of 0.085 indicated a narrower particle size distribution than in JS-3o (PDI 0.097) and suggested by the static light

scattering data. Electron microscopic pictures revealed different particle shapes for JS-3o and JS-3. The formulation JS-3o resulted in spherical particles, while the particles in JS-3 showed a different structure of a baseplate with lipid topping. The assumed structure of a baseplate with lipid topping provided different sizes in the static light scattering dependent from the orientation of the particle. PCS measurements just observed the congruent diffusion behaviour of the particles.

It was concluded that all developed formulations provided large conformance in the particle size distribution with the market product. Differences occurred mainly in the presence of particle amounts above 300 nm and the distribution width. As the producer specifications allowed particles size from 120 nm to 170 nm (z-average), batch to batch variations could provide much broader size distribution than the developed formulations. Following, the adjuvant effect should not be interfered as long as 90 % of the particle volume is below 300 nm. Additional, the different preparation regimen of the market product had to be taken in account. While AddaVax<sup>TM</sup> was filtered terminally by a 0.22  $\mu\text{m}$  filter, the samples were not filtered except for animal experiments which required sterility. Due to the flexibility of the emulsion droplets, also larger particles can pass a 0.22  $\mu\text{m}$  filter, but microsized particles will be excluded.

#### 4.3.4.2 Nanoparticle Tracking Analysis (NTA)

Nanoparticle tracking analysis calculates the particle size from the diffusion track of the single particles, applying the Stokes-Einstein equation. Table 13 presents the NTA results as volume weighted distribution. The NTA results were in good agreement with the dynamic and static light scattering data for AddaVax<sup>TM</sup>, JS-1, JS-2, JS-3o, JS-3o Lyo and JS-4. The low investigated particle number of 300 particles during 5 measurement cycles tracking 60 particles each, had strong impact on the  $D_{(0.9)}$  values. The detection of a large particle increased the  $D_{(0.9)}$  value of AddaVax<sup>TM</sup> and led to large deviation of the  $D_{(0.9)}$  values between the measurement cycles. Nevertheless, a narrower particle size distribution was evaluated by NTA in general. For JS-1, JS-3o and JS-4 the  $D_{(0.1)} - D_{(0.9)}$  width was estimated with 50 nm instead of 140 nm by static light scattering. The obtained number weighted distribution in Figure 22 explains the influence of large particles around 200 nm and 300 nm in the formulation JS-2. Although just a low particle number differed from JS-1 and JS-4, the mean was increased from 136 nm for JS-1 and JS-4 to 209 nm for JS-2. AddaVax<sup>TM</sup> differed from

JS-1 and JS-4 mainly in higher particle numbers between 180 nm and 200 nm which were responsible for the increased  $D_{(0,9)}$  value and mean particle size.

**Table 13.** Size distribution of the developed formulations and AddaVax<sup>TM</sup> determined by NTA. Data were calculated from the number weighted distribution to a volume weighted distribution under the assumption of compact spherical particles.

Formulation	$D_{(0,1)}$	$D_{(0,5)}$	$D_{(0,9)}$	Mean
AddaVax <sup>TM</sup>	109 nm	131 nm	175 nm	150 nm
JS-1	103 nm	120 nm	158 nm	136 nm
JS-2	109 nm	142 nm	222 nm	209 nm
JS-3	129 nm	160 nm	213 nm	182 nm
JS-3o	102 nm	127 nm	153 nm	137 nm
JS-3o Lyo	132 nm	181 nm	250 nm	214 nm
JS-4	105 nm	124 nm	156 nm	135 nm

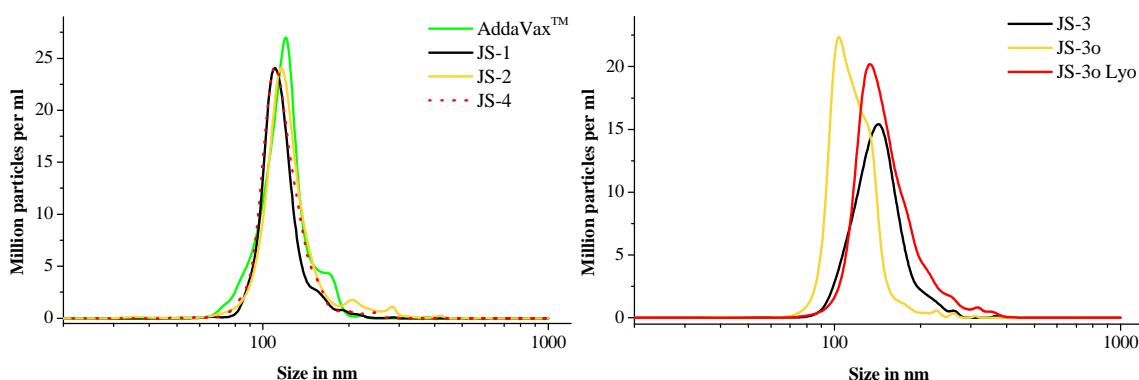


**Figure 22.** Particle number weighted size distribution of JS-1, JS-2 and JS-4 in comparison to AddaVax<sup>TM</sup> (left) and of the solid lipid nanoparticle formulations JS-3, JS-3o and the lyophilisate of JS-3o (right). Results were determined by nano tracking analysis.

The lyophilised form of JS-3o and JS-3 showed not only the occurrence of small amounts of larger particles. The particle size distributions were shifted to larger particle sizes, while the distribution width remained constant (Figure 22). The strongly diluted samples of JS-3o Lyo indicated an increase in particle size by the lyophilisation, instead of a reversible aggregation. It has to be taken in account for JS-3 that the applied measurement principles were comparable to photon correlations spectroscopy. Following, the NTA results of JS-3 were comparable to PCS, but resulted in larger particles sizes than in static light scattering. This difference was explained by the non-spherical shape as base plate with lipid topping. While NTA and PCS determine the hydrodynamic diameter independent from the orientation of the dispersed particles, the determined size in the static light scattering is dependent from the observed side.

#### 4.3.4.3 Asymmetrical Flow Field-Flow Fractionation (AF4)

Asymmetrical Flow Field-Flow Fractionation (AF4) in combination with Multi Angle Laser Light Scattering (MALLS) provided the possibility to characterise heterogeneous particle size distributions over a broad particle size range. The method benefits from an initial separation of the particles in the flow channel in accordance with their particle size. The exact particle size distribution is then determined by static light scattering of the prior separated particles. Figure 23 presents the elution profiles of the squalene containing solid lipid nanoparticles JS-3o and the market product AddaVax<sup>TM</sup>. Although the elution profiles were comparable, they differed in a second larger particle species in JS-3o, which was eluted after 60 min. A larger maximal particle size in JS-3o could be concluded from the eluted particle size vs. time diagram. Nevertheless, in the particle size distribution (Figure 24) the main particle fraction of JS-3o was 10 nm smaller than AddaVax<sup>TM</sup>, but a second particle species between 500 nm and 650 nm occurred in JS-3o.

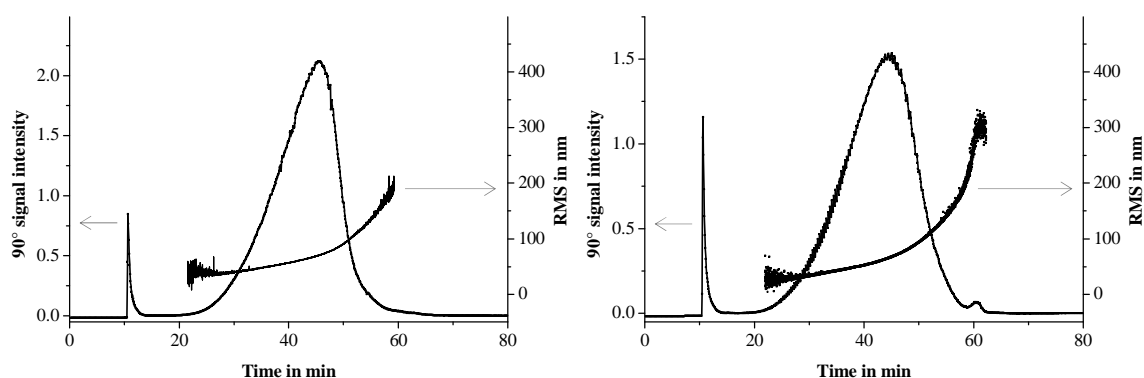


**Figure 23.** AF4/MALLS elution profile (detector signal at 90° vs. time) and root mean square radius (RMS) vs. time of AddaVax<sup>TM</sup> (left) and the solid nanoparticle formulation JS-3o (right).

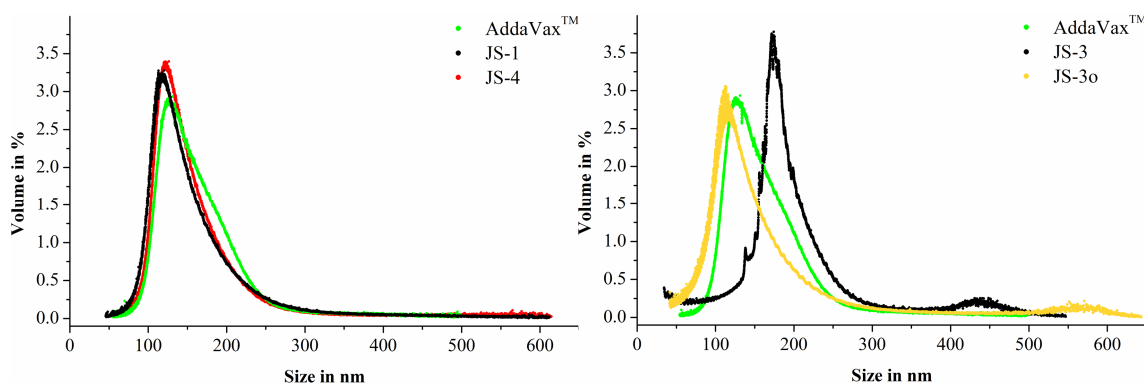


**Figure 24.** Size distribution of JS-1 and JS-4 in comparison to AddaVax<sup>TM</sup> (left) and the solid formulations JS-3 and JS-3o in comparison to AddaVax<sup>TM</sup> (right) determined by AF4/MALLS.

The  $D_{(0.5)}$  and  $D_{(0.9)}$  of JS-3o were with 120 nm and 178 nm, 10 nm smaller than in AddaVax<sup>TM</sup>. The second particle species above 500 nm affected the large particle means of 288 nm for JS-3o and 220 nm for AddaVax<sup>TM</sup>. The particle size distribution of JS-3 was determined 45 nm larger than for JS-3o. Especially the  $D_{(0.1)}$  value increased to 145 nm, whereas it was determined with 67 nm by static light scattering. Similar differences were already investigated by dynamic light scattering and nano tracking analysis, but could be explained by the particle shape. However, this result was contradictive to the static light scattering results which based on the same measurement principles. Therefore, aggregation tendencies during the focus step were assumed.

**Table 14.** Size distribution of JS-1, JS-3, JS-3o, JS-4 and AddaVax<sup>TM</sup> determined by AF4/MALLS. Data represent the average of 3 measurements.  $Mean_{geom.}$  represents the mass weighted geometric diameter.

Formulation	$D_{(0.1)}$	$D_{(0.5)}$	$D_{(0.9)}$	$Mean_{geom.}$
AddaVax <sup>TM</sup>	106 nm	132 nm	189 nm	220 nm
JS-1	100 nm	121 nm	175 nm	270 nm
JS-3	147 nm	179 nm	228 nm	277 nm
JS-3o	85 nm	120 nm	178 nm	288 nm
JS-4	103 nm	128 nm	177 nm	283 nm

The lecithin stabilised formulation JS-2 and the lyophilised form of JS-3o could not be investigated with AF4/MALLS. Both formulations interacted with the membrane of the flow channel or aggregated during the focus step. JS-2 had already shown massive instabilities with citrate buffer and during the filtration through a 0.2  $\mu\text{m}$  PES filter. Even the application of lower focus flows and bidistilled water as eluent did not improve the separation of JS-2.

The squalene nanoemulsions JS-1, JS-4 and AddaVax<sup>TM</sup> showed a uniform size distribution around 130 nm and were in good agreement with the static light scattering data. While the  $D_{(0.5)}$  and  $D_{(0.9)}$  values were nearly comparable around 130 nm and 180 nm, the mean differed especially for JS-4, which has shown minimal particle amounts between 500 nm and 600 nm. AF4/MALLS confirmed a minimal larger  $D_{(0.5)}$  of AddaVax<sup>TM</sup> and a broader size distribution compared to JS-1 and JS-4, as already determined by NTA. All mean diameters (Table 14) were larger than determined by NTA and static light scattering. The calculation of the particle size distribution over the

whole elution peak always included very small amounts, less than 0.25 % of the particle volume, with a size over 400 nm. These particles had a huge impact on the mean particle size. Especially for JS-3o, a second particle species was detectable between 500 nm and 650 nm. Experiments with filtered nanodispersions excluded aggregation effects during the focusing step. No other method was powerful enough to detect this small amounts of large particles and thus it underlined the power AF4/MALLS. The detected differences between the developed formulations were within the batch to batch variations of AddaVax<sup>TM</sup>. An influence on the adjuvant effect was not expected.

#### 4.3.4.4 Electron Microscopy

Size and shape of the solid lipid nanoparticle formulations were investigated by transmission electron microscopy. The particle shape is important for the interpretation of the size measurement data, as the measurement methods assume spherical particle shapes. Nanoemulsions were described as small spherical droplets. Their spherical structure has been investigated sufficiently elsewhere [64,180,181]. In contrast, the shape of solid lipid nanoparticles has been found in a wide range, depending on the exact lipid and emulsifier composition and the preparation method [177,182]. Jores *et al.* observed highly anisotropic platelet structures of Poloxamer stabilised glycerol dibehenate nanoparticles. Dependent on their spatial orientation, they occurred as needles, circles or ovals. The incorporation of medium-chain triglycerides changed their shape to nanospoons, meaning the liquid lipid was sticking as a droplet on the solid lipid platelets [121]. Furthermore, also spherical, rotund, rhombic and even completely irregular geometric forms have been described for solid lipid nanoparticles [183,184].

The lipid particles of the Tween 80 and Span 85 stabilised formulation JS-3 were visualised by electron microscopy as disk like, oval and spherical structures (Figure 25). Especially the oval structures showed a high contrast at one particle side like a solid baseplate covered with a droplet of the liquid squalene. The disks were visible as platelets with high contrast. Otherwise the spherical structures provided only a low contrast. The high contrast could be explained with a higher density or an increased sample thickness. It was concluded that the different structures derived from just one main particle species of a baseplate covered with a droplet of the liquid lipid. Dependent on the spatial orientation, spherical structures were observable in the top view and disks in the side view. All other angels of vision resulted in the typical baseplate with lipid topping.

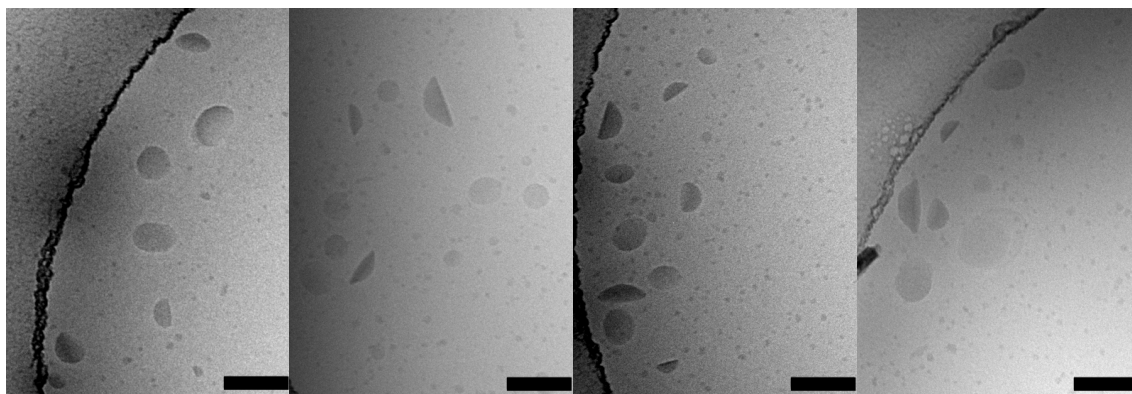


**Figure 25.** Cryo transmission electron microscopic pictures of the Tween 80 and Span 85 stabilised SLN formulation JS-3. Scale bars represent 100 nm.

Different from that, the particles of the Poloxamer 188 stabilised formulation JS-3o occurred as oval, round and polygonal geometries (Figure 26). Although these particles did not form ideal spheres like nanoemulsions, the found geometries could be regarded as sphere-like structures. No separation tendencies were observed, as the particles provided a homogeneous contrast in the cryo electron micrographs. Both formulations differed only in the amount and composition of the emulsifiers. The preparation method and the composition of the lipid phase remained constant. Thus, the difference in the particle shape was attributed to the emulsifiers. During the hot melt homogenisation the particle size reduction led to a massive increase of the particle surface. The emulsifiers had to cover the surface of the hot emulsion droplets and particles during the crystallisation to prevent from coalescing.

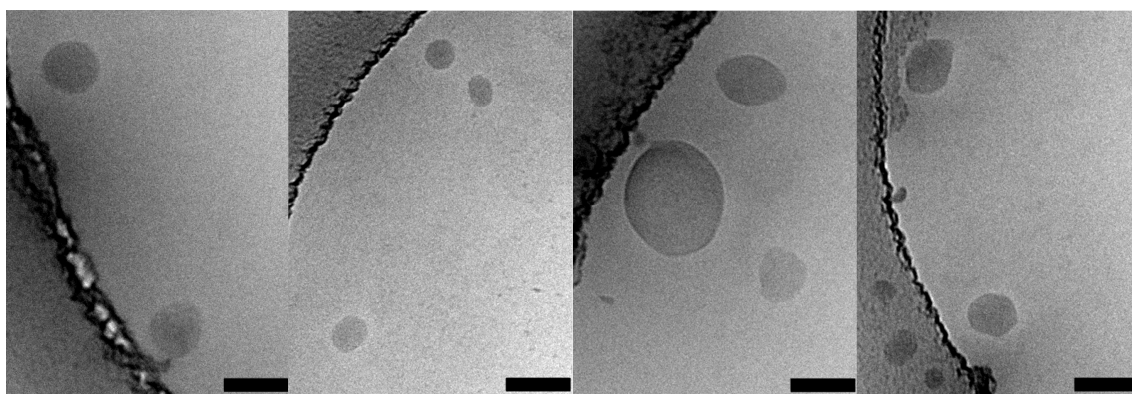


**Figure 26.** Cryo transmission electron microscopic pictures of the Poloxamer 188 stabilised SLN formulation JS-3o. Scale bar represents 100 nm.

As the sample preparation for the cryo electron microscopy comprised a filtration step through a 0.22  $\mu\text{m}$  filter to get rid of larger interfering particles, especially in the formulation JS-3, this method was not used for size determination.

As it was not possible to clarify the process of particle growth during the freeze drying, it was investigated electron microscopically. Both samples showed a comparable particle size and geometry (Figure 27). An increase of particles below 50 nm by the freeze drying process can be discussed in the right micrograph in Figure 27, but this result is limited, because of the low investigated numbers of particles by electron microscopy. The negative stained TEM samples confirmed the irregular geometric form of the particles in JS-3o, but encouraged the assumption of sphere like structures. The particle size distribution between 30 nm and 200 nm agreed with the PCS and static light scattering measurements.

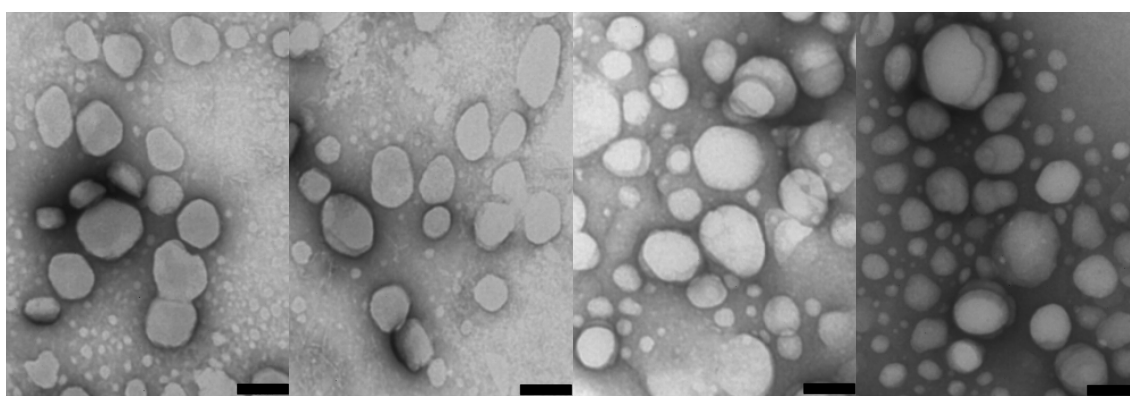


**Figure 27.** Transmission electron microscopic pictures of JS-3o before (both left) and after freeze drying (both right). Samples were prepared by negative staining with uranyl acetate. Scale bars represent 100 nm.

#### 4.3.4.5 Zeta Potential

The zeta potential is a key parameter for the stability of nanoparticle formulations. High electric charges below -30 mV and over 30 mV provide sufficient repulsion forces, and thus prevent the system from aggregation [185]. Dispersed in liquids, particles are surrounded by an electric double layer on the particle surface. The electric double layer is caused by the particle charge. Particle charges derived from charged components of the particles like imperfect crystals, ionic emulsifiers, adsorption of ions from the media or charged bulk material itself. The charge of the particle itself is characterised by the Nernst potential. It is followed by the inner Helmholtz layer of negative charges and the outer Helmholtz layer of counter ions, forming together the Stern potential. The less fixed diffuse layer is attached, until the neutral charge in distance from the particle is achieved. The zeta potential is defined as the surface charge at the shear plane [186]. For reliable measurements low salt concentrations around a conductivity of 1  $\mu\text{S}/\text{cm}$  are favored to ensure the right formation of the electric double layer on the particle surface.

High salt concentrations, multiple charged ions and the pH-value have great influence on the zeta potential [187]. Hence, nanoemulsions for parenteral nutrition are isotonicated with non-charged components like glycerol or are mixed directly before their administration with physiological salt solution to maintain a high zeta potential during storage for stability reasons [188]. Adding peptisators like citrate, tartrate or diphosphate can overcompensate the Nernst potential, meaning that they are attached to the surface and provide a more negative potential to stabilise the system [187]. For adjuvant systems an influence of the zeta potential on the immunogenicity is under discussion. Although the exact mechanism and distinct role of the surface charge is not clear yet, positively charged particles are favored for an improved antigen delivery to dendritic cells and macrophages [14,15].

Except JS-2, all formulations were prepared in 10 mM sodium citrate solution which is known as a peptisator. Adding sodium citrate to formulation JS-2 caused aggregation immediately, probably because of an interaction between the stabilisers and citrate. As 0.9 % sodium chloride had no influence on the stability of JS-2, this effect could not be caused by a higher ion strength. The exact mechanism remained unclear as saponins were charged negatively and phosphatidylcholine of the lecithin Lipoid S 100 was uncharged. An ionic interaction between contrary charges could be excluded. Table 15 shows the results of the zeta potential measurements.

All samples had a negative charge. A negative charge is a well-known phenomenon for lipid particles and emulsions in aqueous solutions, due to the adsorption of negatively charged ions in the Helmholtz layer [189]. Furthermore, the negative charges could be caused by impurities of free fatty acids in the emulsifiers or in the high melting lipid Softisan 154 in the solid formulations, respectively. The zeta potential of -15 mV in 10 mM and -23 mV in 5 mM sodium chloride solution of AddaVax<sup>TM</sup> was observed in all other samples except JS-3o. The increased ion strength of the 10 mM sodium chloride solution led to a fast decrease of the potential in the diffuse layer. Thus, the zeta potential in the 5 mM sodium chloride solution was more negative. The formulation JS-3o consisted of 5 % Poloxamer 188 as emulsifier, which is known to stabilise the particles by steric interactions, and was characterised with less negative zeta potentials of -8 mV and -12 mV in 10 mM and 5 mM sodium chloride. As the hydrophilic polyethylene glycol chains stabilised the particles sterically, electric forces were not necessary to provide a stable formulation [190]. Thus, a nearly neutral charge

was expected for JS-3o. Different salt concentrations and pH-values had just a minor influence on the Poloxamer 188 containing formulations, which were less sensitive to the pH-value and ion strength. The highly negative zeta potentials in bidistilled water for all formulations were attributed to the inappropriate measurement conditions. Bidistilled water did not provide a sufficient conductivity and interfered with the right formation of the electric double layer. Measurements in pure water have often been performed in the literature, but do not give meaningful results. Measurements in 1:10 diluted Sørensen phosphate buffer at pH 7.4 resulted in a zeta potential around -30 mV, providing a high stability for the Poloxamer free formulations. The pH increase from 6.5 to 7.4 changed the particle charge to a more negative zeta potential by 8 mV. Only JS-3o and JS-4 were not influenced by the pH shift, concluding that the zeta potential is mainly dependent on the emulsifier, especially the presence of Tween 80. Higher pH values lead to an extended grade of deprotonation of weak acids like free fatty acids, causing a more negative potential. Determination in 5 mM and 10 mM sodium citrate at pH 6.5 resulted in less negative potentials than in Sørensen buffer and sodium chloride. The used citrate concentrations were already too high to act as a peptisator. A pH effect could be excluded, as it agreed with the examined pH value in Sørensen buffer. The effect of citrate was attributed to the multiple charged ions. Multiple charged ions act like high ion concentrations by a faster potential decrease in the diffuse layer.

For further development of the formulations, the use of cationic emulsifiers like N,N-Di-( $\beta$ -stearoylethyl)-N,N-dimethyl ammonium chloride could lead to a positive zeta potential. Cationic particles and emulsions can provide an additional adjuvant effect [14,15,89].

**Table 15.** Zeta potential of the investigated squalene containing nanoparticle formulations.

<b>Formulation</b>	<b>Diluent</b>	<b>Zeta potential</b>
<b>AddaVax™</b>	Sodium chloride 5 mM	-22.8 mV ± 0.5 mV
	Sodium chloride 10 mM	-15.2 mV ± 0.3 mV
	1:10 Sørensen buffer pH 6.5	-20.1 mV ± 0.6 mV
	1:10 Sørensen buffer pH 7.4	-27.9 mV ± 0.7 mV
	Sodium citrate pH 6.5 5 mM	-14.5 mV ± 0.9 mV
	Sodium citrate pH 6.5 10 mM	-10.0 mV ± 0.7 mV
	Bidistilled water	-44.5 mV ± 0.8 mV
<b>JS-1</b>	Sodium chloride 5 mM	-22.2 mV ± 0.5 mV
	Sodium chloride 10 mM	-16.0 mV ± 0.1 mV
	1:10 Sørensen buffer pH 6.5	-24.8 mV ± 0.7 mV
	1:10 Sørensen buffer pH 7.4	-32.9 mV ± 0.6 mV
	Sodium citrate pH 6.5 5 mM	-17.2 mV ± 0.1 mV
	Sodium citrate pH 6.5 10 mM	-11.0 mV ± 0.1 mV
	Bidistilled water	-48.0 mV ± 0.6 mV
<b>JS-2</b>	Sodium chloride 5 mM	-25.4 mV ± 0.1 mV
	Sodium chloride 10 mM	-17.1 mV ± 0.5 mV
	1:10 Sørensen buffer pH 6.5	-27.7 mV ± 0.8 mV
	1:10 Sørensen buffer pH 7.4	-36.4 mV ± 1.1 mV
	Bidistilled water	-34.4 mV ± 0.6 mV
<b>JS-3</b>	Sodium chloride 5 mM	-21.9 mV ± 0.4 mV
	Sodium chloride 10 mM	-13.2 mV ± 0.5 mV
	1:10 Sørensen buffer pH 6.5	-19.2 mV ± 0.3 mV
	1:10 Sørensen buffer pH 7.4	-27.5 mV ± 0.1 mV
	Sodium citrate pH 6.5 5 mM	-14.4 mV ± 0.1 mV
	Sodium citrate pH 6.5 10 mM	-10.1 mV ± 0.3 mV
	Bidistilled water	-42.1 mV ± 0.7 mV
<b>JS-3o</b>	Sodium chloride 5 mM	-11.6 mV ± 0.4 mV
	Sodium chloride 10 mM	-7.8 mV ± 0.2 mV
	1:10 Sørensen buffer pH 6.5	-8.2 mV ± 0.4 mV
	1:10 Sørensen buffer pH 7.4	-9.3 mV ± 0.1 mV
	Sodium citrate pH 6.5 5 mM	-5.6 mV ± 0.4 mV
	Sodium citrate pH 6.5 10 mM	-2.3 mV ± 0.2 mV
	Bidistilled water	-40.8 mV ± 1.1 mV
<b>JS-4</b>	Sodium chloride 5 mM	-21.2 mV ± 0.3 mV
	Sodium chloride 10 mM	-14.2 mV ± 1.5 mV
	1:10 Sørensen buffer pH 6.5	-25.0 mV ± 1.6 mV
	1:10 Sørensen buffer pH 7.4	-27.1 mV ± 0.4 mV
	Sodium citrate pH 6.5 5 mM	-14.8 mV ± 0.7 mV
	Sodium citrate pH 6.5 10 mM	-10.9 mV ± 0.6 mV
	Bidistilled water	-42.1 mV ± 0.4 mV

#### 4.3.4.6 Differential Scanning Calorimetry (DSC)

DSC allows the investigation of endothermic and exothermic processes, such as melting, crystallisation and glass transition, in solid materials like solid lipids. It provides information about polymorphisms, eutectic mixtures and crystal ordering [191]. Aim of the study was to characterise the behaviour of the solid lipid matrix in the solid lipid nanoparticle formulation. For the low concentrated SLN dispersions, especially with low amounts of Softisan, they were concentrated prior differential calorimetric measurements by ultracentrifugation on an Optima MAX XP (Beckmann Coulter, Brea, USA) at 100000 g for 15 min. This did not change the melting behaviour nor the size distribution. The particles were easily redispersible and provided a better signal to noise ratio.

The Softisan 154 derived from hydrogenated palm oil consisting of different saturated triglycerides with palmitic and stearic acid as main fatty acids. The bulk material had a melting point at 58°C, confirming with the supplier data. As common for solid triglycerides, Softisan 154 showed polymorphisms. Triglycerides can crystallise in three different modifications and can be transformed monotropically from the  $\alpha$ - over the  $\beta$ - to the thermodynamically stable  $\beta$ -modification [192]. Beside the melting peak of the  $\beta$ -modification at 58°C, there was a second smaller melting peak of the less stable  $\alpha$ -modification at 49°C. Especially for tristearin, a slow transition into the thermodynamic stable form has been reported [193]. Reheating clarified the formation and transition of the  $\alpha$ - into the preferred  $\beta$ -modification (Figure 28). The bulk material crystallised at 42°C.

Replacement of half of the hard fat amount by liquid squalene, shifted the melting point to 52°C and it prevented the lipid from forming different modifications as well. As the liquid squalene interfered the crystallisation of the lipid, the crystallisation temperature decreased to 33°C. Likewise, the formulation as nanoparticles decreased the solidification temperature by 14 K to 19°C for Softisan/squalene (1:1) and 29°C for Softisan as solid lipid phase. The crystallisation temperature below room temperature made it necessary to cool the formulation on ice to ensure stability. Additionally, the Tween 80 and Span 85 stabilised formulation JS-3 showed a 10 Kelvin decreased crystallisation temperature compared with JS-3o. This effect was attributed to the type and amount of emulsifiers, hindering the crystallisation, as the size distribution remained constant. Nevertheless, it was not possible to determine the extent of the

solidification point depression of this effect from the size effect. The structure of the stabiliser has an important influence on the crystallisation and can even promote the nucleation by orientating the triglyceride molecules [194]. Helgason *et al.* have discussed the influence of the surfactant concentration on the lipid crystal structure. With growing amounts of Tween 20, the crystallisation temperature of tripalmitin SLNs decreased and changed the melting behavior. They proposed that the tightly packed surfactant shell may protect the lipid core from crystallisation [195]. In contrast to the crystallisation temperature, the melting temperatures of the SLN formulations decreased just by 2 K. A size dependent shift of the melting temperature is known from literature and can be explained by the Gibbs-Thomson equation [196]. Furthermore, adsorbed emulsifiers onto the surface of the nanoparticles could interfere the melting process [197]. The size dependency broadened the melting and crystallisation peak as well, because of the particle size distribution from 50 nm to 300 nm instead of a distinct particle species.

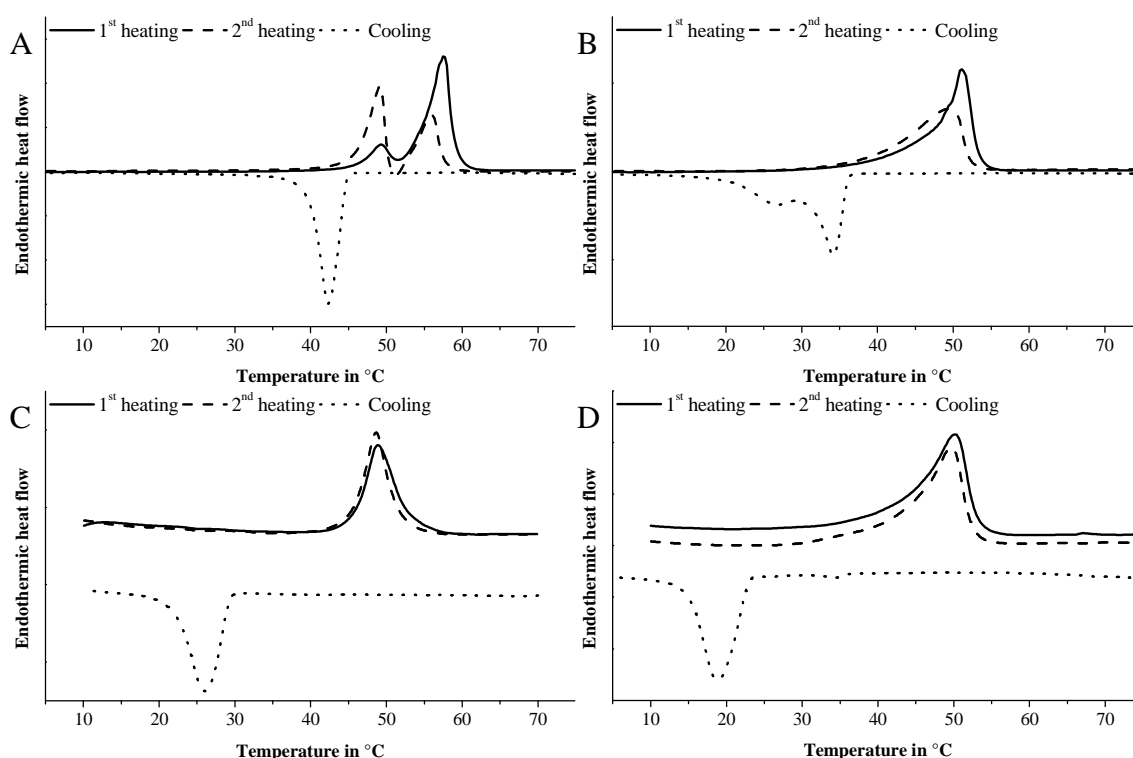


**Figure 28.** DSC thermograms of Softisan 154 (A) and Softisan 154/Squalene (1:1) as bulk materials (B) in comparison to the solid lipid nanoparticles composed of 10 % Softisan 154 (C) and 10 % Softisan 154/Squalene (1:1) (D).

Adding 25 %, 50 % and 75 % squalene to the triglyceride led to a linear decrease of the melting and solidification temperature. The linear correlation between the squalene content of 0 % to 75 % and the decrease in melting respectively crystallisation

temperature indicated the homogeneous distribution of the squalene in the matrix of the solid lipid [198]. As shown in Figure 29, the melting and crystallisation point decrease was linear for the bulk material as well for the SLN formulations. Different from the bulk material, the melting temperature for the nanosized formulations was always 2 K lower than the bulk material. Moreover, the crystallisation temperature of the nanoparticles was decreased by 14 K at each relevant squalene concentration. The two different melting points of Softisan 154 nanoparticles represent the formation of modifications. As the mixture of Softisan with squalene has not shown different modifications, the stable  $\beta$ -form has been used for comparison.

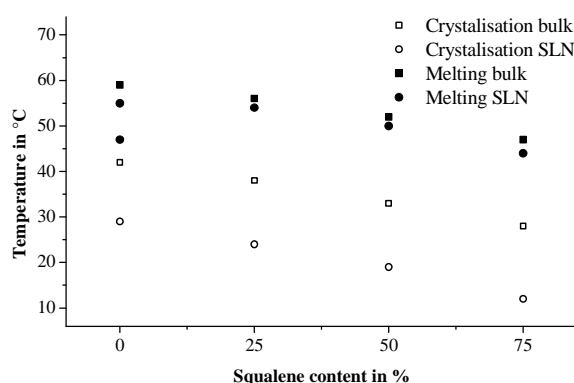


**Figure 29.** Influence of the addition of 25 % to 75 % liquid squalene to Softisan 154 on the melting and crystallisation points. Circles are characterising the behaviour of the bulk material in comparison to the solid lipid nanoparticles (squares).

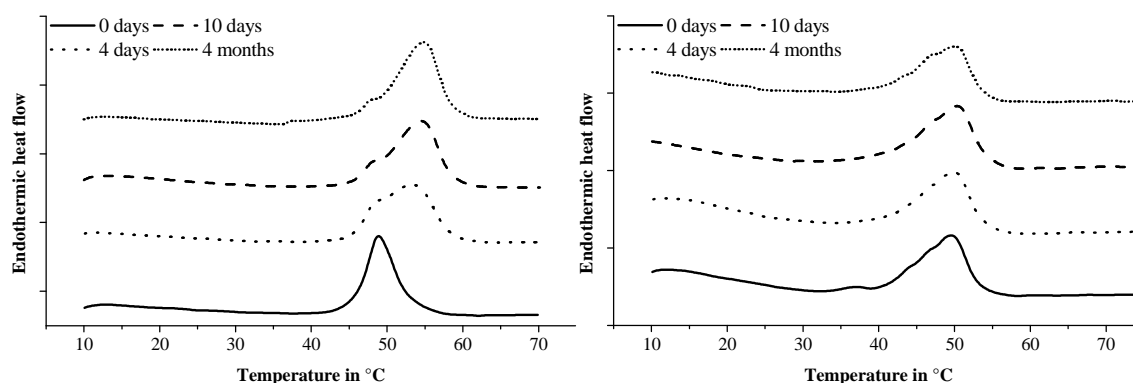


**Figure 30.** Primary heating curve of the solid lipid nanoparticles containing Softisan 154 (left) or Softisan 154 and squalene 1:1 (right) as lipid matrix directly after the preparation and stored up to 4 months at 4°C.

Figure 30 shows the primary melting peaks of the optimised solid squalene formulation (JS-3o) and squalene-free placebo formulation. There was no change in the melting peaks for JS-3o over 4 months, confirming the crystallisation of squalene and Softisan in the stable modification. Compared with this, the squalene-free formulation changed to the stable  $\beta$ -modification. During storage the melting temperature increased from

48°C at the day of preparation to 55°C after 4 months storage at 4°C. The melting peak at 48°C confirmed with the melting temperature of the meta stable  $\alpha$ -modification in the bulk material. The transformation completed 3°C below the maxima of the stable  $\beta$ -form of the bulk material at 58°C, because of the melting point depression of nanoparticles. The conversion was nearly finished after 10 days. After 4 days, both melting points were visible in the thermogram, forming a broad melting range instead of two distinct maxima. Especially for long chain triglycerides and complex triglycerides like Softisan 154, a slow or even incomplete transition into the stable  $\beta$ -modification was reported by Bunjes *et al.* [196]. Additional, the size distribution of the squalene-free formulation changed over time from a unimodal distribution of 126 nm to a bimodal distribution with maxima at 126 nm and 11  $\mu$ m. The size increase was much slower than the change in the thermic analysis. Likewise, the peak of the second heating curve was at the same temperatures at all time points. This ensured that the melting point shift was a phenomenon of different lipid modifications and not a size effect. However, it was assumed that the size increase was induced as a consequence of the formation of platelets in the  $\beta$ -modification and is described in detail in section 4.3.3.

#### 4.3.4.7 X-Ray Diffraction

Triglycerides occur in three different crystal modifications and can be transformed monotropically from the  $\alpha$ - over the  $\beta'$ - to the thermodynamically stable  $\beta$ -modification [192]. Wide angle X-ray diffractometry was used to investigate the exact modifications of the squalene containing (JS-3o) and squalene-free nanoparticles (PS-154) directly after preparation and after storage at 4°C.

Figure 31 shows the diffraction patterns of the four formulations. The maxima of the reflexes confirmed for the stored PS-154 and both forms of JS-3o. The short spacings of the fatty acid chains were calculated with 0.46 nm for the reflexes at 22.5°, 0.39 nm for 26.8° and 0.37 nm for the reflexes at 28°. The determined short spacings were in full agreement with the stable  $\beta$ -modification of a binary mixture of tristearin and tripalmitin [199,200]. In contrast to the squalene containing formulation JS-3o, the Softisan nanoparticles crystallised initially in a different modification. From the strong reflex at 25° a short spacing of 0.41 nm was calculated which agreed with the literature data of the  $\alpha$ -modification [199,200]. A transition into the  $\beta$ -modification was already indicated in the freshly prepared Softisan nanoparticles by the weak reflexion signal at 22.5°C. These results verified the DSC results which suggested an immediate

crystallisation for the squalene containing formulation into the stable  $\beta$ -modification. Additional, it confirmed the crystallisation of the Softisan nanoparticles in the  $\alpha$ -modification and its transition into the stable  $\beta$ -modification during storage.

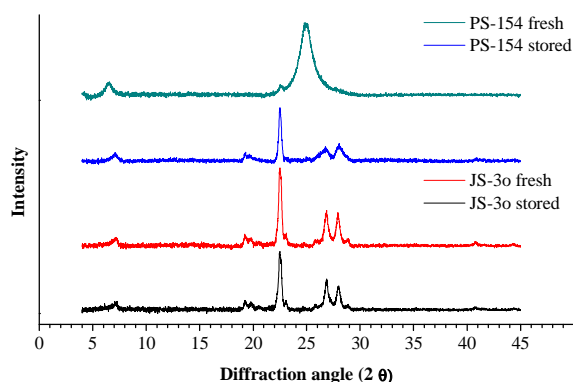


**Figure 31.** X-ray diffraction of the squalene-free nanoparticles PS-154 and JS-3o directly after preparation and after storage at 4°C.

#### 4.3.4.8 $^1\text{H}$ -Nuclear Magnetic Resonance

$^1\text{H}$ -NMR spectroscopy is widely used for the structural clarification of organic chemical compounds like active pharmaceutical ingredients, polymers and proteins [201,202]. Nevertheless, standard  $^1\text{H}$ -NMR is limited to liquid and dissolved compounds, as a limited mobility of protons and following a massive decrease in proton relaxation times (spin-spin relaxation) leads to line broadening or complete disappearance of the proton signal. This provided the possibility to characterise the microenvironment e.g. in gels with a decreased mobility or highly mobile protons in supercooled melts [203,204].  $^1\text{H}$ -NMR spectroscopy can contribute to study the interactions between the solid lipid phase and an incorporated liquid lipid like in nanostructured lipid carriers [198,205,206]. The line width at half amplitude has often been calculated to assess the mobility [183].

The  $^1\text{H}$ -NMR spectra of JS-3o, consisting of 50 % squalene and 50 % hard fat as disperse lipid phase, and of a squalene nanoemulsion are given in Figure 32. The proton signals of squalene (Greek letters) and Poloxamer 188 (Latin letters) in the structural formulas were assigned to the spectra, corresponding to Jores *et al.* and Pogliani *et al.* [205,207]. As Softisan 154 was not mobile at room temperature, its protons were not detectable in standard  $^1\text{H}$ -NMR. Trimethylsilylpropionate was used as internal standard at 0 ppm. Due to the preparation in 80 % bidistilled water, a large water peak occurred at 4.8 ppm, but did not interfere with other signals. There was no difference of the proton signals of Poloxamer 188 at 3.7 ppm (protons a+b+d) and at 1.1 ppm (proton e)

in JS-3o and the nanoemulsion. Although the mobility of the emulsifier at the surface could be restricted, the high Poloxamer 188 concentration provided sufficient free Poloxamer 188 for sharp signals. The proton signals of the methyl groups (peak  $\alpha$ ) at 1.6 ppm and of the methylene groups (peak  $\gamma$ ) at 2 ppm showed a massive line broadening, indicating a limited mobility. Although the different methyl and methylene groups in squalene were not magnetical equivalent and their exact signals in  $^1\text{H-NMR}$  spectroscopy have been described, chemical shifts of 2.0 ppm for all methylene groups and 1.6 ppm for the methyl groups were assumed because of their near peaks and for simplification [207].

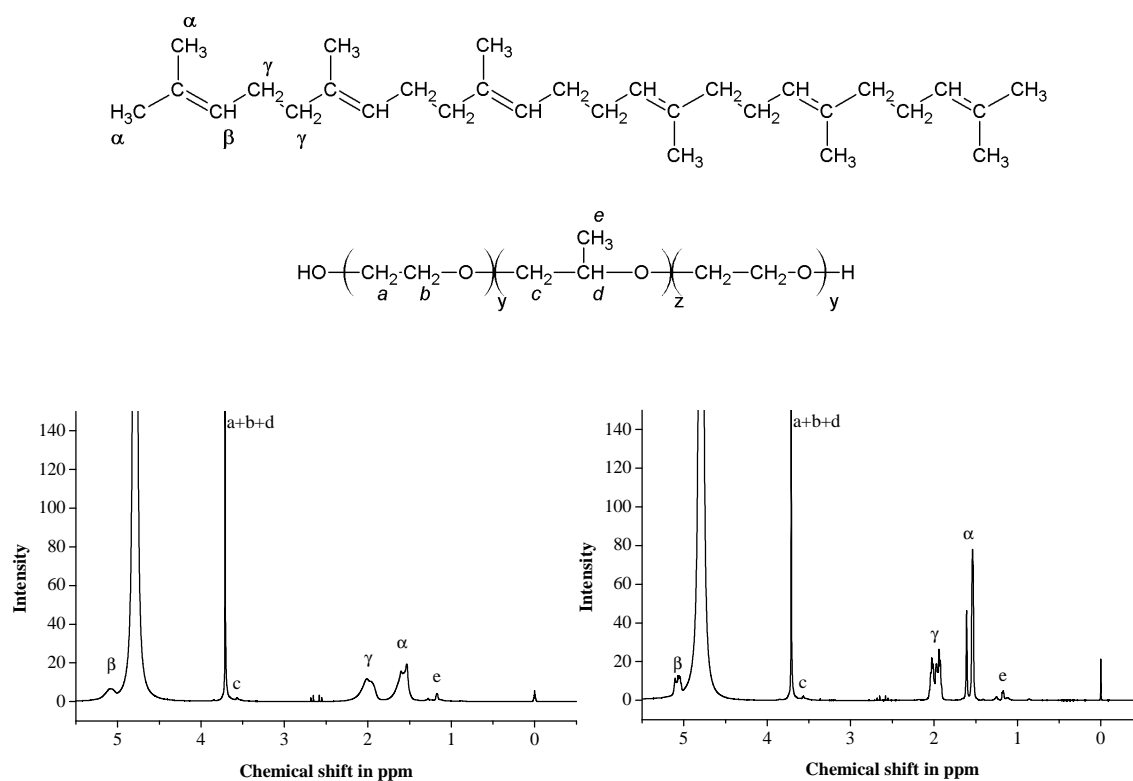


**Figure 32.**  $^1\text{H-NMR}$  spectra of JS-3o (left) and a nanoemulsion of squalene and Poloxamer 188 (right). The Latin letters refer to the proton signals of Poloxamer 188 (lower structural formula) and Greek letters refer to the proton signals of squalene (upper structural formula).

Figure 33 shows the detailed investigation of the proton peaks of squalene at 1.6 ppm and 2 ppm dependent from the concentration of Softisan 154. Already at the lowest Softisan concentration of 25 %, it was impossible to determine the line width at half amplitude, as the distinct peaks changed to broad signals, comprising several proton species. As a result of line broadening, the peak amplitude decreased dramatically. The broadened and reduced peaks were attributed to the immobilisation of the squalene in the lipid matrix causing shorter relaxation times (spin-spin relaxation). The highly

restricted mobility in the lipid matrices was further increased by the addition of more Softisan 154. Pure Softisan SLNs were investigated as negative control and showed, except the proton peaks of Poloxamer 188 and water, no proton peaks of the triglyceride because of their full solid structure and very low relaxation times.

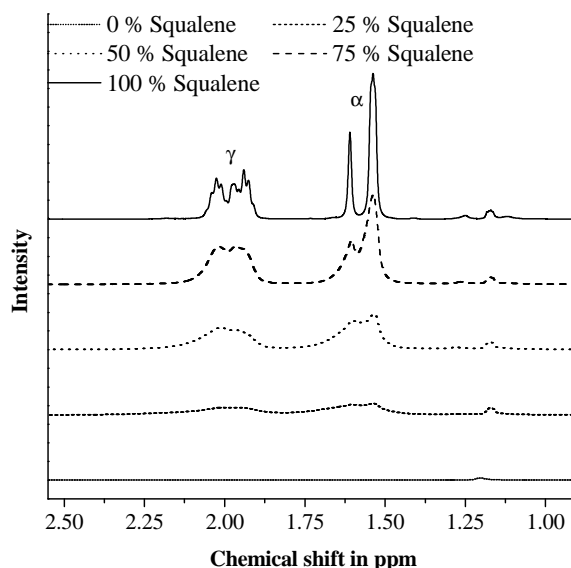


**Figure 33.**  $^1\text{H-NMR}$  spectra of the squalene signal at a chemical shift of 2 ppm and 1.6 ppm in Softisan 154 nanoparticles containing of 0 %; 25 %; 50 % (JS-3o); 75 % squalene and a squalene nanoemulsion. All formulations were stabilised with 5 % Poloxamer 188.

In comparison with the literature data, the mixture of squalene and Softisan 154 has shown strong interactions already at high liquid lipid concentrations. Jennings *et al.* and Jores *et al.* investigated nanostructured lipid carriers based on glycerol behenate and medium chained triglycerides [198,205]. Already at low liquid lipid concentrations like 16 % and 10 %, both described distinct NMR peaks of the incorporated lipid. Because of the relative high mobility of the medium chained triglycerides and in accordance with EPR experiments, Jores *et al.* proposed a model of a solid lipid core with liquid drops at the surface [205].

The  $^1\text{H-NMR}$  experiments suggested an increasing limitation in the mobility of squalene with increasing Softisan amounts. Thus, a homogeneous distribution of the squalene as nanosized liquid domains in the solid triglyceride was assumed. This was in agreement with the DSC measurements which revealed a linear correlation between the squalene content and the melting point depression. Furthermore, the X-ray experiments confirmed the presence of crystalline glycerides and disproved changes in the crystal structure in the nanoparticles.

### 4.3.5 Cytotoxicity Assay

The cytotoxicity tests were carried out with a sulforhodamine B (SRB) assay on human colon fibroblasts (CCD-Co18). Several cell lines e.g. BALB/c 3T3 cells, foreskin fibroblasts, mouse macrophages and colon carcinoma cells were used in the literature to estimate the cytotoxicity [88,208,209]. The ideal cell line should simulate the conditions at the side of application and action. Although human colon fibroblasts are not subcutaneous cells, they behave comparable to subcutaneous cells and benefit from their ability to proliferate on their own. In comparison, immortalised cells are always modified and do not represent the natural cell behaviour, especially tumor cell lines have a lower sensitivity to toxic substances [210].

Many immune stimulants are cytotoxic and raise severe side effects. Crude saponins and to a lower extent also purified saponin fractions cause haemolysis [42]. Paraffin containing adjuvants like CFA and IFA affect granulomas at the injection side. In consequence, they are not used in human vaccines due to their toxicity, although they are providing excellent immune stimulating effects [36]. Although it is an adjuvant mechanism, especially for squalene nanoparticles, to provoke a locally determined inflamed area, it is necessary to ensure good biocompatibility [68]. The effect of the formulations was compared with the effect caused by their emulsifiers at the same used concentration and minimum essential medium (MEM) as positive control.

Comparing the market formulation AddaVax<sup>TM</sup> with the identical adjuvant system JS-1 carried out massive toxic effects of both of them at the three highest concentrations (Figure 34). Only the lowest concentration of 0.0086 % lipid in AddaVax<sup>TM</sup> had no effect on the CCD-Co18 cells. The toxic effects were mainly raised by the squalene based nanoemulsions because of the good biocompatibility of Tween 80 and Span 85. Tween 80 is one of the approved O/W emulsifiers for parenteral applications in humans and known for its good compatibility [88,211]. Tween 80 and Span 85 were just toxic in its highest concentrations of 0.125 % Tween 80 and Span 85. Already at the second highest concentration of 0.025 %, the viability was at 75 %. Lower concentrations had no influence on the cells. In the literature, IC<sub>50</sub> values have been evaluated between 0.02 % and 0.08 % dependent on the test system [212]. In contrast, JS-1, JS-3 and AddaVax<sup>TM</sup> completely inhibited cells from proliferating except of dilution 1:125. At the lowest concentrations the cell viability was evaluated with 92 % for AddaVax<sup>TM</sup>, 40 % for JS-1 and 67 % for JS-3. The lipid phase of JS-3 consisted of a mixture of

squalene and Softisan 154 in equal parts. Differences between the market product AddaVax<sup>TM</sup> and the replica JS-1 might have occurred, due to different purity of the excipients or contamination during the production process.

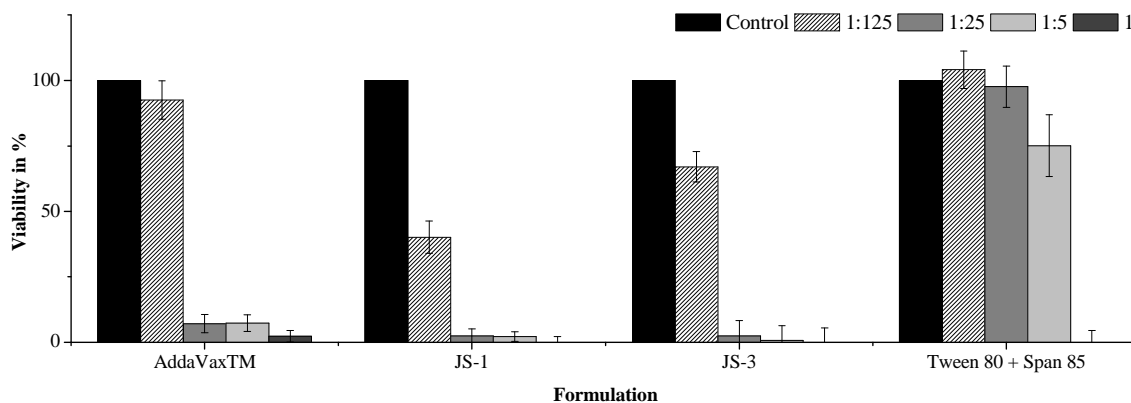


**Figure 34.** Influence of the concentration of AddaVax<sup>TM</sup>, JS-1, JS-3 and the used emulsifiers Tween 80 and Span 85 on the cell viability in comparison with untreated cells as control. Mean  $\pm$  standard deviation.

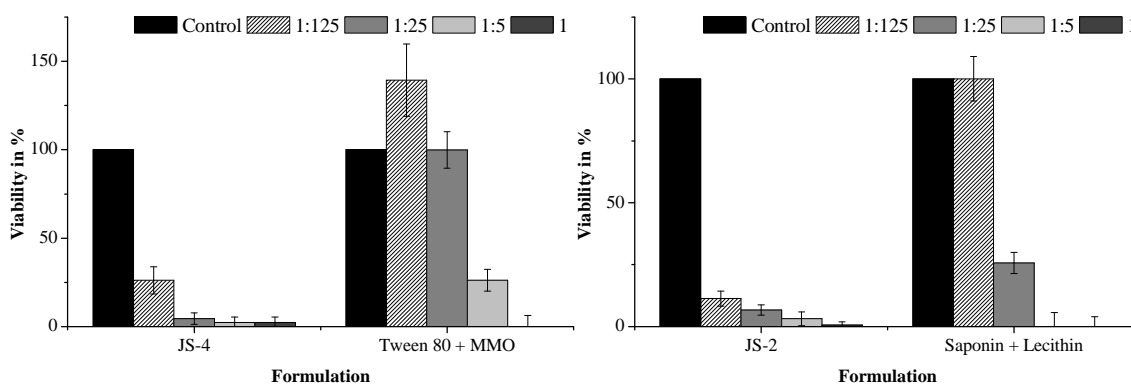


**Figure 35.** Influence of the concentration of JS-4 (left) and JS-2 (right) and their appropriate emulsifiers on the cell viability in comparison with untreated cells as control. Mean  $\pm$  standard deviation.

The toxicity of the formulations was the result of the toxicity of the emulsifiers and the lipid phase. As Tween 80 + mannide monooleate and saponin + lecithin had toxic effects itself, the squalene containing formulations were more toxic than the other formulations (Figure 35). On the other hand, cells can be protected from the emulsifiers by trapping them on the surface of the lipid particles [213]. The mixture of saponin and lecithin showed massive cytotoxic effects. Although the concentration of saponin in dilution 1:25 was just 12.5  $\mu$ g per ml, 75 % of the cells were not viable. Together with the influence of squalene, the incubation with formulation JS-2 caused no remaining cell viability on all evaluated concentrations.

Saponin is well known for its cytotoxic and haemolytic effects. Hence, purified saponin fractions like Quil A or QS-21 are favored, although the toxic effects could not be eradicated completely [214]. An alternative strategy is the formulation of ISCOMS. Saponin, lecithin and cholesterol formed cage like structures of 40 nm and showed no toxic side effects [90]. Rönnerberg *et al.* reported that Quil B, the most toxic and best immune stimulating fraction of *Quillaja* saponins, lysed erythrocytes already at 5 µg per ml. They estimated the same amount as IC<sub>50</sub>, using a MTT cytotoxicity test [215]. In comparison with the IC<sub>50</sub> estimated by Rönnerberg, the toxicity in the experiments with crude saponin and lecithin was at the same level.

The formulation JS-4 had a high toxicity, too. The cell viability at the highest dilution was just at 25 %. JS-4 differed from JS-1 just in the substitution of Span 85 to mannide monooleate, emphasising toxic effects of mannide monooleate. Comparing the emulsifiers Tween 80 + Span 85 with Tween 80 + mannide monooleate revealed a lower biocompatibility of Tween 80 + MMO. For similar effects Tween 80 + Span 85 could be 5 times more concentrated.

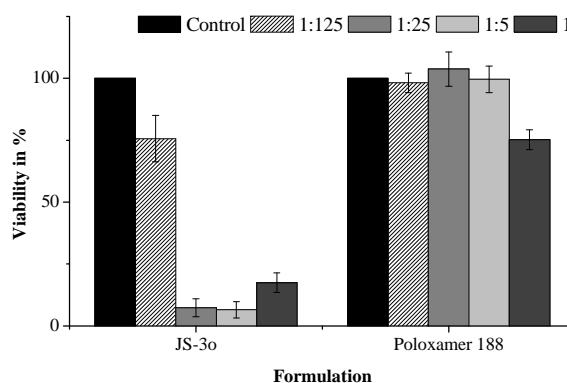


**Figure 36.** Influence of the concentration of JS-3o and the emulsifier Poloxamer 188 on the cell viability in comparison with untreated cells as control. Mean  $\pm$  standard deviation.

Figure 36 shows the cytotoxic effects of the leading formulation JS-3o compared with Poloxamer 188. Poloxamer 188 showed nearly no toxic effects. Even in the highest concentration, when 0.5375 % emulsifier was applied to the cells, the viability was about 75 %. Lower concentrations caused no toxic effects. At the highest concentration, there was no remaining cell viability for the other emulsifiers. In addition, this emulsifier concentration was 4 times higher than the concentration of Tween 80, Span 85 and mannide monooleate and even 17 times higher than the saponin concentration in dilution 1. This proved the excellent biocompatibility of Poloxamer 188. Furthermore JS-3o showed the best biocompatibility of all developed

formulations followed by JS-3. This indicated that squalene may be the toxic ingredient, as fifty percent of the squalene had been replaced by hard fat in both formulations. For lipid nanoparticles, composed of glyceryl dibehenate or glyceryl trimyristate, it has been shown that there was no cytotoxic effect up to 10 % lipid nanoparticles [213]. The cytotoxic effects of squalene nanoparticles at concentrations above 0.01 % confirmed with the theory of causing a local inflamed area as mode of action.

In the immunisation trials, no local reactions were observable except for the saponin containing formulation. Also the toxic effect of JS-2 was not severe, just slightly irritant, limited to the injection side and limited for some days after the application. In contrast, CFA caused massive irritations which increased over the time, because of the non-degradability of paraffin oil. Beside the local inflammation, it resulted in hair loss and bites at the injection sides.

### **4.3.6 *In Vivo* Experiments Adjuvants Development**

#### **4.3.6.1 Immunisation Trials in Mice**

The developed formulations JS-1; -2; -3; -4 were tested in an immunisation trial with VAK911. To ensure comparability, the squalene amount was adjusted to 2.15 mg per injection. All vaccinated mice showed a reliable antibody production. The replica of AddaVax™ JS-1 had the same effect as the market product. As the production by the hot melt emulsion method and high pressure homogenisation could not be run under aseptic conditions, this confirmed that no impurities like pyrogens led to an increased immune response.

There was no difference between the liquid (JS-1) and the solid squalene formulation (JS-3). Although the adjuvant effect of saponins and its purified derivatives are well known, the addition of saponin did not further stimulate the antibody response in JS-2 [42,48]. It was not able to increase the adjuvant effect in the formulation JS-4 by the use of mannide monooleate as lipophilic emulsifier. The stimulating effect of mannide monooleate was mainly attributed to impurities [160]. All squalene containing groups induced antibody titres at the same level (Figure 37). It was concluded that the adjuvant effect was mainly dependent on the nanosized squalene. It has to be taken into account that these findings were limited to the experimental setup with IBDV VP2 antigen in mice. The immune stimulating effects of adjuvants are highly dependent on the antigen,

animal species and the route of administration [31]. Otherwise, the immune response is not only limited to the humoral immune response. Examining the antibody response is not able to investigate the cellular immune response e.g. by cytotoxic T-lymphocytes [216]. Especially saponins are capable to induce the production of cytotoxic T-lymphocytes as further adjuvant effect [42,217]. However, the humoral immune response is expected as the dominant defense mechanism against the infectious bursal disease virus. The current assessment of protective vaccines is only based on the quantity of the produced antibodies [102,218]. Further immunological tests were not performed in mice. Histopathological investigations and challenge experiments were performed in the target organism.

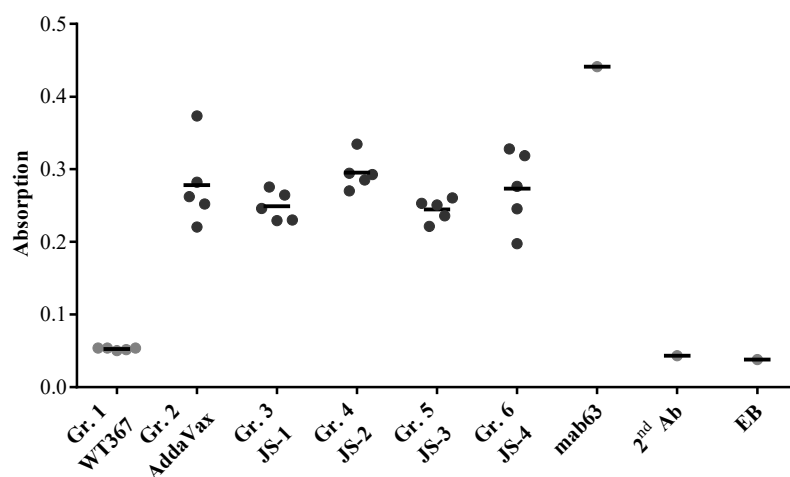


**Figure 37.** ELISA results of AT19: The absorption was determined as parameter for the immune response in mice against VAK911, adjuvanted with the developed nanosized squalene formulations JS-1; -2; -3; -4 and AddaVax<sup>TM</sup>, in comparison to the response against WT367. ELISA buffer (EB), mab63 and 2<sup>nd</sup> antibody were examined as controls for the ELISA. The exact group arrangement is explained in Table 16.

**Table 16.** Group arrangement and immunisation conditions of AT19, examining the effect of the developed nanosized squalene containing formulations.

Group	Yeast	Adjuvant	Amount	Schedule	Processing
1	WT367	AddaVax <sup>TM</sup>	3x 0.1 mg	2-2-1	Standard
2	VAK911	AddaVax <sup>TM</sup>	3x 0.1 mg	2-2-1	Standard
3	VAK911	JS-1	3x 0.1 mg	2-2-1	Standard
4	VAK911	JS-2	3x 0.1 mg	2-2-1	Standard
5	VAK911	JS-3	3x 0.1 mg	2-2-1	Standard
6	VAK911	JS-4	3x 0.1 mg	2-2-1	Standard

Except the saponin containing formulation JS-2, all developed formulations provided excellent biocompatibility. The saponin groups provoked slight irritations at the injection sides, but were much weaker than of Freund's Adjuvant. The slight local inflammation was limited to the application side and cured after some days. In contrast, CFA and IFA caused massive irritations, because of the non-degradability of paraffin oil, and they increased over time. Beside the local inflammation, it resulted in hair loss and bites at the injection sides. Nevertheless, all mice showed a comparable gain in their body weight during the experiment.

Because of the comparable immune stimulation of the developed adjuvants and the promising storage conditions, as dried powder of the solid squalene particles, the solid lipid nanoparticle formulation was further developed. The formulation JS-3 was optimised with the aim to get a formulation with a higher lipid content which can be sterilised and freeze-dried. This optimised formulation JS-3o and its steam sterilised and freeze-dried forms were investigated in a mice immunisation trial.

**Table 17.** *Group arrangement and immunisation conditions of AT21, examining the effect of steam sterilisation and lyophilisation of the leading developed formulation JS-3o.*

Group	Yeast	Adjuvant	Amount	Schedule	Processing
1	WT367	AddaVax <sup>TM</sup>	3x 0.1 mg	2-2-1	Standard
2	VAK911	AddaVax <sup>TM</sup>	3x 0.1 mg	2-2-1	Standard
3	VAK911	JS-3o	3x 0.1 mg	2-2-1	Standard
4	VAK911	JS-3o Autocl.	3x 0.1 mg	2-2-1	Standard
5	VAK911	JS-3o Lyoph.	3x 0.1 mg	2-2-1	Standard

Like the other squalene containing nanosized formulations, JS-3o and its derivatives were adjusted to 2.15 mg squalene per injection and induced a comparable antibody response as the market product AddaVax<sup>TM</sup> (Figure 38). Although the freeze-dried form differed in the particle size distribution with a z-average of 190 nm instead of 145 nm, this had no influence on the adjuvant effect. All animals reacted with a reliable antibody production. The slight differences in the mean antibody titres were attributed to the low group size of 5 mice per group and the large standard deviations.

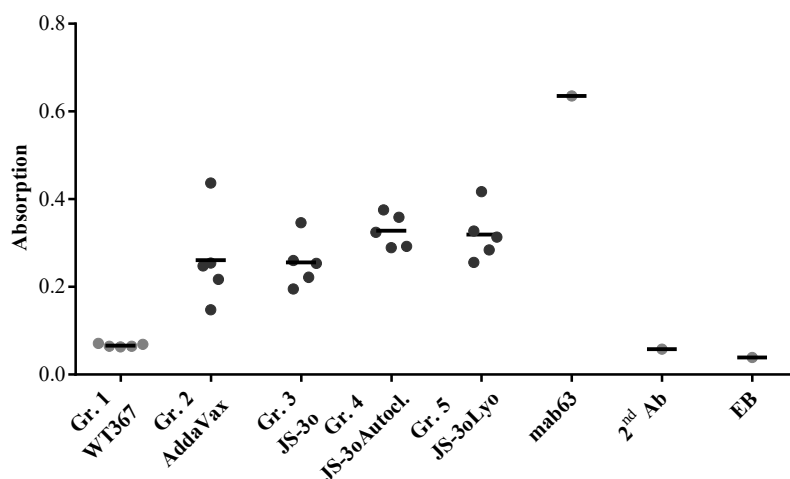


**Figure 38.** ELISA results of AT21: The absorption was determined as parameter for the immune response in mice against VAK911, adjuvanted with JS-3o, its sterilised and lyophilised forms and AddaVax<sup>TM</sup>, in comparison to the response against WT367. ELISA buffer (EB), mab63 and 2<sup>nd</sup> antibody were examined as controls for the ELISA. The exact group arrangement is explained in Table 17.

The final mice immunisation trial AT23 was performed to investigate the dose dependency and to compare the immune response with an unadjuvanted yeast vaccine. Furthermore, the immune stimulating effect of squalene-free SLNs, based on Softisan 154 and Poloxamer 188, were examined, as the adjuvant effect of solid lipid nanoparticles as “stable biocompatible adjuvant” has been reported and patented [86,88]. The standard squalene amount 2.15 mg, 0.54 mg and 8.6 mg per injection were tested for the dose dependency. As the lipid phase of JS-3o contained of squalene and Softisan 154 in equal parts, the lipid concentration was the double of the squalene concentration. Additional, the placebo lipid formulation PS154 was applied at the same dose.

The unadjuvanted VAK911 caused no production of antibodies against IBDV VP2, confirming that an adjuvant is necessary for a sufficient immune response (Figure 39). For JS-3o there was a dose dependent immune response. At the lowest squalene concentration, antibodies were only detectable in 2 of 5 mice. Increasing the squalene amount led to a more reliable antibody response. All vaccinated mice showed an immune reaction with the standard and 4-fold adjuvant amount. The mean absorption, as surrogate for the antibody titre, increased with the squalene amount. Interestingly, the squalene increase made the response more reliable, but the maximal antibody response was not influenced. It was assumed that a certain adjuvant amount is necessary to induce the immune reaction. A further stimulating effect can just be expected for none

or partly responding mice. A dose dependent effect of the antigen and MF59<sup>®</sup> amount has already been shown for influenza A/H5N1 in humans. Only 25 % of the standard dose of MF59<sup>®</sup> was sufficient to induce a strong immune response. In contrast, increasing the antigen amount to the 4-fold dose provided just low additional stimulating effects [219,220]. Because of the low costs and good availability of the adjuvants, it is favoured to increase the adjuvant amount instead of the antigen amount or numbers of immunisations. As the higher adjuvants dose did not cause side effects, it should be tested for further experiments and antigens.

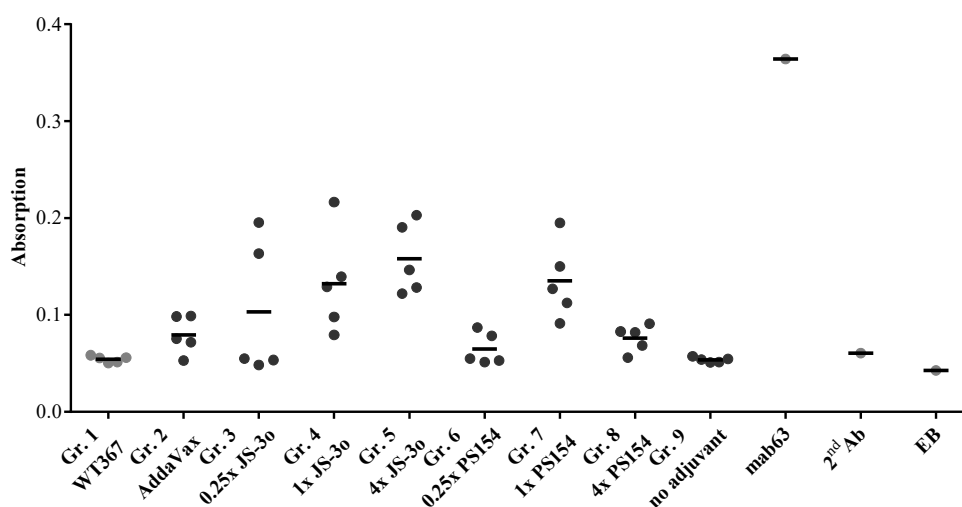


**Figure 39.** ELISA results of AT23: The absorption was determined as parameter for the immune response in mice against VAK911, adjuvanted with the standard, 4-fold and 0.25-fold dose of JS-3o and PS-154, AddaVax<sup>TM</sup> and without adjuvant, in comparison to the response against WT367. ELISA buffer (EB), mab63 and 2<sup>nd</sup> antibody were examined as controls for the ELISA. The exact group arrangement is explained in Table 18.

**Table 18.** Group arrangement and immunisation conditions of AT23, examining the dose response correlation of JS-3o and the adjuvants properties of squalene-free SLNs.

Group	Yeast	Adjuvant	Amount	Schedule	Processing
1	WT367	AddaVax <sup>TM</sup>	3x 0.1 mg	2-2-1	Standard
2	VAK911	AddaVax <sup>TM</sup>	3x 0.1 mg	2-2-1	Standard
3	VAK911	25 % JS-3o	3x 0.1 mg	2-2-1	Standard
4	VAK911	100 % JS-3o	3x 0.1 mg	2-2-1	Standard
5	VAK911	400 % JS-3o	3x 0.1 mg	2-2-1	Standard
6	VAK911	25 % PS154	3x 0.1 mg	2-2-1	Standard
7	VAK911	100 % PS154	3x 0.1 mg	2-2-1	Standard
8	VAK911	400 % PS154	3x 0.1 mg	2-2-1	Standard
9	VAK911	no	3x 0.1 mg	2-2-1	Standard

The placebo formulation PS154 did not or just minimal interacted with the immune system at the lowest and highest concentrations. Surprisingly, the standard lipid concentration resulted in antibody titres. Impurities or other mistakes during the sample preparation like transposition of samples were made responsible for this result, as there was no antibody response at the highest concentration. Additionally, the control group with AddaVax<sup>TM</sup> showed only minor immune reactions, underlining the theory of sample transpositions. This led to a partly repetition of the experiment.

The test of the squalene-free SLNs was repeated. VAK911 was adjuvanted with the three different concentrations of PS154 and was compared against the standard squalene amount of JS-3o. In contrast to the single dose of JS-3o, no dose of the placebo SLNs were able to induce an immune reaction. This clarified that the squalene in the nanometre range was responsible for the adjuvant effect. Although it has been claimed by Müller *et al.* that solid lipid nanoparticles act as an adjuvant [86], this was in contradiction to the performed experiments for the squalene-free system. Furthermore, they were just able to demonstrate an adjuvant effect of their reported formulations which were composed of known adjuvants [88]. An immune stimulating effect could be assumed, due to their composition. Paraffin was introduced by Jules Freund in 1937 in IFA and CFA [30]. Paraffin is not used in humans and current adjuvants development avoids its use, because of its toxicity and serious side effects, like the formation of granulomas and necrosis at the injection side [36]. The use of Esterquat 1 (N,N-Di-( $\beta$ -stearoylethyl)-N,N-dimethyl ammonium chloride) as cationic emulsifier to develop particles with an positive surface charge is a common adjuvant mechanism [47,89,221]. Positively charged particles enhanced the uptake by macrophages and dendritic cells [14,15].

#### **4.3.6.2 Tracking of the Squalene Based SLN Formulation**

The mechanism of the adjuvant effect of squalene has not been fully understood yet. Early investigations by Ott *et al.* with radiolabelled nanosized squalene and antigen showed a fast clearance of squalene and the antigen from the injection side after intramuscular application. Six hours after application, only 10 % of the squalene and 25 % of the antigen were present at the injection side. After 5 days, just 5 % squalene and 0.05 % antigen remained [68]. Thus, the formation of a local depot for a controlled release of antigen and adjuvant over a several days, as it is known for water in oil emulsion like Freund's Adjuvant, can be excluded. However, squalene stimulates the

immune system by causing a local immunocompetent environment at the area of injection. For HIV envelope protein gp120 antigen in mouse, it has been shown that the antibody titre just increased by injection of the antigen and MF59<sup>®</sup> at the same injection side [222]. Furthermore, a delayed injection of an antigen intramuscularly in rabbits, 24 h after the injection of MF59<sup>®</sup> at the same side, had the same effect as injected together. Otherwise, there was no effect, if the antigen was applied 24 h before the adjuvant [68].

To investigate the biodistribution of this special SLN formulation, the optimised formulation JS-3o was labelled fluorescently with DiR and tracked by non-invasive multispectral fluorescence imaging. DiR is characterised by its fluorescence in the near infrared range (excitation maximum at 748 nm and emission maximum at 780 nm) [223], providing a good tissue penetration, due to minimal absorption on water, blood and cells in the range between 650 nm and 950 nm [224]. Lipophilic fluorescence tracers like DiR have been used in several studies to track nanoparticle formulations [179,225]. To quantify the fluorescence results, the concentration of DiR was 0.4 % of the lipid content. Concentrations up to 0.5 % are below the quenching range and consequently give a linear correlation between the dye concentration and the fluorescence intensity [225,226].

The particles were produced as described in chapter 3.1. The fluorescence dye was dissolved in the liquid lipid mixture at 65°C during the particle preparation. To get rid of not encapsulated dye, the formulation was centrifuged for 30 min at 200000 g on an Optima MAX XP (Beckmann Coulter, Brea, USA). The unencapsulated dye and the Poloxamer 188 containing aqueous phase were withdrawn and the particles were resuspended in fresh medium. After three purification cycles, more than 92 % DiR was entrapped in the particles. Neither the incorporation of DiR nor the ultracentrifugation steps had a substantial effect on the particle size distribution (Figure 40). Unstained JS-3o and the raw formulation were characterised by the same median particle size  $D_{(0.5)}$  around 125 nm and z-average around 140 nm, but differed in their uniformity. For JS-3o no particle was larger than 317 nm. In contrast, 7 % of the fluorescently labelled particles (volume weighted) exceeded this size up to a size of 10  $\mu\text{m}$ . As a side effect beside the purification from untrapped dye, ultracentrifugation influenced the size distribution positively. High centrifugal forces up to 200000 g did not lead to aggregation of the particles and narrowed the size distribution. Small particles were

removed, because of their higher speed of diffusion, and withdrawn with the centrifugate. Larger particles aggregated because of their large contact area and could not be resuspended in fresh media. The size distribution of the purified formulation with a z-average of 125 nm and a PDI of 0.059 confirmed with the specifications of the commercial available AddaVax™ (120-170 nm).

Because of the structure as an amphiphile and its former use to stain membranes, the fluorescence dye could interact at the oil-water interface. The high amount of unencapsulated dye, with 45 % before the purification steps, confirmed that the dye was solubilised by the emulsifier Poloxamer 188. At room temperature the critical micelle concentration of Poloxamer 188 is around 0.1 % [227,228]. With increasing amounts of the surfactant the surface becomes saturated and consequently aggregates of tensides molecules are formed. Micelles represent an ideal environment for the uptake of lipophilic molecules like DiR [229,230]. After the purification step, the lipid content had been measured in the purified formulation with 39.7 mg per ml by weighting the remaining lipid mass after vaporization the media and by fluorescence measurements. Each mouse obtained a dose of 2.15 mg squalene and 0.1 mg VAK911 in a volume of 120 µl of isotonic phosphate buffer pH 7.2. Three mice were investigated 0 h, 12 h and 24 h after the immunisation and then twice a week over 23 days.

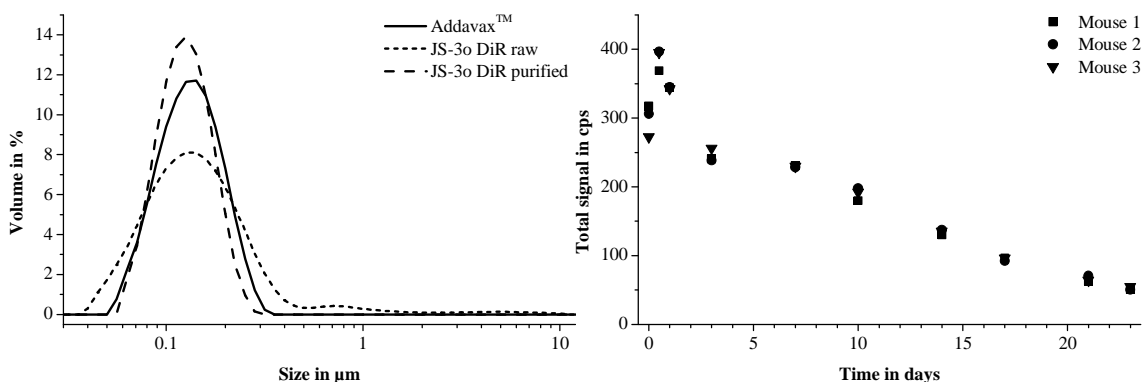


**Figure 40.** Left: Size distribution of DiR labelled squalene nanoparticles before and after purification in comparison to AddaVax™. Right: Fluorescence intensity of DiR labelled JS-3o in three mice over 23 days.

In the first 12 h after application the fluorescence intensity increased by 30 % because of local distribution processes. After subcutaneous application into the nuchal fold, the formulation spread locally over the back of the neck. Comparing the fluorescence signal after 12 h resp. 24 h with the intensity directly after the application in Figure 41 showed an expansion of the illuminating area and a decrease of the maximal fluorescence

intensity. In addition, the fast resorption of the applied liquid volume decreased the sample thickness and so the thickness of light absorbing layers. Although near infrared light is known for its relative low absorption on water and cells, this effect caused the increase of the total fluorescence signal within the first 12 h (Figure 40) [224]. For the calculation of the amount of the remaining formulation, the fluorescence intensity of the DiR spectra over the whole imaging area was reduced by the intensity of the untreated mouse. The translocation of the fluorescent formulation is clearly visible in Figure 41, when the fluorescence signal changed from a defined area with a high intensity, directly after application, to a larger less specific area. In mouse 2 the formulation migrated even to the left subaxillary area, as clearly notable after 12 h and 24 h in Figure 42 (arrow A).

Within the next 22 days the distribution did not change, but the fluorescence intensity declined congruently in all animals to 13 % at day 23. Beside the subcutaneous dislocation and the elimination, the biodistribution of the formulation was investigated fluorescently from the ventral side (Figure 42).

All three mice showed a fluorescence signal in the axillary area, indicating an accumulation in the subaxillary lymph nodes (arrow B). Lymph nodes on both sides right and left were affected, excluding just an effect of the migrated particles like on the left side of mouse 2. For lipid particles it is well known that they can be eliminated by lymphatic uptake [231,232]. However, there was no fluorescence signal in the lymph nodes after preparation at day 23, indicating that the elimination of the formulation had been finished.

Mouse 1 und 2 showed strong fluorescence signals of DiR in the area of the bladder and preputial gland with maxima within the first days after application (arrow C). During this period the elimination rate of the lipid nanoparticles reached its maximum. As mouse 3 showed not fluorescence signal in the bladder and the urine was fluorescently active, this was attributed to urination prior the measurements as a common effect to anaesthesia. Furthermore, this proved the accumulation in the bladder instead of the preputial gland. The signal in the bladder did not represent an accumulation of the formulation in the bladder, it represented the excreted fluorescence dye amount per time. Therefore, a renal excretion of biotransformed DiR can be assumed.

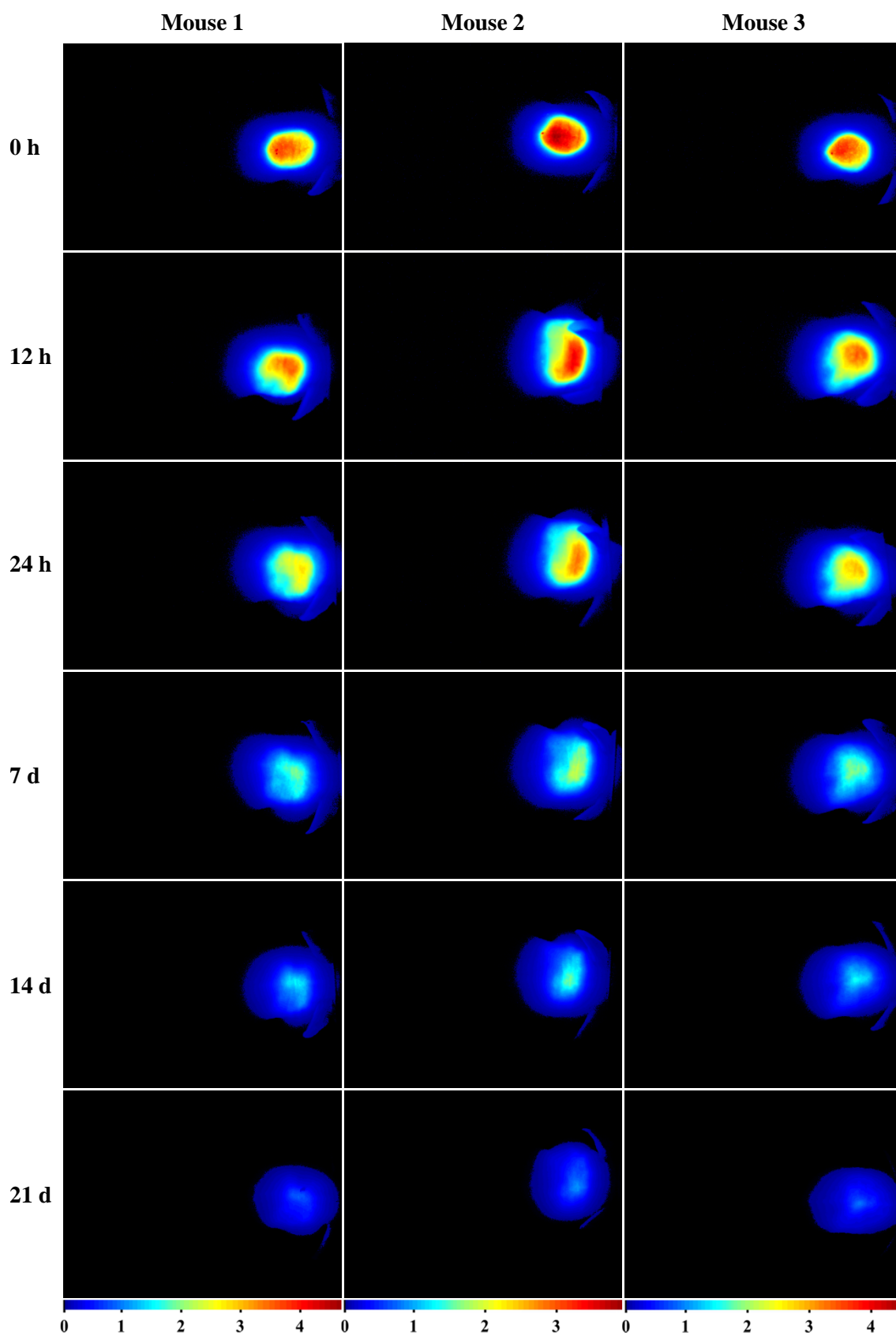


**Figure 41.** Time dependent fluorescence intensity of DiR labelled nanoparticles JS-30 on the back of three male SKH-1 mice over 21 days. Scales represent the unmixed fluorescence intensity of DiR in each mouse.

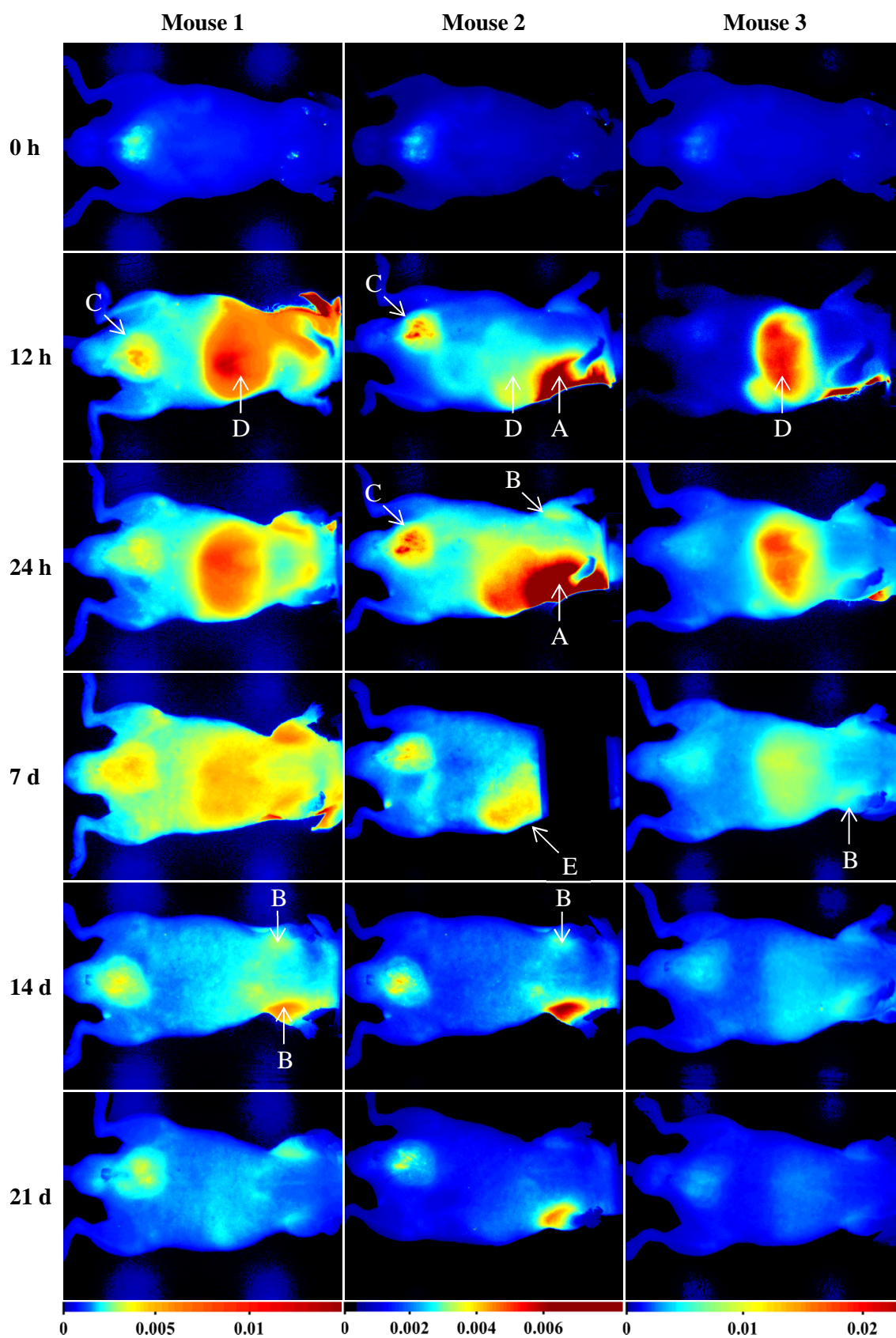


**Figure 42.** Time dependent fluorescence intensity of DiR labelled nanoparticles JS-30 on the ventral side of three male SKH-1 mice over 21 days. Scales represent the unmixed fluorescence intensity of DiR in each mouse. The arrows indicate the following regions: A subaxillary area, B subaxillary lymph nodes, C bladder, D and E liver.

All mice showed massive accumulation tendencies of the fluorescently labelled nanoparticles in the livers already 12 h after the application (arrow D). The lower fluorescence intensity of the liver in mouse 2 can be explained by the migration of the SLNs from the neck to the left flank. In the following, the high intensity on the left side was caused by the applied formulation and masked the fluorescence signals of the liver. Nevertheless, a detailed view and coverage of the large fluorescence signal of the translocated formulation proved the accumulation in the liver after 7 days (arrow E). The accumulation in the liver was dominant during the whole examination period, but decreased with further elimination of the formulation. It was attributed to the elimination of nanoparticles by the reticuloendothelial system and due to the rich blood supply [233]. The reticuloendothelial system comprises the phagocytic cells of the immune system, mainly of tissue macrophages in lymph nodes, the spleen and the Kupffer cells in the liver [234]. Polyethylene glycol is known to provide a stealth effect. The presentation of hydrophilic structures on the surface of nanoparticles protected them from their uptake by macrophages [235]. This phenomenon was desired for nanoparticles to increase their circulation time and to ensure the accumulation of cytostatics in tumors for example [236]. As the developed formulation was eliminated slowly after the subcutaneous application, there was no need to establish a stealth effect. In contrast, for vaccine formulations it is a common strategy to promote the uptake of the antigen by immune competent cells [34]. The AddaVax™ control verified the absence of negative effects of Poloxamer 188 on the immunogenicity in all immunisation experiments.

Elimination and biodistribution studies of MF59® were performed in the past by Ott *et al.* to investigate the adjuvant mechanism. After intramuscular application of radiolabelled squalene and antigen the elimination was followed for 5 days. Both were eliminated very fast in the first 6 h, disconfirming the theory of the formation of a local antigen depot. Five days after the immunisation just 5 % of the squalene remained at the injection side [68]. More detailed investigations, comparing the distribution and accumulation of the squalene, were performed in 1999 by Dupuis *et al.*, using radiolabelled <sup>3</sup>H-squalene and fluorescently labelled squalene. After intramuscular injection, the half-life period was estimated with 42 h, but it was eliminated from the injection side with a shorter half-life period of 2.5 h. Large quantities were distributed

rapidly to the blood, liver and inguinal fat, already after 4 h [67]. Additionally, the adjuvant had been detected in the draining lymph nodes [67,70].

The work has shown a similar elimination kinetic and distribution to the liver and lymph nodes. In contrast to the literature, the formulation remained at the injection site for longer times. As the assumed adjuvant mechanism of nanosized squalene is the generation of a local inflamed area, this could provide an enhanced immune stimulating effect [222].

#### **4.3.6.3 Immunisation Trials in the Target Organism Chicken**

The infectious bursal disease virus causes significant economic losses in poultry farms by its mortality, exceeding 50 % for very virulent strains [99], and long-lasting immunosuppression by the destruction of the lymphoid follicles in the bursa of Fabricius, making the animals susceptible for secondary infections. Because of the various possible secondary infections and the varying virulence, the exact economic loss could not be calculated [237]. Nevertheless, the gumboro disease was described as the most important disease in the global chicken production [103].

The immunisation of the target species was investigated with the optimised VAKJS71, adjuvanted with the sterilised and freeze-dried form of JS-30, in comparison with the commercial adjuvant AddaVax<sup>TM</sup>. WT367 and PBS were given as negative controls. The exact group arrangement is explained in Table 19. During the immunisation study the antibody titres were monitored weekly. Before the first immunisation, no VP2 antibodies were detectable in any animal, ensuring the absence of IBDV pathogens in the SPF chickens. The antibody titres of the immunisation and challenge experiment are given in Figure 43.

After 10 days, all vaccinated chickens showed an immune reaction with low antibody titres. Full seroconversion was reached after the second application. Six days after the boost, a strong antibody response with mean titres of 5000 was raised by both squalene containing formulations. Although the immune response was reliable in all animals, the titres differed in a range from 3500 to 7000. During the following seven days, the antibody titres increased only slightly, indicating the necessity of the booster immunisation for a reliable immune response.

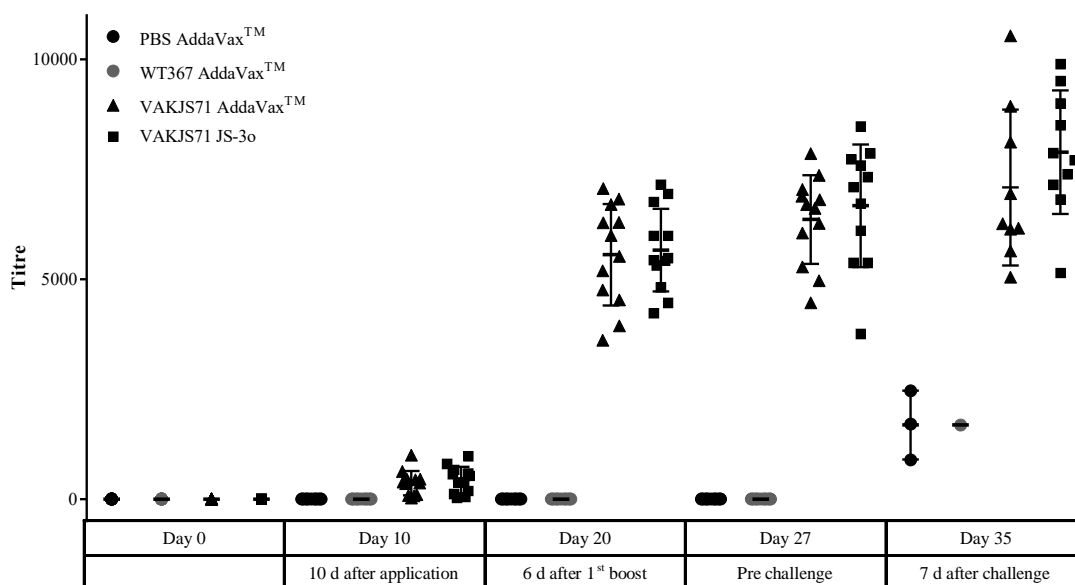


**Figure 43.** HTV8: Development of the antibody titres in chickens against VP2 in with AddaVax<sup>TM</sup> and JS-3o adjuvanted VAKJS71 in comparison to PBS control and antigen free WT367 over 35 days. The exact group arrangement is explained in Table 19. Single values and mean  $\pm$  standard deviation.

**Table 19.** Group arrangement and immunisation conditions of HTV8, investigating the adjuvant effect of AddaVax<sup>TM</sup> and JS-3o in chickens.

Group	Yeast	Adjuvant	Amount	Schedule	Processing
1, PBS	no	AddaVax <sup>TM</sup>	2x 10 mg	2-2	Standard
2, WT367	WT367	AddaVax <sup>TM</sup>	2x 10 mg	2-2	Standard
3, AddaVax <sup>TM</sup>	VAKJS71	AddaVax <sup>TM</sup>	2x 10 mg	2-2	Standard
4, JS-3o	VAKJS71	JS-3o Autocl.+ Lyo.	2x 10 mg	2-2	Standard

To estimate the protectivity, half of the groups were challenged with  $10^4$  EID of a very virulent IBDV strain (vvIBDV Strain 89163/7.3, Etteradossi, France) [134]. The remaining unchallenged animals were used as control groups for the histopathological examinations and the bursa to bodyweight ratio. All adjuvants were able to raise full protection against the very virulent IBDV strain (Table 20). No VAKJS71 immunised chicken died or has shown any clinical signs of morbidity, like ruffled feathers, exhaustion, dehydration and watery diarrhoea [237]. In contrast, all animals of the negative controls have shown severe clinical symptoms and 90 % of the WT367 and 66 % of the PBS negative control group died. The virus challenge induced the production of antibodies in both negative control groups at higher levels than 10 days after the first immunisation in the vaccine groups. This clarified the potential of live-

attenuated viruses because of their promoted recognition and interaction with the immune system. Infection with vvIBDV increased the antibody titres in the vaccine groups only slightly, confirming that a third immunisation was not necessary.

**Table 20.** Morbidity and mortality of the JS-3o and AddaVax<sup>TM</sup> adjuvanted yeast vaccine VAKJS71 in comparison to antigen free yeast VAK367 and PBS control.

Group	Morbidity	%	Mortality	%
1, PBS	9/9	100 %	6/9	66 %
2, WT367	10/10	100 %	9/10	90 %
3, AddaVax <sup>TM</sup>	0/9	0 %	0/9	0 %
4, JS-3o	0/10	0 %	0/10	0 %

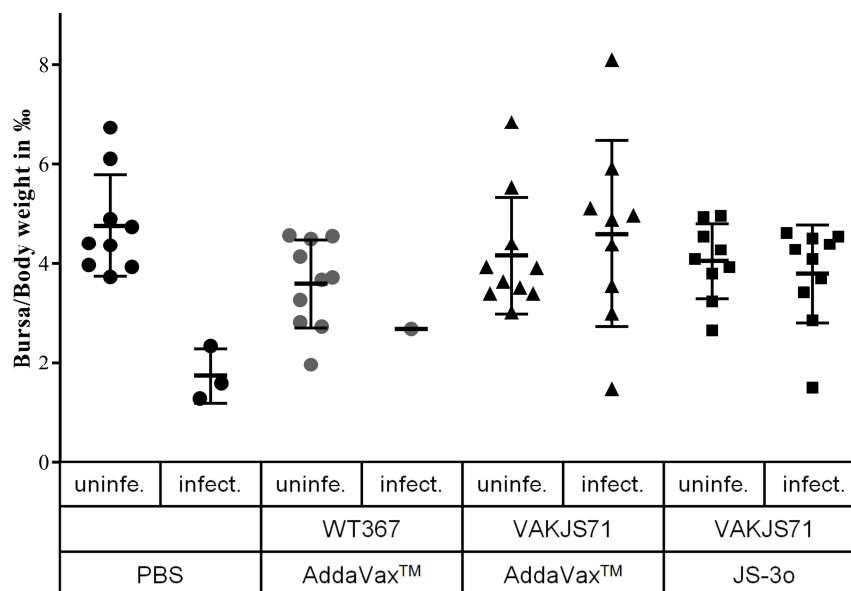


**Figure 44.** Bursa to body weight ratio of infected (*infect.*) and uninfected (*uninfe.*) subgroups of the challenge experiment of HTV8. Single values and mean  $\pm$  standard deviation.

Finally, all chickens were sacrificed and the body and bursa weights were determined to calculate the bursa to bodyweight ratios with the formula by Sarachai *et al.* [238]. In the challenged subgroups of the PBS resp. VAK367 group, just three resp. one chicken were available for the determination of the bursa to body weight ratio, because of the high mortality of the vvIBDV strain (Figure 44). These surviving animals showed a massive decrease in their bursa to bodyweight ratio. As the infectious bursal disease virus causes massive damage and atrophy of the bursa, the weight ratio can be used to determine the severeness of the infection. The challenge of VAKJS71 vaccinated

chickens had no influence on the bursa to body weight ratio and corresponded with the good protection of the examined vaccine formulations.

Initially, the bursa lesions were investigated macroscopically and assessed by the bursa lesion score from 0 to 4 as following: 0 unchanged, 1 gel like swollen, 2 petechial haemorrhages, 3 complete haemorrhages and atr. for completely atrophied. Furthermore, the bursa samples were fixated with formalin and stained with haematoxylin and eosin to be investigated microscopically. The samples were assessed by the histology score introduced by Sharma *et al.* in 1989 on the basis of lymphoid necrosis and depletion [238]. According to the affected parts of the lymphoid follicles, less than 5% led to a histo score of 0; 5-25 % to a score of 1; 25-50% to a score of 2; 50-75 % to 3 and more than 75 % affected lymphoid follicles led to a histo score of 4.

**Table 21.** Bursa lesion score and histology score of the bursa of Fabricius of the challenged and control groups in HTV8.

Group		Lesion Score					Histo Score				
		0	1	2	3	atr.	0	1	2	3	4
1, PBS	Unchallenged	9x	0	0	0	0	9x	0	0	0	0
	Challenged	0	1x	3x	1x	4x	0	0	0	0	9x
2, WT367	Unchallenged	10x	0	0	0	0	10x	0	0	0	0
	Challenged	0	0	4x	4x	2x	0	0	0	0	10x
3, AddaVax™	Unchallenged	10x	0	0	0	0	10x	0	0	0	0
	Challenged	7x	2x	0	0	0	6x	1x	1x	1x	0
4, JS-3o	Unchallenged	9x	0	0	0	0	9x	0	0	0	0
	Challenged	8x	2x	0	0	0	8x	0	1x	0	1x

Table 21 presents the lesion and histo scores of HTV8. All unchallenged animals showed no macroscopic and histopathological changes in the bursa of Fabricius. In contrast, the challenge of unvaccinated animals led to massive damage of the bursa of Fabricius. Already the macroscopic investigation revealed a complete atrophy of the bursa in 4 chickens in the PBS group and 2 chickens in the WT367 group. The remaining animals in these groups showed all severe macroscopic changes of the bursa with lesion scores of 2 and 3, except one chicken with a lesion score of 1. Nevertheless, the histopathological investigation resulted in a histo score of 4 for all unvaccinated animals in group 1 und 2, indicating a nearly full atrophy of the lymphoid follicles. The

macroscopic determined lesion score can just be applied as initial assessment, as the detailed depletion of the lymphatic tissue can just be examined microscopically.

Both squalene adjuvanted groups were protected partially. 80 % of the JS-3o adjuvanted and challenged chickens showed no macroscopic lesion or histological signs of necrosis in the lymphatic tissue and were fully protected. However, in two chickens the lymphoid tissues were affected. Already in the macroscopic investigation, a lesion score of 1 was determined for 2 animals in the JS-3o group. The damage was assessed with a histo score of 2, moderate damage, and a score of 4, complete depletion of the lymphatic tissues. The AddaVax<sup>TM</sup> group reacted comparably, 67 % were fully protected and each one of three bursae had a histo score of 1; 2 and 3, while the macroscopic investigation only assessed a lesion score of 1 in two animals. The protection was attributed to the adjuvant effect of the nanosized squalene. Interestingly, the differences between the vaccinated animals appeared only in the histology, while the antibody responses, morbidities and bursa to bodyweight ratios were comparable. Comparing the raised antibody titres with the lesion scores and the bursa to body weight ratios did not reveal a correlation. Although the control groups proved that a protective effect was associated with the production of antibodies, high antibody titres were not accompanying necessarily with low histo and lesion scores and high bursa to body weight ratios. These findings were in contrast with the current method to assess the quality of IBDV vaccines just on the amount of induced antibodies [102,218]. Experiments using thymectomy and Cyclosporine A to silence the T-cell response, indicated, that T-lymphocytes were necessary to ensure a full protection [218].

Vaccination with mild and intermediate strains of live attenuated viruses have shown to cause damage in the bursa itself [102]. Despite this side effects intermediate and intermediate plus vaccines were not fully protective against vvIBDV. 75 % of the intermediate plus vaccinated chickens developed a lesion score of 3 or 4 after challenge with vvIBDV and led to a decrease in the bursa to body weight ratio [108]. The developed vaccine system of VAKJS71, adjuvanted with JS-3o, reached a higher protectivity against vvIBDV. Only 10 % reacted with a bursa score of 3 or higher and the bursa to body weight ratio did not decrease. Most commercially available IBDV vaccines are less effective in the presence of maternally antibodies and do not provide protection against very virulent strains [106]. Additional, the use of a single antigen, instead of a live attenuated vaccine, prevented from infection and lesion by the vaccine.

---

Further experiments should be performed using an increased adjuvant amount. The mice experiments revealed that an increase of the adjuvant amount has made the immune response more reliable.

## **5 Conclusion and Outlook**

Aim of this work was to develop a vaccine formulation for a novel yeast based vaccine against the infectious bursal disease virus in chicken. As the yeast vaccine is storable as dry powder at room temperature for years, the final formulation should contain the adjuvant as dry powder. The ideal adjuvant would provide a strong antibody response, excellent biocompatibility and stability as well as cheap production costs to be competitive with the market products.

Primary immunisation trials have shown comparable adjuvant effects of the squalene containing nanoemulsion AddaVax<sup>TM</sup> and the gold standard Complete Freund's Adjuvant in mice. AddaVax<sup>TM</sup> is also known as MF59<sup>®</sup> and has been used in more than 150 million immunisations in humans since its approval in 1997 [60]. The formulation of squalene together with the high melting lipid Softisan 154 resulted in a solid lipid nanoparticle formulation. Additionally, saponins and mannide monooleate were introduced to squalene nanoemulsions to promote the adjuvant effect of the squalene nanoemulsion. All liquid lipid formulations were prepared by high pressure homogenisation at room temperature resp. using the hot melt emulsion homogenisation method for the solid lipids.

The size of all adjuvant systems was characterised in detail by static and dynamic light scattering, nanoparticle tracking analysis and AF4/MALLS. All nanoparticle formulations were preparable in the size range of the market product AddaVax<sup>TM</sup> 120-170 nm. Nevertheless, the saponin containing formulation and the primary SLN formulation JS-3 showed a broader particle size distribution and were only stable for 2 months. All other developed formulations were nearly identical to AddaVax<sup>TM</sup> and provided excellent stability over 12 months. The final formulation contained 5 % squalene, 5 % Softisan 154 and was stabilised with 5 % Poloxamer 188. It could be autoclaved successfully without any change in the particle size distribution and freeze-dried with 10 % sucrose and 2 % PVA. The mean particle diameter of the resuspended lyophilisate just increased by 20 nm by the formation of a second particle species around 1 µm, comprising only 1.5 % of the particle volume. At 4°C the lyophilisate showed no change in the particle size over one year. Even at 25°C, it was stable for 6 months, providing the possibility of storage at room temperature after dispensing to

the user resp. veterinarian. Then the application of the formulation has to be assured within 6 months.

The incorporation of squalene into the Softisan matrix has been investigated by DSC, <sup>1</sup>H-NMR and X-ray diffractometry. Adding squalene to Softisan forced the recrystallization of the hard fat in the stable  $\beta$ -modification. In contrast to this, a placebo SLN formulation of Softisan resulted in an instable modification after preparation and transition into the stable modification within 7 days. The linear decrease of the melting temperature by the addition of squalene to Softisan, X-ray and <sup>1</sup>H-NMR data suggested a homogeneous distribution of the squalene as nanosized liquid domains in the solid triglyceride matrix.

Tests on cytotoxicity revealed a toxic effect of the squalene nanoparticles itself. This was explained with the adjuvant mechanism of nanosized squalene by the induction of a local inflamed and immunocompetent area at the injection side. The toxicity of the emulsifiers was compared with the emulsifiers of the market product. While even high concentrations of Poloxamer 188 had no influence on the cell viability, saponin was cytotoxic as expected. In contrast to Freud's Adjuvant, the final formulation provided excellent biocompatibility in mice and chicken. Only the saponin containing formulation showed slight signs of irritation at the injection side for some days after the injection.

Tracking of the fluorescently labelled formulation JS-3o supported the theory of a local immunocompetent area. The largest quantities remained at the injection side for 23 days. Lower amounts were detected in the liver and the lymph nodes. The strong accumulation in the liver was attributed to the elimination of the nanoparticles by the reticuloendothelial system.

Immunisation trials in mice verified the immune stimulating effect of all squalene based adjuvants. There were no differences between any processed formulation and additional adjuvants like MMO and saponins in comparison to the market product AddaVax<sup>TM</sup>. Although different arms of the immune system can be stimulated by different adjuvants, only the antibody response is used for the assessment of IBDV vaccines [102,218]. The main adjuvant effect was attributed to the nanosized squalene. Increased adjuvants concentrations indicated a dose dependent adjuvant effect. While an increased squalene amount did not improve the antibody response of well reacting animals, it decreased the

number of non or partly responding animals. Squalene-free solid lipid nanoparticles did not stimulate the immune system.

Immunisation trials in chickens resulted in comparable antibody titres of the final freeze-dried formulation and AddaVax<sup>TM</sup>. Further challenge experiments in chickens, using a very virulent IBDV strain, resulted in full protectivity in both groups. Unvaccinated chickens showed massive bursa lesions and 67-90 % of the unvaccinated animals died. Whereas no vaccinated animal showed signs of sickness, the histopathological investigation of the bursa revealed bursa lesions in 20-30 % of the animals. In contrast to commercial live attenuated vaccines against very virulent IBDV, the yeast vaccine did not cause bursa lesions itself. Further experiments should be performed using an increased squalene dose.

The final formulation JS-3o fulfilled the main requirements of the ideal adjuvant. The final ready to use vaccine formulation was storable as dry powder of the yeast vaccine and the adjuvant. It provided an excellent immune stimulating effect on the level of AddaVax<sup>TM</sup>, sterility, stability and could be produced in large scales using the preparation methods of MF59<sup>®</sup>. Further improvements of the final formulation should focus on the storage stability at room temperature and the squalene amount. Both could be achieved with a higher melting lipid like glycerol behenate instead of Softisan 154. The preparation process was limited by the homogenisation temperature of 65°C. Nanomilling of squalene lipid mixtures could be an alternative to the high pressure homogenisation at higher temperature. The use of organic solvents should be avoided.

In addition to the adjuvants development, the yeast vaccine was processed with the aim to achieve a defined particle size distribution, sterility and to optimise the immune response to the yeast vaccine. It was possible to inactivate and sterilise the yeast vaccine with 25 kGy resp. 50 kGy  $\gamma$ -irradiation on dry ice without major influence on the antigen amount and the immunogenicity. The  $\gamma$ -irradiation with 50 kGy assured sterility in accordance with the pharmacopoeia and replaced the inactivation step at 90°C for 2 h. Disruption of the yeast cells indicated a strengthened immune response by an enhanced release of the antigen. This effect was limited to low antigen amounts which affected only a low or no immune response. An additional adjuvant effect by  $\beta$ -glucans of the disrupted yeast cell walls could not be demonstrated. Ultrasonication was applied successfully to provide yeast material with a defined particle size. Independent from the

size of the clumped yeast material, the treated yeast occurred mainly in mono- and dimers with constant particle sizes. Ultrasonication had no influence on the integrity of the cell wall and stability of the antigen. Nevertheless, a size dependent immune response to the yeast material was not detectable in immunisation trials in mice. Additionally, the size decrease of the yeast material was performed to develop a controlled release formulation.

The formation of an antigen depot is a common adjuvant principle to increase the interaction time between the antigen and the immune system. Although the yeast vaccine provided very good protectivity, their major drawbacks are the multiple immunisations. For further experiments the formulation should release the antigen over 2-4 weeks to make the booster injections redundant. Initial experiments have already been performed using a matrix of lecithin and hard fat for the controlled release. Softisan based microparticles with encapsulated fluorescently labelled yeast showed no yeast release except an initial burst release of partly encapsulated yeast at the first days. Adding lecithin, it was possible to control the release. The addition of 50 % lecithin extended the release period to 7 days and the addition of only 25 % lecithin extended the release period to 14 days. Nevertheless, the differences in the antigen release did not confirm with the antibody response. Because of the high applied yeast amount and the initial release, all formulations induced a strong antibody response against IBDV. This promising system should be investigated with lower antigen amounts and an additional adjuvant like the developed squalene based SLN formulation.

## **6**     **Appendix**

### **6.1**    **References**

- [1] Plotkin SL, Plotkin SA. A short history of vaccination. *Vaccines*. 2004;5:1–16.
- [2] Gross CP, Sepkowitz KA. The myth of the medical breakthrough: Smallpox, vaccination, and Jenner reconsidered. *Int J Infect Dis*. 1998;3(1):54–60.
- [3] Jenner E. An inquiry into the causes and effects of the variolae vaccine (1798). *The Challenge of Epidemiology: Issues and Selected Readings*. Washington, DC: World Health Organization. 1988:31–2.
- [4] Riedel S. Edward Jenner and the history of smallpox and vaccination. *Proc (Bayl Univ Med Cent)*. 2005;18(1):21–5.
- [5] Hammarsten JF, Tattersall W, et al. Who discovered smallpox vaccination? Edward Jenner or Benjamin Jesty? *Trans Am Clin Climatol Assoc*. 1979;90:44–55.
- [6] Barquet N, Domingo P. Smallpox: The triumph over the most terrible of the ministers of death. *Ann Intern Med*. 1997;127(8):635–42.
- [7] Mercer AJ. Smallpox and epidemiological-demographic change in Europe: The role of vaccination. *Popul Stud*. 1985;39(2):287–307.
- [8] Klein S, Schöneberg I, et al. Vom Zwang zur Pockenschutzimpfung zum Nationalen Impfplan. Die Entwicklung des Impfwesens vom Deutschen Kaiserreich bis heute. *Bundesgesundheitsbl*. 2012;55(11):1512–23.
- [9] Fenner F, Henderson DA, et al. *Smallpox and its eradication* World Health Organization. Geneva, Switzerland. 1988.
- [10] Breman JG, Arita I. The confirmation and maintenance of smallpox eradication. *N Engl J Med*. 1980;303(22):1263–73.
- [11] Baxter D. Active and passive immunity, vaccine types, excipients and licensing. *Occup Med*. 2007;57(8):552–6.
- [12] Ada G. Overview of vaccines and vaccination. *Mol Biotechnol*. 2005;29(3):255–72.
- [13] Akira S, Uematsu S, et al. Pathogen recognition and innate immunity. *Cell*. 2006;124(4):783–801.
- [14] Foged C, Brodin B, et al. Particle size and surface charge affect particle uptake by human dendritic cells in an in vitro model. *Int J Pharm*. 2005;298(2):315–22.

- [15] Thiele L, Merkle HP, et al. Phagocytosis and phagosomal fate of surface-modified microparticles in dendritic cells and macrophages. *Pharm Res.* 2003;20(2):221–8.
- [16] Seong S, Matzinger P. Hydrophobicity: An ancient damage-associated molecular pattern that initiates innate immune responses. *Nat Rev Immunol.* 2004;4(6):469–78.
- [17] Kohler KA, Banerjee K, et al. Vaccine-associated paralytic poliomyelitis in India during 1999: Decreased risk despite massive use of oral polio vaccine. *Bull World Health Organ.* 2002;80(3):210–6.
- [18] Laver WG, Webster RG. Preparation and immunogenicity of an influenza virus hemagglutinin and neuraminidase subunit vaccine. *Virology.* 1976;69(2):511–22.
- [19] Broder KR, Cortese MM, et al. Preventing tetanus, diphtheria, and pertussis among adolescents: Use of tetanus toxoid, reduced diphtheria toxoid and acellular pertussis vaccines recommendations of the Advisory Committee on Immunization Practices (ACIP). *MMWR Morb Mortal Wkly Rep.* 2006;55(RR-3):1–34.
- [20] Tandrup Schmidt S, Foged C, et al. Liposome-based adjuvants for subunit vaccines: Formulation strategies for subunit antigens and immunostimulators. *Pharmaceutics.* 2016;8(1):7–29.
- [21] Garçon N, Leroux-Roels G, et al. Vaccine adjuvants. *Understanding Modern Vaccines: Perspectives in Vaccinology.* 2011;1(1):89–113.
- [22] Reinert P. Vaccins sous-unités polysaccharidiques. *Rev Prat.* 1995;45(12):1484–7.
- [23] Douglas RM, Paton JC, et al. Antibody response to pneumococcal vaccination in children younger than five years of age. *J Infect Dis.* 1983;148(1):131–7.
- [24] Stein KE. Thymus-independent and thymus-dependent responses to polysaccharide antigens. *J Infect Dis.* 1992;165(Suppl 1):S49-52.
- [25] Leitner WW, Ying H, et al. DNA and RNA-based vaccines: Principles, progress and prospects. *Vaccine.* 1999;18(9):765–77.
- [26] Leroux-Roels I, Borkowski A, et al. Antigen sparing and cross-reactive immunity with an adjuvanted rH5N1 prototype pandemic influenza vaccine: A randomised controlled trial. *Lancet.* 2007;370(9587):580–9.
- [27] Freund J, Thomson KJ. Antibody formation and sensitization with the aid of adjuvants. *J Immunol.* 1948;60(3):383–98.
- [28] Le Moignic P. Application to man of vaccines consisting of emulsions in fatty substances (lipo-vaccines). *Comptes Rendus Biologies.* 1916;29:352–8.

- [29] Glenny AT, Pope CG, et al. Immunological Notes XVII–XXIV. *J Pathol.* 1926;29(1):31–40.
- [30] Freund J, Casals J, et al. Sensitization and antibody formation after injection of tubercle bacilli and paraffin oil. *Exp Biol Med.* 1937;37(3):509–13.
- [31] Petrovsky N, Aguilar JC. Vaccine adjuvants: Current state and future trends. *Immunol Cell Biol.* 2004;82(5):488–96.
- [32] Mbow ML, Gregorio E de, et al. New adjuvants for human vaccines. *Curr Opin Immunol.* 2010;22(3):411–6.
- [33] Marciani DJ. Vaccine adjuvants: Role and mechanisms of action in vaccine immunogenicity. *Drug Discov Today.* 2003;8(20):934–43.
- [34] Cox JC, Coulter AR. Adjuvants-A classification and review of their modes of action. *Vaccine.* 1997;15(3):248–56.
- [35] Freund J. The effect of paraffin oil and mycobacteria on antibody formation and sensitization; A review. *Am J Clin Pathol.* 1951;21(7):645–56.
- [36] Billiau A, Matthys P. Modes of action of Freund's adjuvants in experimental models of autoimmune diseases. *J Leukoc Biol.* 2001;70(6):849–60.
- [37] Even M, Young K, et al. In vivo investigation of twin-screw extruded lipid implants for vaccine delivery. *Eur J Pharm Biopharm.* 2014;87(2):338–46.
- [38] O'Hagan DT, Rahman D, et al. Biodegradable microparticles as controlled release antigen delivery systems. *Immunology.* 1991;73(2):239–42.
- [39] Jiang W, Gupta RK, et al. Biodegradable poly(lactic-co-glycolic acid) microparticles for injectable delivery of vaccine antigens. *Adv Drug Deliv Rev.* 2005;57(3):391–410.
- [40] Joshi VB, Geary SM, et al. Biodegradable particles as vaccine delivery systems: Size matters. *AAPS J.* 2013;15(1):85–94.
- [41] Jakse G; Wolff J. *Endokrine Therapie des fortgeschrittenen Prostatakarzinoms, Multicenter-Studie mit Enantone® Monats-Depot-Langzeitverlaufskontrolle.* Berlin: Springer; 1992. ISBN: 978-3-642-76867-5.
- [42] Sun H, Xie Y, et al. Advances in saponin-based adjuvants. *Vaccine.* 2009;27(12):1787–96.
- [43] Soltysik S, Wu JY, et al. Structure/function studies of QS-21 adjuvant: Assessment of triterpene aldehyde and glucuronic acid roles in adjuvant function. *Vaccine.* 1995;13(15):1403–10.

- [44] Amselem S, Domb AJ, et al. Lipospheres as vaccine carrier system: Effects of size, charge and phospholipid composition. *Vacc Res.* 1992;1:383–95.
- [45] Grgacic EV, Anderson DA. Virus-like particles: Passport to immune recognition. *Methods.* 2006;40(1):60–5.
- [46] Glück R, Mischler R, et al. Immunopotentiating reconstituted influenza virus virosome vaccine delivery system for immunization against hepatitis A. *J Clin Invest.* 1992;90(6):2491–5.
- [47] Lincopan N, Espíndola NM, et al. Novel immunoadjuvants based on cationic lipid: Preparation, characterization and activity in vivo. *Vaccine.* 2009;27(42):5760–71.
- [48] Malaria vaccine: WHO position paper-January 2016. *Wkly Epidemiol Rec WHO.* 2016;91(4):33–51.
- [49] Coffman RL, Sher A, et al. Vaccine adjuvants: Putting innate immunity to work. *Immunity.* 2010;33(4):492–503.
- [50] Eisenbarth SC, Colegio OR, et al. Crucial role for the Nalp3 inflammasome in the immunostimulatory properties of aluminium adjuvants. *Nature.* 2008;453(7198):1122–6.
- [51] Ghimire TR, Benson RA, et al. Alum increases antigen uptake, reduces antigen degradation and sustains antigen presentation by DCs in vitro. *Immunol Lett.* 2012;147(1-2):55–62.
- [52] Kundi M. New hepatitis B vaccine formulated with an improved adjuvant system. *Expert Rev Vaccines.* 2007;6(2):133–40.
- [53] Fox CB. Squalene emulsions for parenteral vaccine and drug delivery. *Molecules.* 2009;14(9):3286–312.
- [54] Murray RK. Harper's illustrated biochemistry, Cholesterol synthesis, transport, and excretion. 26th ed. New York: Lange Medical Books/McGraw-Hill; 2003.
- [55] Miles AP, McClellan HA, et al. Montanide ISA 720 vaccines: Quality control of emulsions, stability of formulated antigens, and comparative immunogenicity of vaccine formulations. *Vaccine.* 2005;23(19):2530–9.
- [56] Aucouturier J, Dupuis L, et al. Montanide ISA 720 and 51: A new generation of water in oil emulsions as adjuvants for human vaccines. *Expert Rev Vaccines.* 2002;1(1):111–8.

- [57] Allison AC, Byars NE. An adjuvant formulation that selectively elicits the formation of antibodies of protective isotypes and of cell-mediated immunity. *J Immunol Methods*. 1986;95(2):157–68.
- [58] Waters RV, Terrell TG, et al. Uveitis induction in the rabbit by muramyl dipeptides. *Infect Immun*. 1986;51(3):816–25.
- [59] Kahn JO, Sinangil F, et al. Clinical and immunologic responses to human immunodeficiency virus (HIV) type 1SF2 gp120 subunit vaccine combined with MF59 adjuvant with or without muramyl tripeptide dipalmitoyl phosphatidylethanolamine in non-HIV-infected human volunteers. *J Infect Dis*. 1994;170(5):1288–91.
- [60] O'Hagan DT, Ott GS, et al. The history of MF59® adjuvant: A phoenix that arose from the ashes. *Expert Rev Vaccines*. 2013;12(1):13–30.
- [61] Asa PB, Cao Y, et al. Antibodies to squalene in Gulf War syndrome. *Exp Mol Pathol*. 2000;68(1):55–64.
- [62] Phillips CJ, Matyas GR, et al. Antibodies to squalene in US Navy Persian Gulf War veterans with chronic multisymptom illness. *Vaccine*. 2009;27(29):3921–6.
- [63] Del Giudice G, Fracapane E, et al. Vaccines with the MF59 adjuvant do not stimulate antibody responses against squalene. *Clin Vaccine Immunol*. 2006;13(9):1010–3.
- [64] Shah RR, O'Hagan DT, et al. The impact of size on particulate vaccine adjuvants. *Nanomedicine*. 2014;9(17):2671–81.
- [65] Calabro S, Tritto E, et al. The adjuvant effect of MF59 is due to the oil-in-water emulsion formulation, none of the individual components induce a comparable adjuvant effect. *Vaccine*. 2013;31(33):3363–9.
- [66] Ott G, Barchfeld GL, et al. Enhancement of humoral response against human influenza vaccine with the simple submicron oil/water emulsion adjuvant MF59. *Vaccine*. 1995;13(16):1557–62.
- [67] Dupuis M, McDonald DM, et al. Distribution of adjuvant MF59 and antigen gD2 after intramuscular injection in mice. *Vaccine*. 1999;18(5-6):434–9.
- [68] Ott G, Barchfeld GL, et al. MF59. Design and evaluation of a safe and potent adjuvant for human vaccines. *Pharm Biotechnol*. 1995;6:277–96.
- [69] Seubert A, Monaci E, et al. The adjuvants aluminum hydroxide and MF59 induce monocyte and granulocyte chemoattractants and enhance monocyte differentiation toward dendritic cells. *J Immunol*. 2008;180(8):5402–12.

- [70] Calabro S, Tortoli M, et al. Vaccine adjuvants alum and MF59 induce rapid recruitment of neutrophils and monocytes that participate in antigen transport to draining lymph nodes. *Vaccine*. 2011;29(9):1812–23.
- [71] Oyewumi MO, Kumar A, et al. Nano-microparticles as immune adjuvants: Correlating particle sizes and the resultant immune responses. *Expert Rev Vaccines*. 2010;9(9):1095–107.
- [72] Bachmann MF, Jennings GT. Vaccine delivery: A matter of size, geometry, kinetics and molecular patterns. *Nat Rev Immunol*. 2010;10(11):787–96.
- [73] Negash T, Liman M, et al. Mucosal application of cationic poly(d,l-lactide-co-glycolide) microparticles as carriers of DNA vaccine and adjuvants to protect chickens against infectious bursal disease. *Vaccine*. 2013;31(36):3656–62.
- [74] Borges O, Cordeiro-da-Silva A, et al. Immune response by nasal delivery of hepatitis B surface antigen and codelivery of a CpG ODN in alginate coated chitosan nanoparticles. *Eur J Pharm Biopharm*. 2008;69(2):405–16.
- [75] Shakweh M, Ponchel G, et al. Particle uptake by Peyer's patches: A pathway for drug and vaccine delivery. *Expert Opin Drug Deliv*. 2004;1(1):141–63.
- [76] Reddy ST, van der Vlies AJ, et al. Exploiting lymphatic transport and complement activation in nanoparticle vaccines. *Nat Biotechnol*. 2007;25(10):1159–64.
- [77] Landesman-Milo D, Peer D. Altering the immune response with lipid-based nanoparticles. *J Control Release*. 2012;161(2):600–8.
- [78] Shimizu Y, Takagi H, et al. Intraperitoneal immunization with oligomannose-coated liposome-entrapped soluble leishmanial antigen induces antigen-specific T-helper type immune response in BALB/c mice through uptake by peritoneal macrophages. *Parasite Immunol*. 2007;29(5):229–39.
- [79] Sugimoto M, Ohishi K, et al. Oligomannose-coated liposomes as an adjuvant for the induction of cell-mediated immunity. *FEBS Lett*. 1995;363(1-2):53–6.
- [80] Pawar D, Mangal S, et al. Development and characterization of surface modified PLGA nanoparticles for nasal vaccine delivery: Effect of mucoadhesive coating on antigen uptake and immune adjuvant activity. *Eur J Pharm Biopharm*. 2013;85(3):550–9.
- [81] Thomas C, Rawat A, et al. Aerosolized PLA and PLGA nanoparticles enhance humoral, mucosal and cytokine responses to hepatitis B vaccine. *Mol Pharm*. 2011;8(2):405–15.

- [82] Moon JJ, Suh H, et al. Antigen-displaying lipid-enveloped PLGA nanoparticles as delivery agents for a Plasmodium vivax malaria vaccine. PLoS ONE. 2012;7(2):1–9.
- [83] Borges O, Silva M, et al. Alginate coated chitosan nanoparticles are an effective subcutaneous adjuvant for hepatitis B surface antigen. Int Immunopharmacol. 2008;8(13):1773–80.
- [84] Filipović-Grcić J, Skalko-Basnet N, et al. Mucoadhesive chitosan-coated liposomes: Characteristics and stability. J Microencapsul. 2001;18(1):3–12.
- [85] Prego C, Paolicelli P, et al. Chitosan-based nanoparticles for improving immunization against hepatitis B infection. Vaccine. 2010;28(14):2607–14.
- [86] Mueller RH, Grubhofer N, et al. Stabilitäts-, Biokompatibilitäts-optimiertes Adjuvans (SBA) zur Erhöhung der humoralen und zellulären Immunantwort DE10024788A1. 2000 May 19.
- [87] Moyano DF, Goldsmith M, et al. Nanoparticle hydrophobicity dictates immune response. J Am Chem Soc. 2012;134(9):3965–7.
- [88] Olbrich C, Müller RH, et al. Stable biocompatible adjuvants-a new type of adjuvant based on solid lipid nanoparticles: A study on cytotoxicity, compatibility and efficacy in chicken. Altern Lab Anim. 2002;30(4):443–58.
- [89] Ott G, Singh M, et al. A cationic sub-micron emulsion (MF59/DOTAP) is an effective delivery system for DNA vaccines. J Control Release. 2002;79(1):1–5.
- [90] Rönnerberg B, Fekadu M, et al. Adjuvant activity of non-toxic Quillaja saponaria Molina components for use in ISCOM matrix. Vaccine. 1995;13(14):1375–82.
- [91] Paillot R, Prowse L. ISCOM-matrix-based equine influenza (EIV) vaccine stimulates cell-mediated immunity in the horse. Vet Immunol Immunopathol. 2012;145(1):516–21.
- [92] Sundquist B, Lövgren K, et al. Influenza virus ISCOMs: Biochemical characterization. Vaccine. 1988;6(1):44–8.
- [93] Mougín B, Bakouche O, et al. Humoral immune response elicited in rats by measles viral membrane antigens presented in liposomes and ISCOMs. Vaccine. 1988;6(5):445–9.
- [94] Morein B, Ekström J, et al. Increased immunogenicity of a non-amphipathic protein (BSA) after inclusion into ISCOMs. J Immunol Methods. 1990;128(2):177–81.

- [95] Müller H, Scholtissek C, et al. The genome of infectious bursal disease virus consists of two segments of double-stranded RNA. *J Virol.* 1979;31(3):584–9.
- [96] Rudd MF, Heine HG, et al. Characterisation of an Indonesian very virulent strain of infectious bursal disease virus. *Arch Virol.* 2002;147(7):1303–22.
- [97] Cosgrove AS. An apparently new disease of chickens: Avian nephrosis. *Avian Dis.* 1962;6(3):385.
- [98] Müller R, Käufer I, et al. Immunofluorescent studies of early virus propagation after oral infection with infectious bursal disease virus (IBDV). *J Vet Med B.* 1979;26(5):345–52.
- [99] Nunoya T, Otaki Y, et al. Occurrence of acute infectious bursal disease with high mortality in Japan and pathogenicity of field isolates in specific-pathogen-free chickens. *Avian Dis.* 1992;36(3):597–609.
- [100] Rosales AG, Villegas P, et al. Immunosuppressive potential and pathogenicity of a recent isolate of infectious bursal disease virus in commercial broiler chickens. *Avian Dis.* 1989;33(4):724–8.
- [101] Faragher JT, Allan WH, et al. Immunosuppressive effect of infectious bursal agent on vaccination against Newcastle disease. *Vet Rec.* 1974;95(17):385–8.
- [102] Tsukamoto K, Tanimura N, et al. Efficacy of three live vaccines against highly virulent infectious bursal disease virus in chickens with or without maternal antibodies. *Avian Dis.* 1995;39(2):218–29.
- [103] van der Sluis W. World poultry diseases update. *World poultry.* 1999;(15):30–2.
- [104] Marina Arnold-Klingbeil. Entwicklung von Kluyveromyces lactis-basierten Vakzinen gegen Infektiöse Bursitis und Influenza [Dissertation]. Martin-Luther-Universität Halle-Wittenberg; 2014.
- [105] Benton WJ, Cover MS, et al. Physicochemical properties of the infectious bursal agent (IBA). *Avian Dis.* 1967;11(3):438–45.
- [106] Müller H, Mundt E, et al. Current status of vaccines against infectious bursal disease. *Avian Pathol.* 2012;41(2):133–9.
- [107] Berg TP. Acute infectious bursal disease in poultry: A review. *Avian Pathol.* 2000;29(3):175–94.
- [108] Rautenschlein S, Kraemer C, et al. Protective efficacy of intermediate and intermediate plus infectious bursal disease virus (IBDV) vaccines against very virulent IBDV in commercial broilers. *Avian Dis.* 2005;49(2):231–7.

- [109] Block H, Meyer-Block K, et al. A field study on the significance of vaccination against infectious bursal disease virus (IBDV) at the optimal time point in broiler flocks with maternally derived IBDV antibodies. *Avian Pathol.* 2007;36(5):401–9.
- [110] Le Gros FX, Dancer A, et al. Field efficacy trial of a novel HVT-IBD vector vaccine for 1-day-old broilers. *Vaccine.* 2009;27(4):592–6.
- [111] European Medicines Agency Veterinary Medicines. EPAR summary: VAXXITEK HVT+IBD: EMEA; 01.01.2007.
- [112] Werling D, Jann OC, et al. Variation matters: TLR structure and species-specific pathogen recognition. *Trends Immunol.* 2009;30(3):124–30.
- [113] Arnold M, Durairaj V, et al. Protective vaccination against infectious bursal disease virus with whole recombinant *Kluyveromyces lactis* yeast expressing the viral VP2 subunit. *PLoS ONE.* 2012;7(9):e42870.
- [114] Krijger J, Baumann J, et al. A novel, lactase-based selection and strain improvement strategy for recombinant protein expression in *Kluyveromyces lactis*. *Microb Cell Fact.* 2012;11:112.
- [115] Breunig KD, Bolotin-Fukuhara M, et al. Regulation of primary carbon metabolism in *Kluyveromyces lactis*. *Enzyme Microb Technol.* 2000;26(9):771–80.
- [116] Anders A, Breunig KD. Evolutionary aspects of a genetic network: Studying the lactose/galactose regulon of *Kluyveromyces lactis*. *Methods Mol Biol.* 2011;734:259–77.
- [117] van Ooyen AJ, Dekker P, et al. Heterologous protein production in the yeast *Kluyveromyces lactis*. *FEMS Yeast Res.* 2006;6(3):381–92.
- [118] Saugar I, Luque D, et al. Structural polymorphism of the major capsid protein of a double-stranded RNA virus: An amphipathic alpha helix as a molecular switch. *Structure.* 2005;13(7):1007–17.
- [119] Bachmair A, Finley D, et al. In vivo half-life of a protein is a function of its amino-terminal residue. *Science.* 1986;234(4773):179–86.
- [120] Filipe V, Hawe A, et al. Critical evaluation of Nanoparticle Tracking Analysis (NTA) by NanoSight for the measurement of nanoparticles and protein aggregates. *Pharm Res.* 2010;27(5):796–810.
- [121] Jores K, Mehnert W, et al. Investigations on the structure of solid lipid nanoparticles (SLN) and oil-loaded solid lipid nanoparticles by photon correlation

- spectroscopy, field-flow fractionation and transmission electron microscopy. *J Control Release*. 2004;95(2):217–27.
- [122] Hoffmann S, Caysa H, et al. Carbohydrate plasma expanders for passive tumor targeting: In vitro and in vivo studies. *Carbohydr Polym*. 2013;95(1):404–13.
- [123] Fraunhofer W, Winter G. The use of asymmetrical flow field-flow fractionation in pharmaceuticals and biopharmaceuticals. *Eur J Pharm Biopharm*. 2004;58(2):369–83.
- [124] Giddings JC. Field-flow fractionation: Analysis of macromolecular, colloidal, and particulate materials. *Science*. 1993;260(5113):1456–65.
- [125] Wittgren B, Wahlund K. Fast molecular mass and size characterization of polysaccharides using asymmetrical flow field-flow fractionation-multiangle light scattering. *J Chromatogr A*. 1997;760(2):205–18.
- [126] Stauch O, Schubert R, et al. Structure of artificial cytoskeleton containing liposomes in aqueous solution studied by static and dynamic light scattering. *Biomacromolecules*. 2002;3(3):565–78.
- [127] Lyklema J. Electrokinetics after Smoluchowski. *Colloids Surf A*. 2003;222(1):5–14.
- [128] Bradford MM. A rapid and sensitive method for the quantitation of microgram quantities of protein utilizing the principle of protein-dye binding. *Anal Biochem*. 1976;72(1-2):248–54.
- [129] Laemmli UK. Cleavage of structural proteins during the assembly of the head of bacteriophage T4. *Nature*. 1970;227(5259):680–5.
- [130] Renart J, Reiser J, et al. Transfer of proteins from gels to diazobenzyloxymethyl-paper and detection with antisera: A method for studying antibody specificity and antigen structure. *Proc Natl Acad Sci USA*. 1979;76(7):3116–20.
- [131] Snyder DB, Lana DP, et al. Differentiation of infectious bursal disease viruses directly from infected tissues with neutralizing monoclonal antibodies: Evidence of a major antigenic shift in recent field isolates. *Avian Dis*. 1988;32(3):535–9.
- [132] Granzow H, Birghan C, et al. A second form of infectious bursal disease virus-associated tubule contains VP4. *J Virol*. 1997;71(11):8879–85.
- [133] Skehan P, Storeng R, et al. New colorimetric cytotoxicity assay for anticancer-drug screening. *J Natl Cancer Inst*. 1990;82(13):1107–12.
- [134] Eterradossi N, Picault JP, et al. Pathogenicity and preliminary antigenic characterization of six infectious bursal disease virus strains isolated in France from acute outbreaks. *J Vet Med B*. 1992;39(9):683–91.

- [135] Kelemen MV, Sharpe JE. Controlled cell disruption: A comparison of the forces required to disrupt different micro-organisms. *J Cell Sci.* 1979;35(1):431–41.
- [136] Klimek-Ochab M, Brzezińska-Rodak M, et al. Comparative study of fungal cell disruption-scope and limitations of the methods. *Folia Microbiol.* 2011;56(5):469–75.
- [137] Stubbs AC, Martin KS, et al. Whole recombinant yeast vaccine activates dendritic cells and elicits protective cell-mediated immunity. *Nat Med.* 2001;7(5):625–9.
- [138] van Asbeck EC, Hoepelman AIM, et al. Mannose binding lectin plays a crucial role in innate immunity against yeast by enhanced complement activation and enhanced uptake of polymorphonuclear cells. *BMC Microbiol.* 2008;8(1):229.
- [139] Seong SK, Kim HW. Potentiation of innate immunity by  $\beta$ -glucans. *Mycobiology.* 2010;38(2):144–8.
- [140] Brown GD, Herre J, et al. Dectin-1 mediates the biological effects of beta-glucans. *J Exp Med.* 2003;197(9):1119–24.
- [141] Kim KS, Yun HS. Production of soluble  $\beta$ -glucan from the cell wall of *Saccharomyces cerevisiae*. *Enzyme Microb Technol.* 2006;39(3):496–500.
- [142] Ostroff GR, Tipper DJ. Yeast cell particles as oral delivery vehicles for antigens WO2007109564A2. 2007.
- [143] Munang'andu HM, Fredriksen BN, et al. Antigen dose and humoral immune response correspond with protection for inactivated infectious pancreatic necrosis virus vaccines in Atlantic salmon (*Salmo salar* L). *Vet Res.* 2013;44(1):7.
- [144] Balasubramanian MK, Bi E, et al. Comparative analysis of cytokinesis in budding yeast, fission yeast and animal cells. *Curr Biol.* 2004;14(18):806–18.
- [145] Sabatinos SA, Forsburg SL. Measuring DNA content by flow cytometry in fission yeast. *Methods Mol Biol.* 2009;521:449–61.
- [146] Fykse EM, Olsen JS, et al. Application of sonication to release DNA from *Bacillus cereus* for quantitative detection by real-time PCR. *J Immunol Methods.* 2003;55(1):1–10.
- [147] Sheetz RM, Dickson RC. Lac4 is the structural gene for beta-galactosidase in *Kluyveromyces lactis*. *Genetics.* 1981;98(4):729–45.
- [148] Dickson RC, Barr K. Characterization of lactose transport in *Kluyveromyces lactis*. *J Bacteriol.* 1983;154(3):1245–51.
- [149] Liu D, Zeng X, et al. Disruption and protein release by ultrasonication of yeast cells. *Innov Food Sci Emerg Technol.* 2013;18:132–7.

- [150] Bzducha-Wróbel A, Błażej S, et al. Evaluation of the efficiency of different disruption methods on yeast cell wall preparation for  $\beta$ -glucan isolation. *Molecules*. 2014;19(12):20941–61.
- [151] Taghavian O, Mandal MK, et al. A potential nanobiotechnology platform based on infectious bursal disease subviral particles. *RSC Adv*. 2012;2(5):1970–8.
- [152] Xu H, Yuan L, et al. Overexpression of recombinant infectious bursal disease virus (IBDV) capsid protein VP2 in the middle silk gland of transgenic silkworm. *Transgenic Res*. 2014;23(5):809–16.
- [153] Maquille A. Drugs radiosterilization: Parameters influencing the selection of the irradiation dose. *Chimie Nouvelle*. 2008;99:15–22.
- [154] Ghoddusi HB, Glatz B. Decontamination of saffron (*Crocus sativus* L.) by electron beam irradiation. *Acta Horti*. 2004;650:339–44.
- [155] Terryn H, Maquille A, et al. Irradiation of human insulin in aqueous solution, first step towards radiosterilization. *Int J Pharm*. 2007;343(1):4–11.
- [156] Taghavian O, Spiegel H, et al. Protective oral vaccination against infectious bursal disease virus using the major viral antigenic protein VP2 produced in *Pichia pastoris*. *PLoS ONE*. 2013;8(12):e83210.
- [157] Bazan SB, Breinig T, et al. Heat treatment improves antigen-specific T cell activation after protein delivery by several but not all yeast genera. *Vaccine*. 2014;32(22):2591–8.
- [158] Greene RS, Downing DT, et al. Anatomical variation in the amount and composition of human skin surface lipid. *J Invest Dermatol*. 1970;54(3):240–7.
- [159] Videira MA, Botelho MF, et al. Lymphatic uptake of pulmonary delivered radiolabelled solid lipid nanoparticles. *J Drug Target*. 2002;10(8):607–13.
- [160] Oda K, Sato Y, et al. Separation and characterization of adjuvant oligosaccharide oleate ester derived from product mixture of mannitol-oleic acid esterification. *Vaccine*. 2004;22(21):2812–21.
- [161] Saul A, Lawrence G, et al. Human phase I vaccine trials of 3 recombinant asexual stage malaria antigens with Montanide ISA720 adjuvant. *Vaccine*. 1999;17(23):3145–59.
- [162] Cox, Sjölander, et al. ISCOMs and other saponin based adjuvants. *Adv Drug Deliv Rev*. 1998;32(3):247–71.

- [163] Lin Y, Al-Suwayeh SA, et al. Squalene-containing nanostructured lipid carriers promote percutaneous absorption and hair follicle targeting of diphencyprone for treating alopecia areata. *Pharm Res.* 2013;30(2):435–46.
- [164] Fang J, Fang C, et al. Lipid nanoparticles as vehicles for topical psoralen delivery: Solid lipid nanoparticles (SLN) versus nanostructured lipid carriers (NLC). *Eur J Pharm Biopharm.* 2008;70(2):633–40.
- [165] Fang Y, Lin Y, et al. Tryptanthrin-loaded nanoparticles for delivery into cultured human breast cancer cells, MCF7: The effects of solid lipid/liquid lipid ratios in the inner core. *Chem Pharm Bull.* 2011;59(2):266–71.
- [166] Bakumov V, Schwarz M, et al. Emulsion processing of polymer-derived porous Si/C/(O) ceramic bodies. *J Eur Ceram Soc.* 2009;29(13):2857–65.
- [167] Trotta M, Debernardi F, et al. Preparation of solid lipid nanoparticles by a solvent emulsification-diffusion technique. *Int J Pharm.* 2003;257(1):153–60.
- [168] Committee for veterinary and medicinal products. EMEA MRL/055/95, Summary report Quillaia saponins. London; 1996.
- [169] Johansson M, Lövgren-Bengtsson K. ISCOMs with different quillaia saponin components differ in their immunomodulating activities. *Vaccine.* 1999;17(22):2894–900.
- [170] Jumaa M, Müller BW. The stabilization of parenteral fat emulsion using non-ionic ABA copolymer surfactant. *Int J Pharm.* 1998;174(1):29–37.
- [171] Innocente N, Biasutti M, et al. Effect of high-pressure homogenization on droplet size distribution and rheological properties of ice cream mixes. *J Dairy Sci.* 2009;92(5):1864–75.
- [172] Benita S, Böhm BHL. Emulsions and nanosuspensions for the formulation of poorly soluble drugs. Stuttgart: CRC Press; 1998. ISBN: 3887630696.
- [173] Abdelwahed W, Degobert G, et al. Freeze-drying of nanoparticles: Formulation, process and storage considerations. *Adv Drug Deliv Rev.* 2006;58(15):1688–713.
- [174] Schwarz, Mehnert. Freeze-drying of drug-free and drug-loaded solid lipid nanoparticles (SLN). *Int J Pharm.* 1997;157(2):171–9.
- [175] Geyer RP. Utilization and tolerance of intravenous fat emulsions. In: Bode HH, Warshaw JB, editors. *Parenteral Nutrition in Infancy and Childhood.* Boston, MA: Springer US; 1974. p. 98–111. ISBN: 978-1-4684-3249-7.

- [176] Ott G, Radhakrishnan R, et al. The adjuvant MF59: A 10-year perspective. In: O'Hagan DT, editor. *Vaccine adjuvants*: Springer; 2000. p. 211–28. (vol. 42). ISBN: 978-1-59259-083-4.
- [177] Mehnert W, Mäder K. Solid lipid nanoparticles: Production, characterization and applications. *Adv Drug Deliv Rev.* 2001;47(2):165–96.
- [178] Siekmann B, Westesen K. Thermoanalysis of the recrystallization process of melt-homogenized glyceride nanoparticles. *Colloids Surf B.* 1994;3(3):159–75.
- [179] Schädlich A, Rose C, et al. How stealthy are PEG-PLA nanoparticles? An NIR in vivo study combined with detailed size measurements. *Pharm Res.* 2011;28(8):1995–2007.
- [180] McClements DJ. Nanoemulsions versus microemulsions: Terminology, differences, and similarities. *Soft Matter.* 2012;8(6):1719–29.
- [181] Grumezescu AM. *Nanotechnology in the agri-food industry-Emulsions*. 3rd ed. San Diego: Academic Press; 2016. ISBN: 978-0-12-804306-6.
- [182] Bunjes H, Koch MHJ, et al. Influence of emulsifiers on the crystallization of solid lipid nanoparticles. *J Pharm Sci.* 2003;92(7):1509–20.
- [183] Noack A, Hause G, et al. Physicochemical characterization of curcuminoid-loaded solid lipid nanoparticles. *Int J Pharm.* 2012;423(2):440–51.
- [184] Ugazio E, Cavalli R, et al. Incorporation of cyclosporin A in solid lipid nanoparticles (SLN). *Int J Pharm.* 2002;241(2):341–4.
- [185] Douglas HE. *Basic principles of colloid science*. Cambridge: Royal Society of Chemistry; 1988. ISBN: 978-0-85186-443-3.
- [186] Delgado AV, González-Caballero F, et al. Measurement and interpretation of electrokinetic phenomena. *J Colloid Interface Sci.* 2007;309(2):194–224.
- [187] Jiang J, Oberdörster G, et al. Characterization of size, surface charge, and agglomeration state of nanoparticle dispersions for toxicological studies. *J Nanopart Res.* 2009;11(1):77–89.
- [188] Barnett MI, Cosslett AG, et al. Parenteral Nutrition. *Drug Saf.* 1990;5(Supplement 1):101–6.
- [189] Voigt R, Fahr A. *Pharmazeutische Technologie*. 10th ed. Stuttgart: Dt. Apotheker-Verl.; 2006. 716 p. ISBN: 9783769235111.
- [190] Lourenco C. Steric stabilization of nanoparticles: Size and surface properties. *Int J Pharm.* 1996;138(1):1–12.

- [191] Gabbott P. Principles and applications of thermal analysis. Oxford, UK: Blackwell Publishing Ltd; 2008. ISBN: 9780470697702.
- [192] Timms RE. Phase behaviour of fats and their mixtures. *Prog Lipid Res.* 1984;23(1):1–38.
- [193] Kellens M, Meeussen W, et al. Synchrotron radiation investigations of the polymorphic transitions of saturated monoacid triglycerides. Part 1: Tripalmitin and tristearin. *Chem Phys Lipids.* 1991;58(1):131–44.
- [194] Skurtys O, Aguilera JM. Formation of O/W macroemulsions with a circular microfluidic device using saponin and potato starch. *Food Hydrocolloid.* 2009;23(7):1810–7.
- [195] Helgason T, Awad TS, et al. Effect of surfactant surface coverage on formation of solid lipid nanoparticles (SLN). *J Colloid Interface Sci.* 2009;334(1):75–81.
- [196] Bunjes H, Koch MHJ, et al. Effect of particle size on colloidal solid triglycerides. *Langmuir.* 2000;16(12):5234–41.
- [197] Bunjes H, Unruh T. Characterization of lipid nanoparticles by differential scanning calorimetry, X-ray and neutron scattering. *Adv Drug Deliv Rev.* 2007;59(6):379–402.
- [198] Jennings V, Mäder K, et al. Solid lipid nanoparticles (SLN) based on binary mixtures of liquid and solid lipids: A H-NMR study. *Int J Pharm.* 2000;205(1):15–21.
- [199] Goto M, Asada E. X-ray diffraction of the binary system tristearin-tripalmitin. *J Jpn Oil Chem Soc.* 1967;16(7):402–6.
- [200] Lutton ES. The polymorphism of tristearin and some of its homologs. *J Am Chem Soc.* 1945;67(4):524–7.
- [201] Rucker G, Neugebauer M, et al. *Instrumentelle pharmazeutische Analytik.* 4th ed. Stuttgart: Wiss. Verl.-Ges.; 2008. 711 p. ISBN: 978-3804723979.
- [202] Wishart DS, Sykes BD, et al. The chemical shift index: A fast and simple method for the assignment of protein secondary structure through NMR spectroscopy. *Biochemistry.* 1992;31(6):1647–51.
- [203] Westesen K, Bunjes H, et al. Physicochemical characterization of lipid nanoparticles and evaluation of their drug loading capacity and sustained release potential. *J Control Release.* 1997;48(2):223–36.
- [204] Metz H, Mäder K. Benchtop-NMR and MRI-a new analytical tool in drug delivery research. *Int J Pharm.* 2008;364(2):170–5.

- [205] Jores K, Mehnert W, et al. Physicochemical investigations on solid lipid nanoparticles and on oil-loaded solid lipid nanoparticles: A nuclear magnetic resonance and electron spin resonance study. *Pharm Res.* 2003;20(8):1274–83.
- [206] Zimmermann E, Souto EB, et al. Physicochemical investigations on the structure of drug-free and drug-loaded solid lipid nanoparticles (SLN) by means of DSC and <sup>1</sup>H NMR. *Pharmazie.* 2005;60(7):508–13.
- [207] Pogliani L, Ceruti M, et al. An NMR and molecular mechanics study of squalene and squalene derivatives. *Chem Phys Lipids.* 1994;70(1):21–34.
- [208] Lewinski N, Colvin V, et al. Cytotoxicity of nanoparticles. *Small.* 2008;4(1):26–49.
- [209] Weyenberg W, Filev P, et al. Cytotoxicity of submicron emulsions and solid lipid nanoparticles for dermal application. *Int J Pharm.* 2007;337(1):291–8.
- [210] Persidis A. Cancer multidrug resistance. *Nat Biotechnol.* 1999;17(1):94–5.
- [211] Floyd. Top ten considerations in the development of parenteral emulsions. *Pharm Sci Technol Today.* 1999;4(2):134–43.
- [212] Arechabala B, Coiffard C, et al. Comparison of cytotoxicity of various surfactants tested on normal human fibroblast cultures using the neutral red test, MTT assay and LDH release. *J Appl Toxicol.* 1999;19(3):163–5.
- [213] Müller RH, Rühl D, et al. Cytotoxicity of solid lipid nanoparticles as a function of the lipid matrix and the surfactant. *Pharm Res.* 1997;14(4):458–62.
- [214] Kensil CR, Patel U, et al. Separation and characterization of saponins with adjuvant activity from *Quillaja saponaria* Molina cortex. *J Immunol.* 1991;146(2):431–7.
- [215] Rönnerberg B, Fekadu M, et al. Effects of carbohydrate modification of *Quillaja saponaria* Molina QH-B fraction on adjuvant activity, cholesterol-binding capacity and toxicity. *Vaccine.* 1997;15(17):1820–6.
- [216] Schütt C, Bröker B. *Grundwissen Immunologie.* 3rd ed. Heidelberg: Spektrum Akademischer Verlag; 2011. XVI, 268 S. ISBN: 3827426464.
- [217] Marciani DJ, Press JB, et al. Development of semisynthetic triterpenoid saponin derivatives with immune stimulating activity. *Vaccine.* 2000;18(27):3141–51.
- [218] Rautenschlein S, Yeh H, et al. The role of T cells in protection by an inactivated infectious bursal disease virus vaccine. *Vet Immunol Immunopathol.* 2002;89(3-4):159–67.

- [219] Keitel W, Groth N, et al. Dose ranging of adjuvant and antigen in a cell culture H5N1 influenza vaccine: Safety and immunogenicity of a phase 1/2 clinical trial. *Vaccine*. 2010;28(3):840–8.
- [220] Della Cioppa G, Vesikari T, et al. Trivalent and quadrivalent MF59®-adjuvanted influenza vaccine in young children: A dose- and schedule-finding study. *Vaccine*. 2011;29(47):8696–704.
- [221] Xiang SD, Scholzen A, et al. Pathogen recognition and development of particulate vaccines: Does size matter? *Methods*. 2006;40(1):1–9.
- [222] O'Hagan DT, Ott GS, et al. The mechanism of action of MF59 - an innately attractive adjuvant formulation. *Vaccine*. 2012;30(29):4341–8.
- [223] Spence MTZ, Johnson ID. *The molecular probes handbook, A guide to fluorescent probes and labeling technologies*. 11th ed. Carlsbad, CA: Life Technologies Corporation; 2010. 1060 p. ISBN: 0982927916.
- [224] Weissleder R. A clearer vision for in vivo imaging. *Nat Biotechnol*. 2001;19(4):316–7.
- [225] Schädlich A, Hoffmann S, et al. Accumulation of nanocarriers in the ovary: A neglected toxicity risk? *J Control Release*. 2012;160(1):105–12.
- [226] Texier I, Goutayer M, et al. Cyanine-loaded lipid nanoparticles for improved in vivo fluorescence imaging. *J Biomed Opt*. 2009;14(5):54005.
- [227] Saski W, Shah SG. Availability of drugs in the presence of surface-active agents. I. Critical micelle concentrations of some oxyethylene oxypropylene polymers. *J Pharm Sci*. 1965;54(1):71–4.
- [228] Maskarinec SA, Hannig J, et al. Direct observation of poloxamer 188 insertion into lipid monolayers. *Biophys J*. 2002;82(3):1453–9.
- [229] Francis MF, Lavoie L, et al. Solubilization of cyclosporin A in dextran-g-polyethyleneglycolalkyl ether polymeric micelles. *Eur J Pharm Biopharm*. 2003;56(3):337–46.
- [230] Shen J, Zhan C, et al. Poly(ethylene glycol)-block-poly(D,L-lactide acid) micelles anchored with angiopep-2 for brain-targeting delivery. *J Drug Target*. 2011;19(3):197–203.
- [231] Reddy LH, Sharma RK, et al. Influence of administration route on tumor uptake and biodistribution of etoposide loaded solid lipid nanoparticles in Dalton's lymphoma tumor bearing mice. *J Control Release*. 2005;105(3):185–98.

- [232] Alex MR, Chacko AJ, et al. Lopinavir loaded solid lipid nanoparticles (SLN) for intestinal lymphatic targeting. *Eur J Pharm Sci.* 2011;42(1):11–8.
- [233] Li R, Eun JS, et al. Pharmacokinetics and biodistribution of paclitaxel loaded in pegylated solid lipid nanoparticles after intravenous administration. *Arch Pharm Res.* 2011;34(2):331–7.
- [234] van Furth R, Cohn ZA, et al. The mononuclear phagocyte system: A new classification of macrophages, monocytes, and their precursor cells. *Bull World Health Organ.* 1972;46(6):845–52.
- [235] Storm G, Belliot SO, et al. Surface modification of nanoparticles to oppose uptake by the mononuclear phagocyte system. *Adv Drug Deliv Rev.* 1995;17(1):31–48.
- [236] Immordino ML, Dosio F, et al. Stealth liposomes: Review of the basic science, rationale, and clinical applications, existing and potential. *Int J Nanomedicine.* 2006;1(3):297–315.
- [237] van den Berg, T P, Eterradossi N, et al. Infectious bursal disease (Gumboro disease). *Rev sci tech Off int Epiz.* 2000;19(2):509–43.
- [238] Sarachai C, Chansiripornchai N, et al. Efficacy of infectious bursal disease vaccine in broiler chickens receiving different vaccination programs. *Thai J Vet Med.* 2010;40(1):9–14.

## 6.2 Supplementary Material

**Laemmli buffer 10x:** 600 mmol/l Tris/HCl pH 6.8  
 20 % SDS  
 20 % Glycerol  
 20 % Mercaptoethanol  
 0.05 % Bromphenol blue  
 20 mmol/l Dithiothreitol

### SDS-PAGE gels:

Stacking gel 4.8 %	Separation gel 12%	Substance
58 %	35 %	Bidistilled water
25 %	25 %	Stacking/separation gel solution
16 %	40 %	30 % Acrylamid solution
1 %	0.5 %	20 % Ammonium peroxydisulfate
0.1 %	0.1 %	Tetramethylethylenediamine

**Stacking gel solution:** 0.5 mol/l Tris/HCl pH 6.8 with 0.4 % SDS

**Separation gel solution:** 1.5 mol/l Tris/HCl pH 8.8 with 0.4 % SDS

**10x SDS running buffer:** 0.25 mol/l Tris Base  
 2 mol/l Glycin  
 1 % (w/v) Na-Dodecylsulfat (SDS)

**10x Transfer buffer:** 0.25 mol/l Tris Base  
 2 mol/l Glycin  
 ad 1 l H<sub>2</sub>O

**1x Transfer buffer:** 100 ml 10x Transfer buffer  
 700 ml H<sub>2</sub>O  
 200 ml MeOH

**10x TBS:** 80 g NaCl  
 24.2 g Tris  
 ad 1000 ml H<sub>2</sub>O  
 pH 6.8 with HCl

**TBS-T:** 0.3 % Tween 20 in TBS

---

<b>Ponceau S:</b>	250 mg PonceauS 2.5 ml Acetic acid ad 250 ml H <sub>2</sub> O
<b>B60 buffer:</b>	50 mM Hepes/KOH pH 7.3 60 mM KAc 5 mM MgAc 0.1% Triton X-100 (v/v) 5 % Glycerol 20 mM Glycerol phosphate 10 mM MgCl <sub>2</sub> 1 mM Dithiothreitol 1 mM Phenylmethylsulfonyl fluoride 1 Tablet Roche protease inhibitor ad 50 ml H <sub>2</sub> O
<b>Beta-Gal buffer:</b>	5 mM Tris/HCl pH 7.8 5 % Glycerol 10 mM KCl
<b>Sörensen phosphahate buffer:</b>	
Solution A:	9.078 g/l KH <sub>2</sub> PO <sub>4</sub>
Solution B:	11.876 g/l Na <sub>2</sub> HPO <sub>4</sub> x 2H <sub>2</sub> O
pH 6.5:	31.3 ml solution B + 68.7 ml solution A
pH 7.4:	81.8 ml solution B + 18.2 ml solution A
<b>Medium fed batch fermentation:</b>	
	20 g/l Peptone 10 g/l Yeast extract 0.5 g/l NH <sub>4</sub> Cl 0.68 g/l MgCl <sub>2</sub> 50 ml/l Potassium phosphate buffer 10 ml/l Supplements 12 mg/l Niacin 0.25 ml/l Sterile antifoam

**2.5x feeding solution fed batch fermentation:**

50 g/l Peptone  
25 g/l Yeast extract  
1.25 g/l  $\text{NH}_4\text{Cl}$   
1.7 g/l  $\text{MgCl}_2$   
125 ml/l Potassium phosphate buffer  
25 ml/l Supplements  
200 g/l Lactose  
30 mg/l Niacin  
0.25 ml/l Sterile antifoam

**Supplements:**

0.1 g/l  $\text{H}_3\text{BO}_3$   
0.3 g/l  $\text{FeSO}_4 \times 7 \text{H}_2\text{O}$   
0.45 g/l  $\text{CaCl}_2 \times 2 \text{H}_2\text{O}$   
0.03 g/l  $\text{CoCl}_2 \times 6 \text{H}_2\text{O}$   
0.03 g/l  $\text{CuSO}_4 \times 5 \text{H}_2\text{O}$   
0.12 g/l  $\text{MnSO}_4 \times \text{H}_2\text{O}$   
0.035 g/l NaI  
0.05 g/l  $\text{Na}_2\text{MoO}_4 \times 2 \text{H}_2\text{O}$   
0.45 g/l  $\text{ZnSO}_4 \times 7 \text{H}_2\text{O}$   
0.15 g/l EDTA

**1 M Potassium phosphate buffer:**

22.99 g/l  $\text{K}_2\text{HPO}_4$   
119.13 g/l  $\text{KH}_2\text{PO}_4$

**YPD medium:**

2 % Pepton  
1 % Yeast extract  
2 % Glucose

**YP medium:**

2 % Peptone  
1 % Yeast extract

---

**PBS 10x:**                    8.00 g NaCl  
                                  0.20 g KCl  
                                  0.20 g KH<sub>2</sub>PO<sub>4</sub>  
                                  0.92 g Na<sub>2</sub>HPO<sub>4</sub>  
                                  ad 100 ml H<sub>2</sub>O  
                                  Adjust pH to 7.4

### 6.3 Acknowledgement

I would like to express my deepest gratitude for any assistance and encouragement I have got me during my PhD studies. Especially I would like to thank:

- Prof. Dr. Karsten Mäder for the opportunity to work under his supervision and his excellent support during my work.
- The heads of the verovaccines project Prof. Dr. Karin Breunig, Prof. Dr. Sven-Erik Behrens and Dr. Hanjo Hennemann for providing me with this promising research topic.
- The group of Prof. Dr. Silke Rautenschlein at the University of Veterinary Medicine Hannover for the realisation of the immunisation trials in chickens.
- The members of the workgroup Pharmaceutical Technology, especially:
  - o Dr. Henrike Lucas, Dr. Hendrik Metz and Dr. Stefan Hoffmann for fruitful scientific discussions and suggestions.
  - o Tom Wersig and Eric Lehner for the pleasant time.
  - o Manuela Woigk, Kerstin Schwarz and Ute Mentzel for routine measurements.
- All members of the verovaccines project for their assistance and training in biological and biochemical methods, especially:
  - o Dr. Martina Behrens and Mandy Koller for performing immunisation trials in mice.
  - o Dr. Hans Caspar Hürlimann and Jenny Wieczorek for strain construction and yeast fermentation.
- Hanne Debergh for her cooperation with the cytotoxicity assay.
- PD Dr. Anette Meister and Dr. Gerd Hause for the electron microscopic images.
- My family for their ongoing support and encouragement.
- Miri for being on my side and her love.

## 6.4 Curriculum Vitae

### Persönliche Daten:

Name: Johannes Jörg Stelzner  
Geburtsdatum: 16.01.1989  
Geburtsort: Dresden

### Berufserfahrung:

Seit 11/2016 Leiter des Pharmazeutischen Technikums bei der Korsch AG

12/2012 bis 10/2016 Doktorand in der Arbeitsgruppe von Prof. Dr. Karsten Mäder an der Martin-Luther-Universität Halle-Wittenberg

04/2012 bis 10/2012 Zweiter Teil des Praktischen Jahres in der Blue Marlin Apotheke in Dresden

11/2011 bis 04/2012 Erster Teil des Praktischen Jahres, als Diplomand in der Arbeitsgruppe von Prof. Dr. Karsten Mäder an der Martin-Luther-Universität Halle-Wittenberg  
Thema: „*Methodenuntersuchung zum quantitativen in vitro und in vivo Fluoreszenz imaging*“

08/2010 bis 09/2010 Praktikum an der Oxford University bei Prof. Dr. Chris Schofield  
Thema: „*Isolierung, Darstellung und Testung von Enzymen der Carbapenembiosynthese*“

03/2010 Wahlpflichtfach bei der Bayer Schering Pharma AG in Wuppertal  
Thema: „*Quantitative PCR Genexpressionsanalysen krankheitsrelevanter Gene an tierischen und humanen Geweben*“

### Ausbildung:

12/2012 Approbation als Apotheker

10/2007 bis 09/2011 Studium der Pharmazie an der Martin-Luther-Universität Halle-Wittenberg

07/2007 Abitur am Hans-Erlwein-Gymnasium in Dresden

## 6.5 Selbstständigkeitserklärung

Hiermit erkläre ich an Eides statt, dass die vorliegende Promotionsarbeit am Institut für Pharmazie der Martin-Luther-Universität Halle-Wittenberg unter Anleitung von Prof. Dr. Karsten Mäder selbstständig bzw. im Rahmen der angegebenen Kooperationen erstellt wurde. Die Dissertation habe ich ohne fremde Hilfe angefertigt und dazu keine anderen als die von mir angegebenen Quellen und Hilfsmittel benutzt. Inhaltlich oder wörtlich übernommene Stellen aus anderen Arbeiten sind als solche kenntlich gemacht.

Ferner erkläre ich, dass ich bisher noch keine Promotionsversuche unternommen habe und diese Promotionsschrift keiner anderen in- oder ausländischen Fakultät vorgelegt wurde.

---

Ort, Datum

---

Johannes Stelzner

## **6.6 Publications**

### **Peer Reviewed Articles**

J. J. Stelzner, M. Behrens, S.-E. Behrens and K. Mäder

Squalene Containing Solid Lipid Nanoparticles, a Promising Adjuvant System for the Immunisation with Yeast Vaccines

(Submitted)

### **Poster Presentations:**

J.J. Stelzner, H. Caysa, S. Hoffmann and K. Mäder

Key Parameters and Limits for Quantification in Optical Imaging

42<sup>nd</sup> CRS Annual Meeting, 2015, Edinburgh, Scotland

J.J. Stelzner, S. Hoffmann, K. Mäder

A Step to Reliable Fluorescence Imaging

9<sup>th</sup> PBP World Meeting, 2014, Lisbon, Portugal